UNIVERSITÀ DEGLI STUDI DI TORINO

DIPARTIMENTO DI FISICA

DOCTORAL PROGRAMME IN PHYSICS & ASTROPHYSICS

Cataloging Active Galactic Nuclei: a Panchromatic View of Extragalactic Sources

by

Harold Andrés Peña Herazo

Degree on Doctor of Phylosophy

Under supervision of:

Prof. Francesco Massaro and **Dr. Vahram Chavushyan**

2020 - Cycle XXXII

Cataloging Active Galactic Nuclei: a Panchromatic View of Extragalactic Sources

por

Harold Andrés Peña Herazo

Doctorado en Ciencias en la Especialidad de Astrofísica

INSTITUTO NACIONAL DE ASTROFÍSICA, ÓPTICA Y ELECTRÓNICA

Bajo la supervisión de:

Dr. Vahram Chavushyan y **Prof. Francesco Massaro**

Tonantzintla, Puebla

Abstract

Cataloging Active Galactic Nuclei (AGNs) had proven to be a powerful tool to study the AGN phenomena, significantly improving our understanding of their statistical properties and helping to discover new classes.

In this thesis, I present our recent efforts devoted to carrying out a research project on cataloging two specific classes of active galaxies: Blazars and Seyfert Galaxies. For the former class, I searched new sources that will be then included in the next release of the Roma-BZCAT, which I participate in. For the latter, I led the release of the first multifrequency catalog of Seyfert galaxies, and I used its results to investigate the large-scale environments up to Mpc scale.

Blazars are the largest population of γ-ray sources associated to date. However, a significant fraction of all γ-ray sources detected by the *Fermi* Large Area Telescope (LAT) still lacks an assigned low-energy counterpart or a firm classification. In the last years, I have been involved in an optical spectroscopic campaign to tackle the challenging problem of searching counterparts, more specifically blazar-like, potentially associated with unassociated/unidentified γ-ray sources.

Thus, in the first part of this thesis, I present all the optical spectroscopic campaign results I participated in since 2017, as well as a summary of all spectroscopic follow-up observations available to date. Also, I present the results of our extensive search in the literature. Both works are devoted to the "γ-ray blazar hunt". In the literature search, we kept track of efforts of different teams that presented the optical spectra of counterparts or potential counterparts of sources listed in *Fermi*-LAT catalogs. Our optical spectroscopic campaign, our group, acquired long-slit optical spectra using several observatories, including Blanco 4-m, SOAR 4-m, OAN-SPM 2.1-m, OAGH 2.1-m telescopes or available in the Sloan Digital Sky Survey (SDSS).

Thanks to our campaign, we discovered and classified $\sim$500 new blazars, including those found in the literature. We carried out our optical spectroscopic campaign between the release of the second and the third *Fermi*-LAT source catalog, classifying about 25% of sources with uncertain nature and discovering a blazar-like potential counterpart for $\sim$10% of UGSs listed therein. In the last data release of the *Fermi*-LAT Point Source Catalog, about 350 sources are classified thanks to the results achieved during our campaign. We conclude that BL Lac objects constitute the most elusive class of blazars since the largest fraction of *Fermi* sources we targeted and identified during our spectroscopic observations show a featureless optical spectrum. The same occurs among all spectra collected from the literature. Finally, we confirm the high reliability of methods based on mid-IR colors, developed to select blazar-like candidate counterparts of unassociated/unidentified γ-ray sources.

The second part of my thesis is then devoted to Seyfert galaxies. I describe the first release of the Turin-SyCAT, a homogeneous and statistically "clean" catalog of Seyfert galaxies created using their multifrequency properties. To build the Turin-SyCAT, I selected Seyfert galaxies based on an extensive literature search and considering multifrequency selection criteria. I visually inspected all spectra available for all selected sources and applied several thresholds to their radio, infrared and optical properties.

The Turin-SyCAT currently includes more than 500 Seyfert galaxies distinguished in type 1 and type 2 based on their emission line properties of optical spectra. From the analysis I carried out, I found that mid-IR colors of type 1 Seyfert galaxies are more concentrated in the W1-W2 vs. W2-W3 color-color diagram than those of Seyfert 2 galaxies. Then, type 1 Seyfert galaxies could appear to have mid-IR colors similar to blazars, but they can be distinguished from them based on their radio-loudness. Additionally, Seyfert 2 galaxies have mid-IR colors similar to quasars but well distinct from those of BL Lac objects. As expected from their spectral properties, type 1 and 2 Seyfert galaxies have a neat distinction when using the $u - r$ color. Finally, we discovered a tight correlation between the mid-IR fluxes at both 12 and 22 μm and hard X-ray fluxes between 15 and 150 keV in agreement with expectations of the AGN unification scenario.

Finally, I present the study on the large-scale environments of Seyfert galaxies as an additional test to verify the predictions of their unification scenario, as an example of the possible use of the Turin-SyCAT resource. According to the unification scenario predictions, we expect similar "behavior" of galaxies lying in the large-scale environments of type 1 and type 2 Seyferts, since observational differences between the two Seyfert types should be only due to orientation with respect to the line of sight. This analysis was restricted to those sources lying in the footprint of the SDSS. I studied the large-scale environment of Seyfert galaxies adopting a procedure based on the spatial distribution of the so-called *cosmological neighbors*, defined as optical sources lying within 2 Mpc from the Seyfert galaxy having all SDSS magnitude flags indicating a galaxy-type object and having a spectroscopic redshift difference with respect to their surrounding sources within $\Delta z = |z_{\rm src} - z| \leq 0.005$, corresponding to the maximum velocity dispersion in groups and clusters of galaxies. I carried out our analysis in different redshift bins, a requirement strictly necessary to avoid cosmological biases and artifacts.

Finally, from my analysis of the large-scale environments of Seyfert galaxies, I discovered no differences in the neighborhoods of type 1 and type 2 up to redshift $z_{\rm src} = 0.15$. However, compared with the radio galaxies' environments, at the same redshift, I indeed found that the latter inhabits richer environments than Seyfert galaxies. This result is in agreement with the evolution of their host galaxies, mostly spirals for Seyfert galaxies and elliptical for radio galaxies.

A mi familia
To my family

Acknowledgements

I am deeply thankful to my supervisors, Francesco and Vahram for their patience, guidance, support, and opportunities along these years.

I also thanks to INAOE, CONACyT and UniTO for their continuous institutional support.

I would like to thank my collaborators: Raffaelle, Teddy, Alessandro, Federica, Nicola, Ana, Víctor, and Raniere for their fruitful advises, chats, discussions and help.

I wish to extend my special thanks to Eleonora Sani for the opportunity of visiting and working at ESO.

A mi familia, gracias por su infinito apoyo y compañía desde la distancia.

A mis amigos con quienes compartí en México, Italia y Chile, gracias por hacer estos años inolvidables.

To you that were part of this astronomical journey, thanks a lot!

Table 1: Acronyms and Abbreviations used in the text.

Acronym/Abbreviation	Description
AGN	Active Galactic Nuclei
AGU	AGN of Uncertain type
BCU	Blazar of Uncertain type
BLL	BL Lac object
BLR	Broad Line Region
BLRG	Broad Line Radio Galaxies
NLR	Narrow Line Region
NLRG	Narrow Line Radio Galaxies
FSRQ	Flat Spectrum Radio Quasar
OVV	Optical Violent Variable
SMBH	Central Supermassive Black Hole
SSRQ	Steep Spectrum Radio Quasars
UGS	Unidentified/Unassociated γ-ray Source
LINER	Low-Ionization Nuclear Emission-line Region
BZB	Roma-BZCAT label for BL Lacs
BZQ	Roma-BZCAT label for Flat Spectrum Radio Quasars
BZG	Roma-BZCAT label for blazars with optical spectra dominated by their host galaxy
1FGL	*Fermi*-LAT First Source Catalog
2FGL	*Fermi*-LAT Second Source Catalog
3FGL	*Fermi*-LAT Third Source Catalog
4FGL	*Fermi*-LAT Fourth Source Catalog
4LAC	The Fourth Catalog of Active Galactic Nuclei Detected by the Fermi Large Area Telescope
FL8Y	Preliminary *Fermi*-LAT 8-year Point Source List
2MASS	The Two Micron All-Sky Survey
3C	Third Cambridge Catalog
3PBC	The Third Palermo BAT Catalog
4C	Fourth Cambridge catalog
6dF	The Six-degree Field Galaxy Survey
BASS	BAT AGN Spectroscopic Survey
BAT105	The Swift-BAT 105 month catalog
DSS	Digital Sky Survey
SDSS	Sloan Digital Sky Survey
FIRST	Faint Images of the Radio Sky at Twenty-Centimeters
FRSC	The ROSAT Faint Source catalog
IBISCAT4	The 4th IBIS/ISGRI Soft Gamma-Ray Survey Catalog
KDEBLLACS	Catalog of KDE-selected candidate BL Lacs
LipCAT	Lipovetski Catalog of Seyfert Galaxies
NVSS	The NRAO VLA Sky Survey
RBSC	The ROSAT Bright Source catalog

Roma-BZCAT	Roma-BZCAT multifrequency catalogue of Blazars
SUMSS	The Sydney University Molonglo Sky Survey
VERONCAT	Veron Catalog of Quasars & AGN
WIBRaLS	WISE Blazar-like Radio-Loud Sources
BAT	The Burst Alert Telescope
INTEGRAL	The INTErnational Gamma-Ray Astrophysics Laboratory
IRAS	Infrared Astronomical Satellite
Pan-STARRS	Panoramic Survey Telescope and Rapid Response System
ROSAT	The ROentgen SATellite
SWIFT	The Neil Gehrels Swift Observatory
Blanco	Victor Blanco 4-m Telescope
Copernico	Copernico 182 cm telescope
Fermi-LAT	Fermi Large Area Telescope
HET	Hobby-Eberly Telescope
Keck	W. M. Keck Observatory
KPNO	Kitt Peak National Observatory
LAMOST	Large Sky Area Multi-Object Fiber Spectroscopic Telescope
GemN	Gemini North Observatory
Magellan	Magellan Telescope
MMT	Mount Hopkins Telescope
NOT	Nordic Optical Telescope
NTT	New Technology Telescope
OAGH	Guillermo Haro Astrophysical Observatory
OAN-SPM	Observatorio Astronomico Nacional San Pedro Mártir
Palomar	Hale 200 inch Telescope at Palomar
SALT	Southern African Large Telescope
SOAR	Southern Astrophysical Research Telescope
TNG	Telescopio Nazionale Galileo
WISE	Wide-field Infrared Survey Explorer
EW	Equivalent Width
KDE	Kernel Density Estimation
IRAF	Image Reduction and AnalysisFacility
SED	Spectral Energy Distribution
SNR	Signal-to-Noise Ratio

Contents

Chapter 1

Active galaxies

In the realm of galaxies, there are those with showing prominent emission arising from their nuclear regions that dominate that of the whole galaxy across the electromagnetic spectrum. Their nuclear radiation is not related to thermal emission from stars or star formation processes, but due to accretion of matter into a central supermassive black hole (SMBH). These astrophysical objects are known as Active Galactic Nuclei (AGNs). In this first chapter of the thesis, I briefly review the basic observational properties of AGNs, with particular attention to those classes: blazars and Seyfert galaxies, subject of this thesis. Then I will conclude highlighting the scientific objectives of my Ph.D. research.

1.1 Observational properties of Active Galactic Nuclei

The first AGNs to be methodologically studied were six spiral galaxies by Carl Seyfert (Seyfert, 1943). These galaxies have stellar-like nuclei brighter than the rest of the galaxy. But it was not until the release of the Third Cambridge Catalogue of Radio Sources (3C), and the identification of stellar-like optical counterpart of the strongest 3C sources, via lunar occultation, with the discovery of quasars (QSOs) as cosmological sources (Schmidt, 1963) that the systematic studied of AGNs gained impulse. It then became evident that Seyfert galaxies shared several properties with this new class, indeed their cosmological distances (i.e., redshift z). However while in the case of a typical Seyfert galaxy their nuclear luminosity is of the same order of magnitude of that emitted by all the stars in the host galaxy (i.e.,$\sim 10^{11}$ $L_{\odot}$), in quasars it can reach 10^{13} L$\odot$ or even more.

Contemporaneously, in the 60s, black-holes passed from theoretical predictions of general relativity to explain the origin AGNs emission. During that time, it was propose the accretion into a SMBH with a mass ($M > 10^5 M\odot$) (Salpeter, 1964; Zel'dovich, 1964; Magorrian et al., 1998; Kormendy & Richstone, 1995), surrounded by an Accretion Disc, that emits radiation from the heated accreting matter (Hoyle & Fowler, 1963; Lynden-Bell, 1969; Rees, 1984). Reaching luminosities of the order of fractions of L_{edd}, with $L_{edd} = l \times 10^{38} M_{BH}/M_{\odot}$ erg s^{-1}, with l equal to 1.26, for pure Hydrogen

and 1.35, for gas with solar metallicity (Netzer, 2015).

Later Khachikian & Weedman (1974); Weedman (1977) classified Seyfert galaxies as type 1 or type 2, depending on the presence of broad emission lines, wider than 1000 km s^{-1}, see Figure 1.3. The physical region responsible for emitting the broad lines observed on the spectra of type 1 AGN is known as Broad Line Region (BLR). Reverberation mapping estimates locate this region at scales of less than a parsec (Blandford & McKee, 1982; Peterson, 1993), with temperatures $\sim 10^4\,K$, and their mentioned Doppler velocities of the order of $\sim 10^{3-4}$ km s^{-1}, due to the gravitational potential well of the SMBH. The BLR is a relatively high-density region as $\gtrsim 10^9\,cm^{-3}$ higher than the electron density in planetary nebulae (Osterbrock & Ferland, 2006).

On the other hand, the region responsible for emitting the broad lines observed on the spectra of type 1 and type 2 AGN is known as Narrow Line Region (NLR). The NLR situates at distances scales of 100 pc, and in some AGN, is resolved spatially at infrared to ultraviolet bands. The FWHM of the NLR is in the range of ∼200-900 km s^{-1}. The electron density of the NLR, lower than the BLR, is in the range of 10^2 to 10^4 cm^{-3} (Osterbrock & Mathews, 1986).

Different surveys filled the luminosity gap between Seyfert galaxies and quasars, with intermediate luminosity objects (Weedman, 1976). The Markarian survey played a central role in this challenge, including hundreds of galaxies characterized by a relatively strong ultraviolet emission (Markarian, 1967). Nearly ∼10% of galaxies listed therein are Seyferts (Huchra & Sargent, 1973). Other surveys contributed to fill this gap using galaxies selected by Zwicky (Sargent, 1970) and the later Palomar-Green survey (Green, 1976). As more Seyferts and quasars were discovered, their separation in luminosity narrowed up to being almost overlapped (see also Burbidge et al., 1963; Osterbrock & Parker, 1965; Pacholczyk & Weymann, 1968; Burbidge, 1968; Schmidt & Green, 1983).

In some AGNs, their Spectral Energy Distribution (SED) in the infrared bands, from 1 to 1000 μm, is dominated by re-emission of radiation by heated dust. This dust is related to a central absorber described in AGNs unification models, located at scales of a few pc and re-emitting radiation of the accretion disk (see, e.g., Mor & Netzer, 2012; Siebenmorgen et al., 2015). I discuss the central role of this absorber in Section 1.5, when talking about unification scenarios.

AGN are also known for their variability. The time scales of their flux variations range from minutes to months (Webb et al., 1988; Green et al., 1993; Ulrich et al., 1997; Vaughan et al., 2003; Abdo et al., 2010b). From their variability, it is possible to constrain the size of the emitting region and estimate the size of the BLR, and consequently, the mass of the SMBH. The most robust method for estimating the mass of the SMBH is reverberation mapping (Blandford & McKee, 1982; Peterson, 1993). This technique relies on the emission line response, of the material surrounding the central source, to the variability of the emitted continuum. It measures the relative time delay between the continuum emission (often measured at λ5100Å) and the flux of an emission line (e.g., Hβ). The delay is estimated using cross-correlating of both light curves. Physically, the time delay is the light travel time from the continuum source to the line emitting region.

Another characteristic is that 10 % of AGNs are classified as radio-loud, parametrized as the flux ratio between an optical to a radio frequency band, e.g., $R = F_{6cm}/F_B$, being radio-loud those with $R > 10$ (Visnovsky et al., 1992; Stocke et al., 1992; Kellermann et al., 1994; Ho & Peng, 2001). Radio-loudness is intrinsically related to the presence of a jet of relativistic charged particles launched in a process linked to the black hole spin (Blandford & Znajek, 1977a; Blandford & McKee, 1982), and extending to distances of up to 100 of kiloparsecs. In some AGN, their jet emission dominates their broadband emission, although there are AGN without detected jet emission.

All these observational properties of AGNs are known thanks decades of efforts and are described in several reviews and books (see e.g. for reviews and books Peterson, 1997; Krolik, 1998; Osterbrock & Ferland, 2006; Tadhunter, 2008; Beckmann & Shrader, 2012; Netzer, 2013; Heckman & Best, 2014).

1.2 Classification

The classification of AGNs is strongly dependent on the different wavelength range, methods, and their bias. Historically, AGNs classification (see Tadhunter, 2008, for a review) are based on their:

- luminosity, e.g., Seyfert vs. quasars or radio-quiet vs. radio-loud;
- radio morphology, Fanaroff–Riley I vs. Fanaroff–Riley II;
- optical morphology, Seyferts vs. quasars or quasars vs. radio galaxies;
- variability, Optical Violent Variables (OVVs) vs. BL Lacs;
- spectral properties, type 1 vs. 2 or Steep Spectrum Radio Quasars (SSRQ) vs. Flat Spectrum Radio Quasars, or Broad Line Radio Galaxies (BLRGs) vs. Narrow Line Radio Galaxies (NLRGs).

Spectral classification of type 1, those that show broad optical emission lines, or type 2, which lacks such broad lines, is not exclusive of Seyfert galaxies. Other classes of AGNs, like quasars, LINERs, and radio galaxies, are classified similarly. However, for decades type 2 quasars were elusive in optical surveys. They were finally observed, thanks to ROSAT and ASCA surveys in the 1990s (Almaini et al., 1995). Later works, showed that for $z \lesssim 0.8$, there are both type 2 and type 1 quasar (Reyes et al., 2008). Considering radio galaxies, they are commonly labeled as BLRG and NLRG for type 1 and 2, respectively.

Another classification based on spectral properties is the one that considers the ionization level of the optical emission lines. Allowing to define objects as Low-Ionization Nuclear Emission Lines Region (LINERS) that present intense low-ionization (e.g., [N II] λ6584, [N II] λ6584, and [S II] λ6731) lines in their spectra (Heckman, 1980). The origin of the emission mechanism has been an open question for decades with several proposed mechanisms that reproduce the observed line ratios. The most promising mechanisms are photoionization by an accretion disk or photoionization from hot stars (Ho, 2008; Heckman & Best, 2014).

Concerning radio frequencies classification, thanks to the first radio surveys like the Third Cambridge Catalogue of Radio Sources (3C) (Edge et al., 1959) in the 50s, it started the cataloging the first radio-emitting AGNs. These objects were the most brilliant quasars discovered at radio frequencies. Other AGNs, including quasars with weaker radio emission, labeled *radio-quiet*, were more challenging to find. They were discovered later, thanks to large spectroscopic surveys, such as First Byurakan Survey (Markarian et al., 1989), Palomar-Green survey (Green et al., 1986), or the Sloan Digital Sky Survey (Abazajian et al., 2005). In such spectroscopic surveys, the dominant population of quasars is radio-weak. Several criteria are used in the literature to discriminate between radio-loud or radio-quiet AGNs, like the flux ratio between the intensity at radio frequencies and an optical band (e.g., $R = \log \frac{f_{radio}}{f_{optical}}$). Where those with a parameter R > 1 are called radio-loud AGNs (Kellermann et al., 1989).

Additionally, based on their spectral radio-frequency shape AGNs are classified as: Flat Spectrum Radio Quasars (FSRQs), with flat spectra towards high frequencies or Steep Spectrum Radio Quasars (SSRQ), if the emission grows towards high frequencies (Beckmann & Shrader, 2012). A dividing line is defined in the spectral index $\alpha = 0.5$ (from $f_\nu \propto \nu^{-\alpha}$, with f_ν the flux at a certain frequency ν), measured at frequencies on the order of GHz. It is also common in the literature to find the term FSRQ simply as blazar (Ajello et al., 2020).

The AGNs classification considering their morphology at radio frequencies, in particular for radio galaxies, led to the classification of Fanaroff-Riley I (FR I) galaxies, with nuclei dominated emission over the extended emission, and Fanaroff-Riley II (FR II) galaxies, with brighter radio-lobes than their nuclei (Fanaroff & Riley, 1974). Figure 1.1 shows the Fanaroff-Riley II Cygnus A radio galaxy, with their extended emission being brighter than the compact nucleus.

1.3 Seyfert Galaxies

Seyfert galaxies are the eldest type of known active galaxy, their observational history begun at the beginning of the past century, when in 1908 Edward A. Fath discovered peculiar emission lines in the nuclear spectrum of the spiral "nebula" NGC 1068 (Fath, 1909) at the Lick Observatory, later confirmed by Vesto M. Slipher in 1917 (Slipher, 1917). At that epoch, the largest fraction of "nebula" objects, known today to be extragalactic sources, showed an optical spectrum dominated by absorption features due to stars while NGC 1068 presented several, relatively bright, emission lines.

About two decades later, Hubble (1926); Humason (1932); Mayall (1934) discovered similar, optical, emission lines in other "nebulae" then classifying them as extragalactic sources. However, we waited until 1943 when Carl Keenan Seyfert, reporting studying five more galaxies similar to NGC 1068, namely: NGC 1275, 3516, 4051, 4151, 7469 established the first class of active galactic nuclei (AGNs), showing emission dominated by their nuclear regions. By the end of the 1950s, the so-called "Seyfert galaxies" were mainly characterized by "extremely" compact nuclei (i.e., <100 pc) with masses of the order of 10^8-10^9 $M_\odot$. They were coupled with emission lines in their optical spectra that were unusually strong and unusually wide. Assuming that the width of these spectral

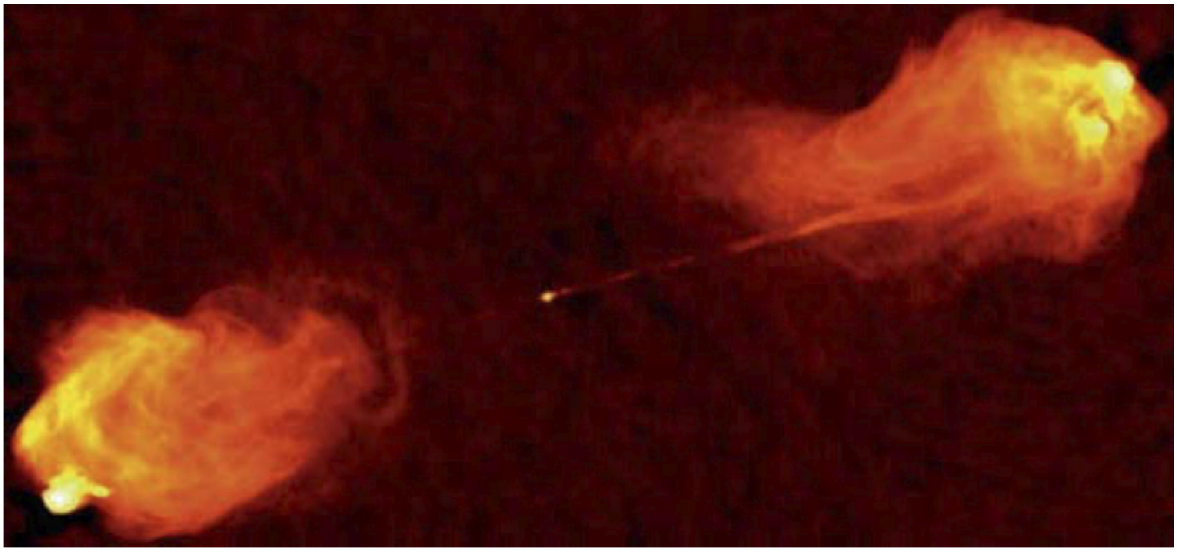

Figure 1.1: Cygnus A, an FR II radio galaxies with lobes that extend up to 50 kpc out of its nuclei. This 5 GHz image was taken with the VLA telescope array with 0.400 resolution (Carilli & Barthel, 1996).

lines is due to the Doppler effect, caused by the ionized gas's motion, gas velocities reach up to several thousand km s^{-1}, far higher than those measured in normal galaxies. At that epoch, the community also started noticing that Seyferts were preferentially hosted in spiral galaxies (Adams, 1977; Heckman, 1978; Simkin et al., 1980; Yee, 1983; MacKenty, 1990; Kotilainen & Ward, 1994; Xanthopoulos, 1996).

A major step in understanding this new class of extragalactic sources was carried out in 1974 when Khachikian and Weedman identified two types/classes of Seyfert galaxies based on the width of their optical emission lines. The presence of permitted emission lines mainly characterizes optical spectra of Seyfert galaxies, like Balmer lines, He IIλ4686, and He Iλ5876, Fe II, and forbidden emission lines, [O II]λ3727, [O III]$\lambda\lambda$4959, 5007, [S II] $\lambda\lambda$6717, 6731 and [N II]$\lambda\lambda$6548, 6584. Balmer lines can present broad (FWHM $> 10^3$ km s^{-1}) and narrow components in their profiles. Seyfert galaxies were initially classified as class 1 or 2 by their relative width of their Balmer or forbidden emission lines(Khachikian & Weedman, 1971, 1974), commonly being use only the relative width of Hβ and Hα to the [OIII] lines (Weedman, 1977; Ho, 2008).

Furthermore, Osterbrock (1981) introduced a more in-depth qualitative classification to account for the range of relative strengths of Hα and Hβ broad components compared with the narrow lines. This definition classifies intermediate types as the broad component gets weaker with the classification number: 1.2, 1.5, and 1.8. Being 1.9, the extreme case in which Hα broad component is detectable but not in $H\beta$.

Several diagnostic diagrams exist to distinguish Seyfert galaxies from other emission-line galaxies, like starburst, star-forming galaxies, or LINERs. These diagnostic diagrams are based on their line intensity ratios and are also useful for investigating the hardness of the ionizing mechanism (Veilleux & Osterbrock, 1987; Kewley et al., 2006; Stasińska et al., 2006). One of the most used diagnostic tools is the BPT diagram

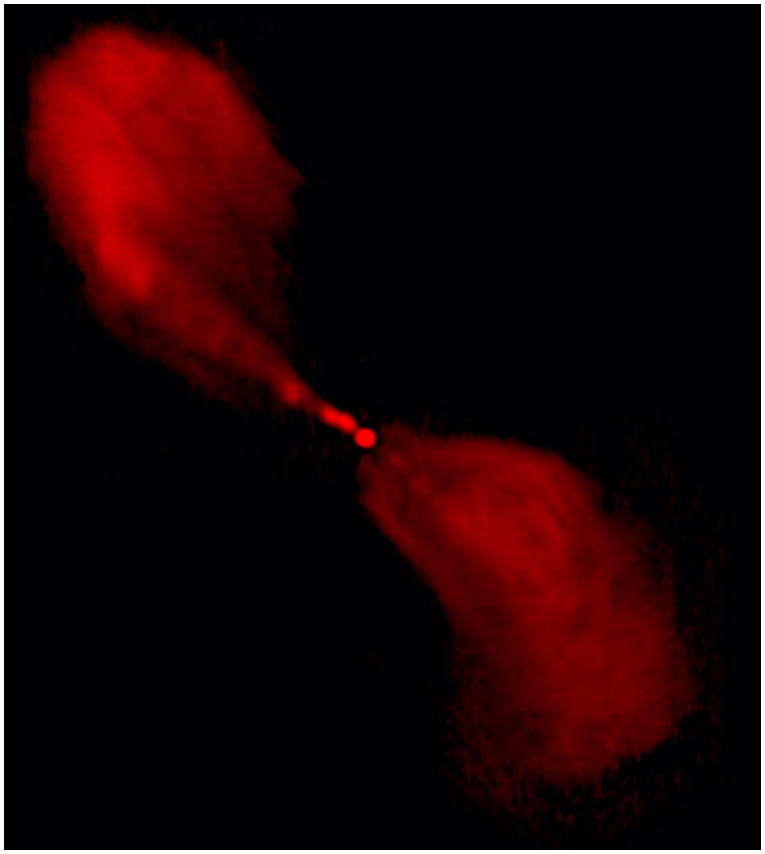

Figure 1.2: FR I Centaurus A VLA 4.9GHz 12.83 × 12.83 arcminutes. Credit: NRAO/AUI/NSF/Univ.Hertfordshire/M.Hardcastle

(Baldwin et al., 1981) based on the comparison between the intensity ratio of [O III] λ5007 over the Hβ and that of the [N II] λ6584 over Hα emission lines, where AGNs are separated from star-forming galaxies (see also Ho et al., 1997; Kewley et al., 2001; Kauffmann et al., 2003; Kewley et al., 2006). It is worth noting that in the BPT diagram Seyfert galaxies and LINERs tend to lie in the same region, having both relative intense low ionization lines (e.g., [OI]λ3727, [OII]λ6300 Heckman, 1980), and thus they could be eventually distinguished according to some empirical criteria as outlined by Schawinski et al. (2007).

At other wavelengths, Seyfert galaxies are commonly known as radio-quiet sources, with radio power typically less than $\sim 10^{40}$ erg s^{-1} (Ho et al., 1995; Ho & Ulvestad, 2001; Chiaraluce et al., 2019).

Their emission at infrared (IR) frequencies is due to several components: continuum emission, dominated by the re-processed radiation arising from the dusty torus heated by the central AGN, where IR luminosities accounts a significant percentage of their bolometric luminosity (Efstathiou & Rowan-Robinson, 1995; Tristram et al., 2007; Nenkova et al., 2008b; Mor et al., 2009; Alonso-Herrero et al., 2011; Siebenmorgen et al., 2015; González-Martín et al., 2019). In addition their IR emission also show (i) a contribution due to star formation (Cid Fernandes et al., 2001; Davies et al., 2007;

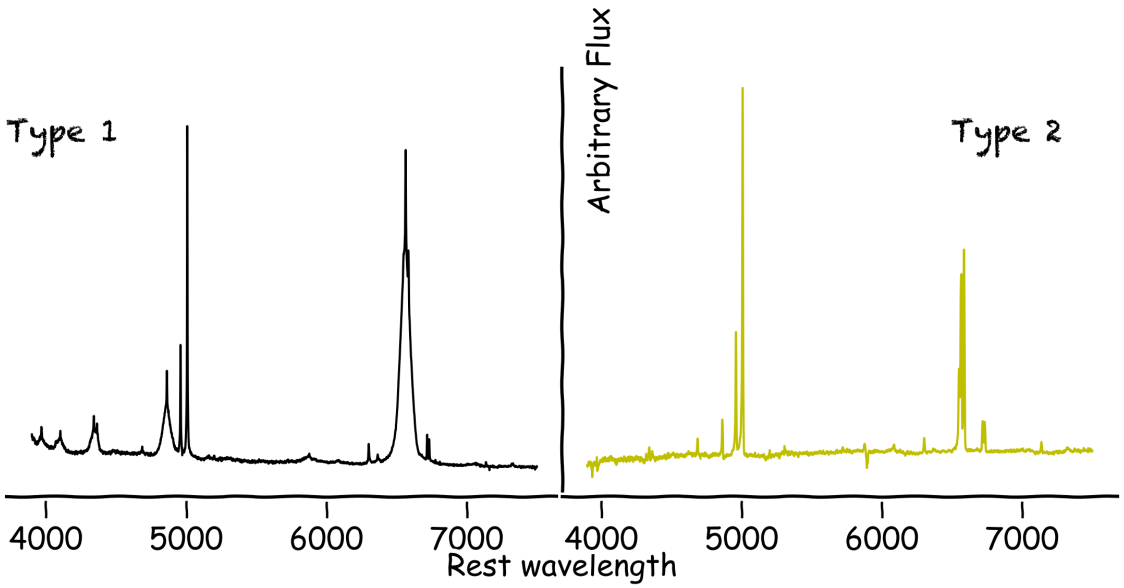

Figure 1.3: We present a type 1 AGN (Left panel) and type 2 (Right panel). Specifically, these sources are the Seyfert galaxies SY1 J0935+2617 SY2 J1135+5657. The difference in both types is the relative widths of their Balmer lines compared with the forbidden lines.

LaMassa et al., 2012; Diamond-Stanic & Rieke, 2012; García-Bernete et al., 2016; Ruschel-Dutra et al., 2017; Esparza-Arredondo et al., 2018); (ii) polycyclic aromatic hydrocarbons, again related with star formation (Peeters et al., 2004; Sani et al., 2010; Gallimore et al., 2010; Calzetti, 2011; Jensen et al., 2017); (iii) emissions lines from fine structure ionic species, e.g., [Ne II] 12.8 μm, [Ne III] 15.5 μm, [Ne V] 14.5 μm, [S IV] 10.5 μm (Ruschel-Dutra et al., 2014) and silicate emissions or other molecular emission (Sturm et al., 2005; Hao et al., 2007; Roche et al., 2007; Mason et al., 2009; Gallimore et al., 2010; Xie et al., 2017; Menezes et al., 2018), often associated with outflows (see e.g., García-Burillo et al., 2014; Morganti et al., 2015; Alonso-Herrero et al., 2019; Feruglio et al., 2020).

At high energies, Seyfert galaxies are also detected in the X-ray band with luminosities $L_{2-10keV} \sim 10^{38-43}$ erg/s (see, e.g., Panessa et al., 2006, for recent work on XMM-Newton and Chandra satellites, and references therein). Their soft X-ray spectra are dominated by a power-law continuum coupled with a high energy cut-off both due to inverse Compton of low energy photons from the accretion disk off relativistic electrons of a "hot" corona (see, e.g. Mushotzky et al., 1980; Haardt & Maraschi, 1991; Singh et al., 2011). There is a "featureless" soft excess Overlaying this X-ray continuum, below a few keV, mainly due to unresolved X-ray emission lines (Fabian et al., 1986; Walter & Fink, 1993; Mehdipour et al., 2011; Gliozzi & Williams, 2020). Above six keV, it is often evident the presence of the Fe Kα fluorescent emission line mainly arising from the reflection of the coronal X-ray emission on the accretion disc and the dusty torus (George & Fabian, 1991; Nandra & Pounds, 1994; Matt et al.,

1996; Markowitz et al., 2008; Patrick et al., 2012; Mantovani et al., 2016).

In the X rays, type 1 and 2 Seyfert galaxies are often distinguished on the basis of their intrinsic absorbing column density, with the latter having $N_{H,int} > 10^{22}$ cm^{-2}; however, there are heavily absorbed Seyfert 1 galaxies mismatching their optical classification (Panessa & Bassani, 2002; Tueller et al., 2008; Beckmann et al., 2009; Corral et al., 2011; Merloni et al., 2015; Ordovás-Pascual et al., 2017). Moreover, local Seyfert 2 galaxies, selected by [O III] flux, show intrinsic column densities $N_H > 10^{24}$ cm^{-2} (Maiolino et al., 1998; Risaliti et al., 1999; Ricci et al., 2015), thus being classified as Compton thick.

The spectra of Seyfert galaxies in the X-ray band can be modeled by a power-law continuum, reflection features, and often an excess in the soft X-rays (Halpern & Filippenko, 1984; Turner & Pounds, 1989). In Figure 1.4 is a representation of a typical Seyfert 1 spectrum and its components. These several components can be disentangled as:

A power-law to model the primary X-rays source of emission that arises from the inverse Compton process of ultraviolet or optical photons in a region of energetic electrons, known as the Corona, with seed photons coming from the accretion disk or synchrotron emission (Dadina, 2008; Beckmann et al., 2009). This continuum has a cut-off at energies of the order of ∼100 keV. This power-law have typical with photon index, $\Gamma \sim 1.7-2.0$, from $F(E) = kE^{-\Gamma}$, and related to the spectral index by $\alpha = \Gamma+1$ (Scott et al., 2011; Brightman & Nandra, 2011).

Over the power-law continuum it is commonly detected an excess below $\sim$ 2 keV (Singh et al., 1985; Arnaud et al., 1985; Turner & Pounds, 1989; Boissay et al., 2014). The origin of this excess is still a mystery, several attempts to explain its nature include emission arising from the hottest part of the accretion disk (Arnaud et al., 1985; Pounds et al., 1986); Comptonization of UV seed photons from the accretion disk in a warm medium $\sim$ 0.3 keV (Magdziarz et al., 1998; Matt et al., 2014); and ionized reflection on a relativistic disk, resulting in blurring the emission lines (Crummy et al., 2006; Vaughan & Fabian, 2004; Ponti et al., 2006).

There are two components produces by the reflection of the primary radiation on the matter: the reflection hump and the iron Kα emission line. The reflection hump is produced by Compton scattering (free-free transition) dominating above ten keV over photoelectric absorption (George & Fabian, 1991; Magdziarz & Zdziarski, 1995). The effect of increasing the ionization state of the reflecting material is the increase of the albedo below ten keV (Ross & Fabian, 1993). The emission iron Kα is emitted by the transition of one electron from the n=2 energy level (L-shell in the Siegbahn notation) to the n=1 energy level (K-shell) after an electron vacancy is left by ionization due to absorption of an X-ray photon. This emission line is a doublet due to spin-orbit interaction on the L-shell, split into two lines with energies 6.404 keV, and 6.391 keV on neutral matter (Fabian et al., 2000). Depending on the iron ionization state these energy can increase to 6.97 keV for Fe XXVI (Ross & Fabian, 1993; Matt et al., 1993; Kaspi et al., 2002; Nandra et al., 2007; Zhou et al., 2011; Patrick et al., 2012).

The X-ray spectra of type 2 objects are different from type 1. Type 2 spectra are dominated by the already discussed reflection components, and the soft excess (Mulchaey et al., 1993; Pounds & Vaughan, 2006; Kammoun et al., 2019; Awaki et al.,

2000; Moran et al., 2001). The continuum component reduced due to the absorbing matter in the line of sight; we will discuss more the absorbing matter in Section 1.5.

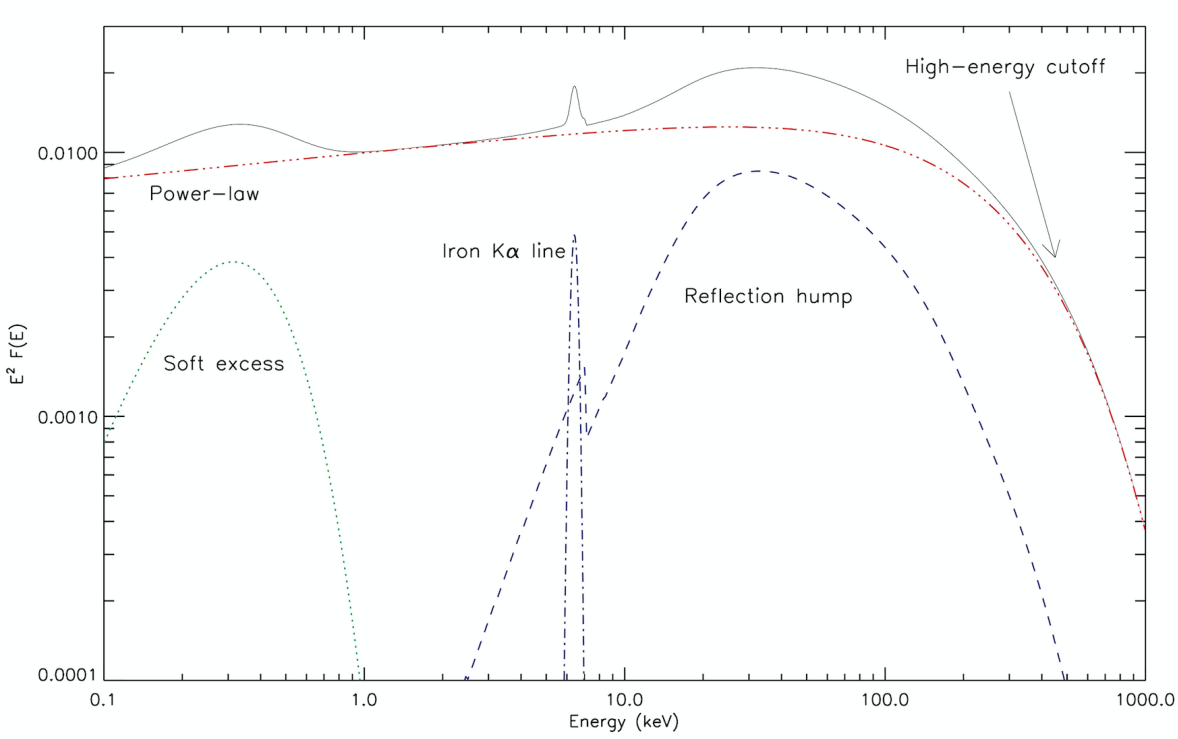

Figure 1.4: Spectrum in the X-ray band of a type 1 Seyfert galaxy. The spectrum is disentangled in several components: in red, the power-law continuum extends to the cutoff energy; green dots are the soft excess below one keV; the blue dashed-dotted line is the iron Kα emission line, and the blue dashed line is the reflection hump. Originally from Ricci (2011).

1.4 Blazars

Blazars are a subclass of radio-loud active galactic nuclei (AGNs), whose emission is dominated by relativistic particles accelerated in a collimated jet, aligned with the line of sight, within a few degrees (Blandford & Znajek, 1977b; Urry & Padovani, 1995). Blazar radiation spans the entire electromagnetic spectrum. Their SEDs consists of two bumps, the low energy one peaking between the infrared and the optical band while the high-energy one in the X-ray or even γ-ray energies (Giommi et al. 1995; Fossati et al. 1998; Abdo et al. 2010c; Abdo et al. 2010d).

There are mainly two different classes of blazars: BL Lac objects and FSRQs. The former class is characterized by an almost featureless optical spectrum, or present only weak (i.e., with equivalent width, EW, less than 5 Å) emission/absorption lines mainly due to their host galaxy (Stickel et al., 1991; Stocke et al., 1991), making their

redshift (i.e., z) estimations challenging (see e.g., Landoni et al., 2014, 2015a, for recent observations).

On the other hand, FSRQs appears as typical quasars in their optical spectra (see Figure 1.5) (Stickel et al., 1991), but showing highly polarized emission from radio to optical frequencies, and flat radio spectra (see. e.g., Healey et al., 2007; Hovatta et al., 2012). In the present work, we adopt the nomenclature of the fifth edition of the Roma-BZCAT, labeling BL Lac objects as BZBs and FSRQ as BZQs (Massaro et al., 2009, 2015a). It is then worth noting that given weak optical features, sometimes present in BL Lacs spectra, that also shows a variable continuum on timescales of hours to minutes, obtaining their redshift estimation is always challenging task (Massaro et al. 2015c).

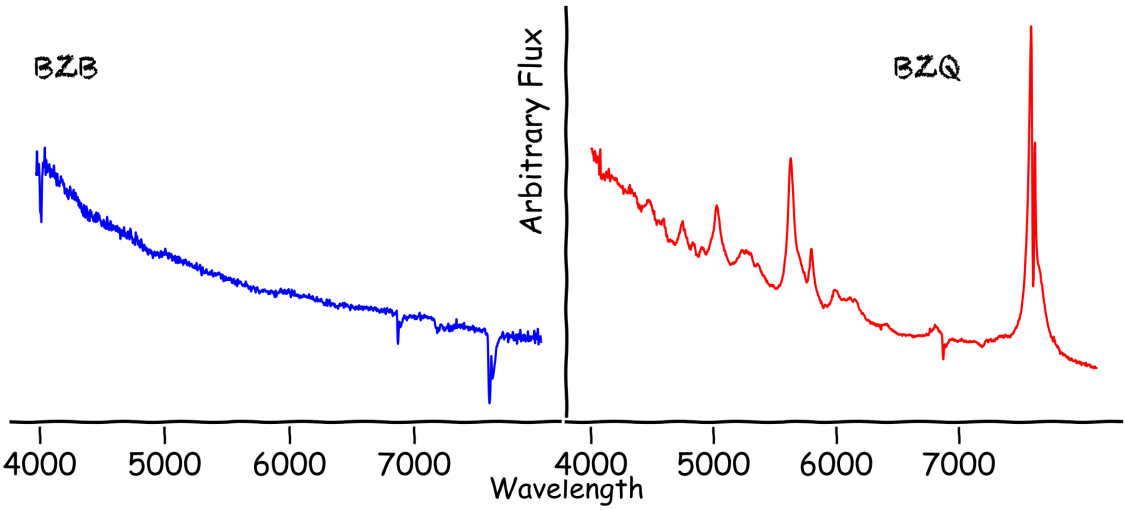

Figure 1.5: Optical spectrum of BL Lac type blazar WISE J031235.70-222117.2 (Left panel) and of the FSRQ 3C 273 (Right panel). Data of 3C 273 was taken from Torrealba et al. (2012)

1.5 The unification scenario

At zero-order, according to the unification model of AGNs (Antonucci, 1993; Urry & Padovani, 1995), type 1 and 2 are intrinsically the same but viewed at different angles with respect to to the line-of-sight, where, in particular, type 2 AGNs are those observed at larger viewing angles thus having the central engine obscured by the presence of a dusty torus (see also Pogge, 1988). Evidence about the role of orientation was found early by Keel (1980), showing that Seyfert 2 galaxies have random orientation while Seyfert 1 galaxies are predominantly orientated face-on. This was later confirmed when Antonucci & Miller (1985) found a hidden Seyfert 1-like spectrum in the polarized light of classical Seyfert 2 NGC 1068.

The central role in the unification scenario its played by a torus-like absorber located at parsec scales that prevents a direct view of the BLR and accretion disk (Antonucci,

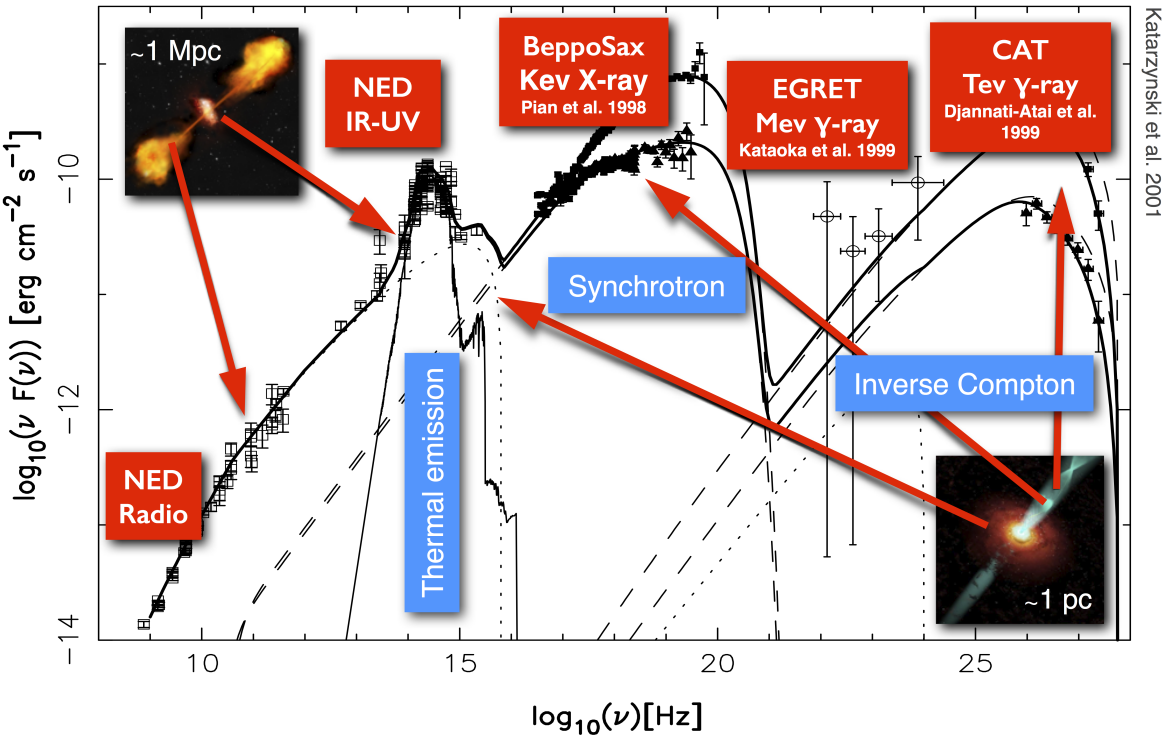

Figure 1.6: Spectral distribution of energy from radio frequencies to the TeV of the blazar Mrk 501. Solid lines show SED in two different states of activity. Dashed and dotted lines show synchrotron emission components. The contribution of the host galaxy is the solid, thin line. The triangles and boxes are data from BeppoSAX (Pian et al., 1998) and CAT (Djannati-Atai et al., 1999). The circles are data from the EGRET satellite (Kataoka et al., 1999). In addition to data from the literature, see Katarzyński et al. (2001).

1993; Urry & Padovani, 1995). Unification is based on two parameters: the inclination of the line of sight with respect to the torus axis and the AGN luminosity (see Netzer, 2015, for a recent review). In the case of jetted AGNs, the radio-unification came with the discovery of relativistic movements in the jets and their anisotropic emission due to relativistic beaming (Cohen et al., 1977; Blandford & Königl, 1979). The angle between the line of sight and the jet explained the spectral index's difference at radio frequencies (Scheuer & Readhead, 1979; Orr & Browne, 1982).

To model the torus emission, there are two approaches (see Netzer, 2015, for a recent review): theoretical hydrodynamic simulations (see, e.g., Wada et al., 2009; Wada, 2012) and phenomenological models based on assumptions of geometry and type of grains.

The phenomenological models differs on the gas distribution: continuous (see e.g., Pier & Krolik, 1992, 1993; Fritz et al., 2006); clumpy (Nenkova et al., 2008a,b); or two-phase, that is a combination of continuous and clumpy distribution (Stalevski et al., 2012). All these models are based on axis-symmetry and with inner edge starting at the dust sublimation radius. Lira et al. (2013) compared different models by fitting the SED of type 2 AGN considering the aperture observations and finding their sample

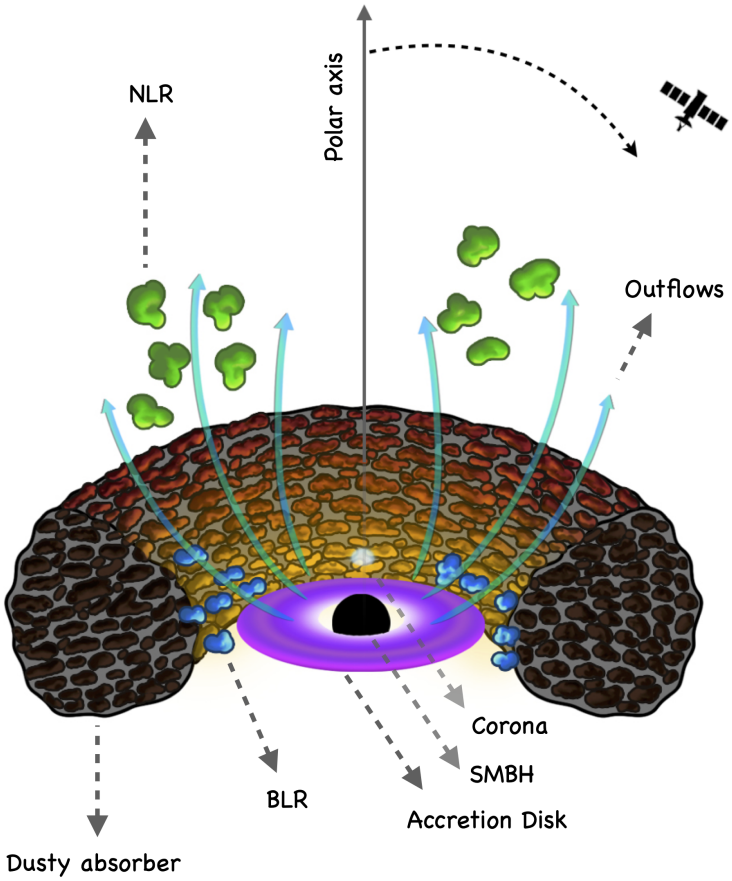

Figure 1.7: A schematic representation of the AGNs unification of radio-quiet objects. At smaller angles between the line of sight respect to the polar axis, the observer would have a direct view of the BLR. At large angles, the dusty absorber prevents a direct view of the central parts.

well fitted by both clumpy and two-phase models, but for half of the sources clumpy models fitted better with an additional black body component.

Further evidence supporting the unification scenario is observations of cones of ISM gas heated, ionized, and getting kinetic energy by the central source radiation, at kpc scales in the host galaxy. This reveals the presence of an absorber with the geometry of a torus (Schmitt & Kinney, 1996; Jaffe et al., 2004; Müller-Sánchez et al., 2011; Fischer et al., 2013; Durré & Mould, 2018; den Brok et al., 2020). These cones are observed in local Seyferts but also at higher redshifts, $z \sim 3$ (den Brok et al., 2020).

With infrared interferometry it was possible to have a close up into AGNs inner regions. With ESO MIDI instrument, 8 to 13 μm, Keck interferometer, and VLTI/AMBER instrument were observed dust emission on parsec scales with dust temperatures $\sim$ 300 to 1400 K (Beckert et al., 2008; Raban et al., 2009; Burtscher et al., 2009; Kishimoto et al., 2011; Hönig et al., 2012; Weigelt et al., 2012; Burtscher et al., 2013; López-Gonzaga et al., 2014, 2016). The VLTI GRAVITY near infrared interferometer detected a rim structure of emission in the inner parsec (0.24 ± 0.03 pc)

of the Seyfert 2 galaxy NGC 1068 offering evidence on the dust sublimation region, i.e., the inner boundary of the dusty absorber (Gravity Collaboration et al., 2020a). Also, with GRAVITY, they resolve the host dust region of eight type 1 AGN (Gravity Collaboration et al., 2020b). The distance of the sublimation region from the central source depends on the sublimation temperature ($T_C \sim 2000$ and $T_{Si} \sim 1500$) and grain composition and size (Baskin & Laor, 2018). This distance offers an estimation of the distance inner part of the dusty torus, supporting the unification scenario as it is a larger distance than the BLR.

Another technique used to estimate the size of the dust emitting region is reverberation mapping (Blandford & McKee, 1982; Peterson, 1993). Dust reverberation mapping is done using NIR emission compared to optical emission (Suganuma et al., 2006; Koshida et al., 2009, 2014; Mandal et al., 2018), also using broad emission lines in the polarized light (Shablovinskaya et al., 2020). These results agree with the unification scenario as the inner radio of the dusty absorber is beyond the BLR size.

In X-rays, the unification scenario's implications are the dependence of different types on the intrinsic absorption, given by the Hydrogen column density, and estimated by modeling the X-ray spectrum. Being type 2 those with $N_{H,int} > 10^{22}$ cm^{-2}.

However, despite the evidence described above, the whole picture appears today more complicated by additional recent discoveries, below we describe the challenges to the geometrical unification scenarios. These challenges include: changing look Seyferts (e.g., Collin-Souffrin et al., 1973; Aretxaga et al., 1999), Seyfert 2 galaxies without absorption in X-rays (Pappa et al., 2001), rare Seyfert galaxies lacking the BLR (Panessa & Bassani, 2002; Shi et al., 2010).

Another phenomenon beyond the unification scenario is the contribution of obscuration at different scales, from nuclear distances to galactic scales. In this case, multiple absorbers can play a role in the observed SED properties. At the BLR distance scales, i.e., at smaller distances than at the torus, there is absorption found by the variability time scales of the X-rays column density (Elvis et al., 2004; Lamer et al., 2003). Beyond the dusty torus, at the host galaxy scales, there are dusty lanes likely part of ISM that absorbs nuclear emission in the line of sight (Matt, 2000; Guainazzi et al., 2005; Lagos et al., 2011; Goulding & Alexander, 2009; Goulding et al., 2012). Dust lanes extinction can be enough to hide the emission of low-luminosity AGN without considering nuclear tours obscuration, challenging the universality of the unification scenario at least for low-luminosity AGN (Prieto et al., 2014). This evidence leads to a complimentary scenario with multiple absorbers with both a Compton–thick ($\tau \ll 1$) absorber at nuclear scales (i.e., the dusty torus) and Compton–thin absorber at larger scales, possibly associated with the host galaxy disc (Maiolino & Rieke, 1995), dust lanes (Matt, 2000) or dusty regions associated with nuclear starbursts (Weaver et al., 2002).

Another factor that can challenge the unification scenario is the role of the environment triggering the AGN activity (e.g., De Robertis et al., 1998; Koulouridis et al., 2006b; Villarroel & Korn, 2014). In particular analyses of the large-scale environments of Seyfert galaxies discovered a significant excess in the number of "companions" compared with non-active galaxies (Petrosian, 1982; Dahari, 1984; MacKenty, 1989; Laurikainen & Salo, 1995; Rafanelli et al., 1995; Salvato & Rafanelli, 1997), and recent

investigations found a difference between of the ambient richness of Seyfert 1 and 2 classes, the latter living in environments with higher galaxy density (Dultzin-Hacyan et al., 1999; Koulouridis et al., 2006b; Jiang et al., 2016; Villarroel & Korn, 2014; Gordon et al., 2017).

1.6 Scientific objectives

The scientific aims and goals of the present thesis are to show how homogeneous, well selected and statistically clean catalogs of AGNs could be used to investigate their properties. Here I focus on two of the major AGN classes: blazars and Seyfert galaxies.

The main aim of the first part of the thesis is to identify and classify blazars as potential counterparts on the *Fermi*-LAT catalogs and increase the number of BL Lac with firm redshift estimations. Another purpose of our campaign is to increase the sample number of the largest homogeneous sample of blazars known to date, the Roma-BzCAT. The main aim of the second part of the thesis is to provide the community with a homogeneous catalog of Seyfert galaxies, the Turin-SyCAT. I present this catalog to study the statistical properties of Seyfert galaxies as well as their large scale environment.

The objectives of my thesis can be summarized as follows:

- Describe our optical campaign for finding and classifying counterparts or potential counterparts of *Fermi*-LAT sources.
- Present the impact of our campaign in the *Fermi*-LAT catalogs and the upcoming release of the Roma-BZCAT.
- Construct the Turin-SyCAT, a homogeneous sample of Seyfert galaxies, using selection criteria that consider their multifrequency characteristics (i.e., optical spectra, radio emission, luminosities).
- Study the Turin-SyCAT sample on different frequencies optical, infrared, and X-ray properties to search for trends or correlations on their emission.
- Study the large-scale environment of the Turin-SyCAT sample as a test of the unification scenario.

Finally, given the large number of acronyms and abbreviations used here, mostly due to different classifications and telescopes used, we summarized them in Table 1.

We use *cgs* units unless otherwise stated. We indicate the WISE magnitudes (Wright et al., 2010) at 3.4, 4.6, 12, and 22 μm as W1, W2, W3, W4, respectively. WISE magnitudes used here are in the Vega system and are not corrected for the Galactic extinction. As shown in our previous analyses (D'Abrusco et al., 2014; Massaro et al., 2016; D'Abrusco et al., 2019), such correction affects only the W1 magnitude for sources lying at low Galactic latitudes (i.e., $|b| < 20°$), and it ranges between 2% and 5% of the magnitude, thus not significantly affecting our results.

We use ΛCDM cosmology with $\Omega_m = 0.286$, and Hubble constant $H_0 = 69.6$ km $s^{-1}Mpc^{-1}$ (Bennett et al., 2014).

Chapter 2

Data acquisition, reduction and analysis

During the whole work related to my Ph.D. thesis and to carry out most of the analyses presented here, I worked on data acquisition, reduction, and analysis of optical observations. I used collected spectra to both the blazar and the Seyfert galaxy research lines. For example, to confirm the blazar nature of associated or unassociated sources during our spectroscopic campaign, it was necessary to observe candidates spectroscopically. Thus, to carry out our follow up campaign, we used several facilities, using the long-slit configuration, in both visiting and remote modes. In this chapter, I describe all telescopes and instruments used in my thesis, including data reduction procedures followed by analyses carried out on archival data.

2.1 Instrument and facilities

We made use of the 2.1 m telescope at the Observatorio Astrofísico Guillermo Haro (OAGH), in Cananea, Mexico. We acquired the data with the Boller & Chivens spectrograph, between April 14^{th} and April 16^{th}, 2018. Collected spectra have a wavelength range from 4000 to 7000 Å and were acquired with a slit width of $2''.5$, getting a final resolution is of 14 Å.

We made extensive use of the 2.1 m telescope at the San Pedro Martir (SPM) Observatory, México. We used the Boller & Chivens spectrograph with a resolution of 2.3 Å grating of 300 l/mm, and a spectral range of 3800 Å to 8000 Å, and resolution of $\sim$ 14 Å. We observe in visiting mode on several runs between 2016 and 2019.

Southern declination sources were observed using two telescopes. I acquired some spectra at the Victor Blanco 4m telescope at Cerro Tololo, Chile, in visiting mode in 2019. We made use of the COSMOS spectrograph (Martini et al., 2014) red grism (r2k), center slit $1.2''$ with OG530 filter. This setup gave a spectral range of 5515-9635 Å and dispersion of 1 Å/pixel. We acquired Hg-Ne comparison lamp spectra on each target position for the wavelength calibration.

The other facility where we acquired southern sources is the Southern Astrophysical Research Observatory (SOAR) 4.1m telescope, at Cerro Pachón, Chile. We used single, long slit mode of the Goodman High Throughput spectrograph (Clemens et al. 2004),

with a slit width of 1.″0 and the 400 l mm^{-1} grating giving a dispersion of $\sim$ 2 Å pixel^{-1}. The observed spectral range was 4000 to 7000 Å , to finally obtain a resolution of 6 Å.

2.2 Data reduction procedure

We performed similar data reduction procedures on all instruments. We acquired two or three different exposures for all our targets, depending on the target's magnitude. Data reduction was then carried out using the Image Reduction and Analysis Facility (IRAF) V2.16 standard reduction packages (Tody & Doug, 1986). Roughly, the data reduction procedure consists of three steps: cosmetic corrections (i.e., bias and flat fielding and cosmic rays removal), wavelength calibration, and flux calibration. The reason for performing cosmetic corrections procedures is to remove any signal not coming from the target of interest but from the instrument's noise, earth atmosphere spectrum, and cosmic rays. I highlighted all IRAF tasks used in italics. An example of raw image of one of the observed targets with all these contributions is presented in Figure 2.2.

First, we performed a bias correction caused by electronic noise. I show an example of bias in the upper panel of Figure 2.1. On each night, we acquired ten bias images. Theses images were taken with the shutter closed and with the shortest possible exposure time, i.e., zero seconds integration time and just readout time. The images were combined using median *imcombine*, to get the master bias. This master bias was then subtracted from the source's, standard star, comparison lamp, and flat field images.

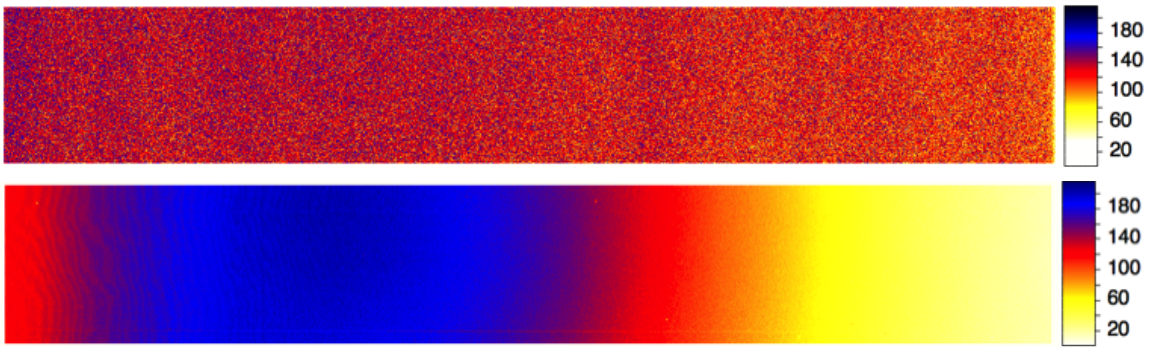

Figure 2.1: *Upper panel*: a master bias. *Lower panel*: a master flat field.

The next step in the cosmetic procedure was to correct for flat fields. We performed this correction as the CCD is not homogeneously illuminated by the telescope and because each pixel of the CCD has different quantum efficiency. During each night of the runs, we acquired five flat field images of a uniformly illuminated screen inside the dome; we did not use or acquired twilight sky flats. We used again *imcombine* task to get the master flat field it then was normalized using *noao.twodspec.longslit.response* task, I show an example of a master flat in lower panel of Figure 2.1. Then, using the *images.imutil.imarith* task, we divided all the images by the master flat field. The last

step of cosmetic corrections was the removal of Cosmic rays. We performed this step using the L.A. Cosmic IRAF algorithm van Dokkum 2001.

The next step was to perform the dispersion axis calibration. To do so, for each set of source images, we acquired a comparison lamp spectral image. Such calibration is intended to fit a wavelength solution to the two-dimensional image. Firstly, we used *noao.twodspec.longslit.identify* to manually identify each emission line in the comparison lamp spectrum extracted from a column or line of the 2D image. Then, we used *noao.twodspec.longslit.reidentify* to automatically re-identify all the lines in the other lines or columns of the 2D lamp image. The third step of the wavelength calibration consists on fit a 2D function, or wavelength solution, of the 2D image with *noao.twodspec.longslit.fitcoords*. Finally, we applied the wavelength solution using the *noao.twodspec.longslit.transform* task.

After calibrating the science images' dispersion axis, we removed the telluric sky spectrum on each image. We performed this step of fitting the sky contribution and remove it using the *noao.imred.generic.background* task. We then extracted the spectrum on each 2D image using *noao.twodspec.apextract.apall* task.

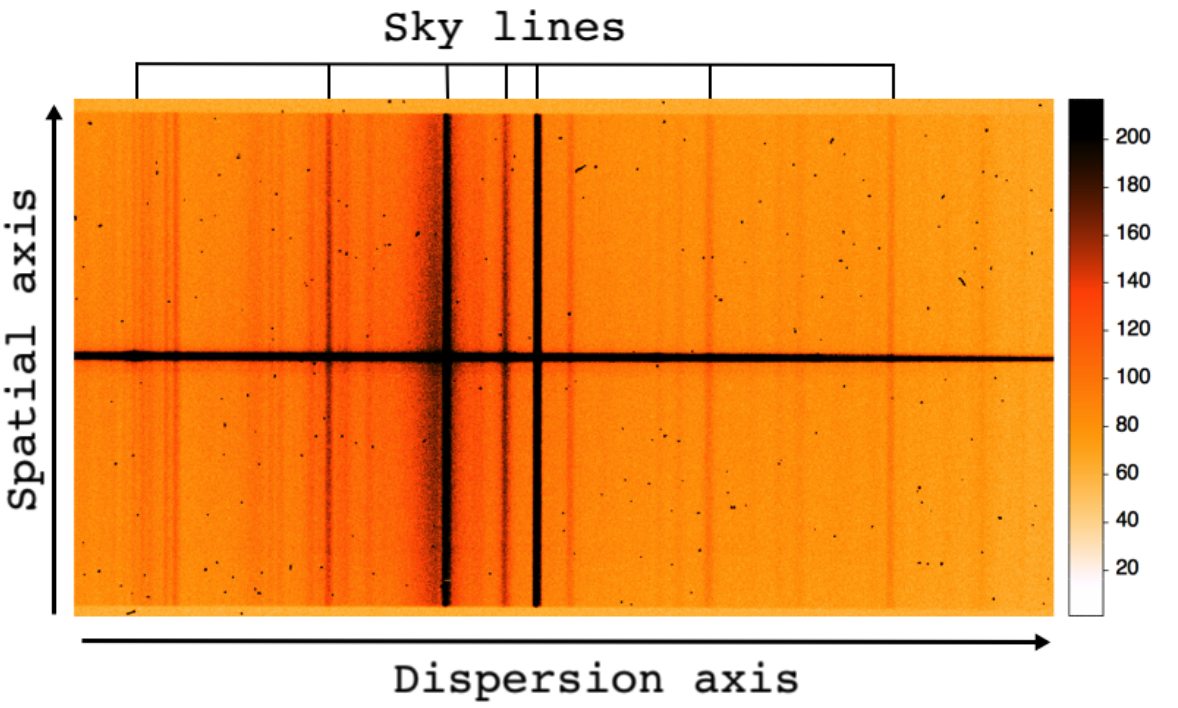

Figure 2.2: Single exposure CCD, horizontal axis is the dispersion direction and vertical axis spatial direction .

During each night, we observed at least one standard spectrophotometric star

to accomplish relative flux calibration. First, we compared our observed spectrum of the standard star with calibration files in the IRAF database spectrum of this star. We performed this comparison using *noao.onedspec.standard* task, which tabulates the observed and calibrated fluxes of the standard star. Based on this tabulation we determined the detector sensitivity as a function of wavelength, using the *noao.onedspec.sensfunc* task. Finally, we calibrated each 1D spectrum *noao.onedspec. calibrate* task. We performed these steps on each source set of images to obtain wavelength and flux calibrated spectra.

Some spectra presented in the current analysis were corrected by galactic extinction using the reddening law of Cardelli et al. (1989) and values of E_{B-V} computed by Schlegel et al. (1998) and reddening and extinction maps of Schlafly & Finkbeiner 2011. Finally, we performed box smoothing for visual representation and, to highlight spectroscopic features, we normalized the spectra to the local continuum.

2.3 SDSS Archival search

We visually inspected all spectra of SDSS sources lying within the positional uncertainty regions, at 95% level of confidence, of our UGS selected sample. Then we selected only those optical sources with blue featureless-like optical spectrum, facilitating its classification as BZBs (i.e. sources with blue optical spectrum with spectral features having $EW < 5$ Å). We did not consider those sources with optical spectral dominated by their host galaxy. We measured the EW of all emission/absorption lines to confirm their nature.

In Figure 2.3, we show the case of FL8Y J0024.1+2401, for which we analyzed all spectra available within the *Fermi* -LAT positional uncertainty region of the FL8Y list including stars, a late-type galaxy and the, previously unknown, BZB. We also report the location of all NVSS sources present in the field, where only a single radio source lies within the positional uncertainty region at 95% level of confidence highlighted with the white ellipse. This radio source is the optical object's counterpart with the typical spectrum of a BL Lac, namely: SDSS J002406.1+240438.3. This strengthens our classification since almost all BL Lacs are known to date have radio counterparts with only a few exceptions (see e.g., Massaro et al. 2017). Thus we claim that SDSS J002406.1+240438.3 could be a potential counterpart of the UGS, which association could be confirmed in the upcoming release of the *Fermi* catalog.

Searching for BZQs in optical surveys is less efficient since they all appear as typical quasars in the optical band and the lack of radio observations, necessary to verify if their spectral index is flat, preventing us from confirming their nature with a similar analysis. All newly discovered optical BZBs lying within the γ uncertainty regions of UGS could be their potential counterparts.

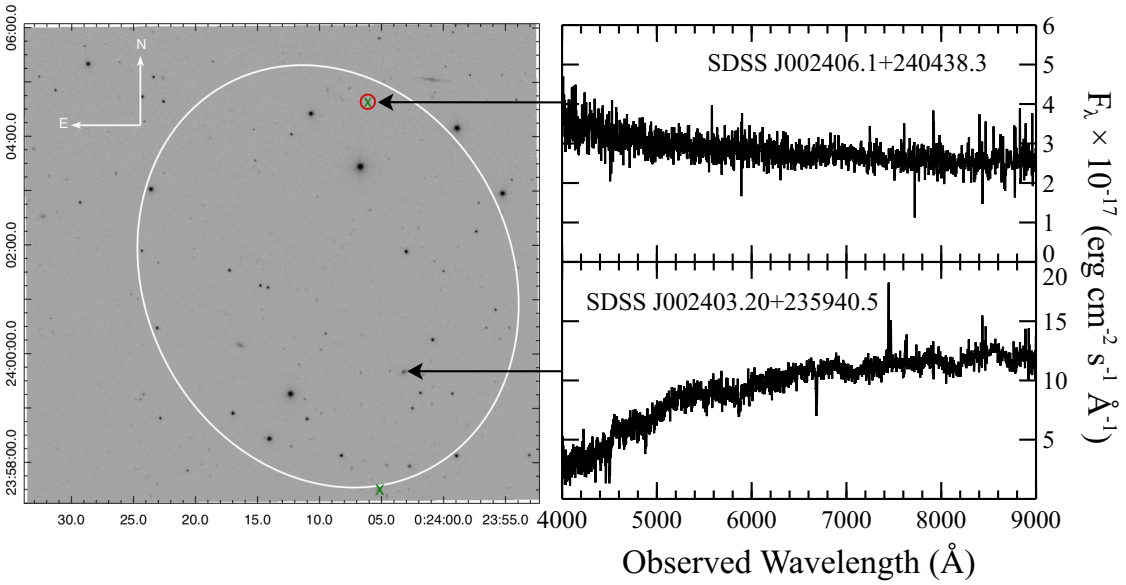

Figure 2.3: We show the optical image of the UGS: FL8Y J0024.1+2401 taken in the i filter and available in the SDSS archive. The white ellipse marks the *Fermi*-LAT positional uncertainty region at a 95% confidence. The red circle indicates the position of the BZB SDSS J002406.1+240438.3 identified and classified thanks to our analysis. Green crosses point all radio sources reported in the NVSS catalog. Insets show all the optical spectra of SDSS sources inspected during our analysis, SDSS J002406.1+240438.3 in the top panel and a typical elliptical galaxy in the bottom one.

Chapter 3

Hunting blazars in the gamma-ray sky: towards the Roma-BZCAT

This chapter is dedicated to all studies I led to search for low energy counterparts of *Fermi*-LAT unidentified/unassociated sources. It is organized as follows. I start introducing both the aim and relevance of the spectroscopic campaign carried out on sources listed in *Fermi*-LAT catalogs. Then I present all results of our observations in the southern hemisphere in section 3.2, corresponding to the first paper I worked. Section 3.3 is indeed devoted to the SDSS archival search and further observations. In Section 3.4, I discuss the state-of-art of our optical spectroscopic campaign. Section 3.5 is devoted to the contribution I provided to the 4LAC catalog. Finally, Section 3.6 is dedicated to the impact of our campaign on the forthcoming release of the Roma-BZCAT.

3.1 Introducing the *Fermi*-LAT Blazar Quest

With the launch in 2008 of the *Fermi* Large Area telescope (*Fermi*-LAT), a new era in the γ-ray astronomy began (Atwood et al., 2009). One of the most challenging key scientific objectives of the *Fermi*-LAT mission, highlighted well before the beginning of scientific operations, is to "identify currently unidentified/unassociated γ-ray sources (UGSs) in the sky" [1].

Amongst all associated γ-ray sources listed in the *Fermi*-LAT catalogs (1FGL, 2FGL, 3FGL and 4FGL, Abdo et al., 2010a; Nolan et al., 2012; Acero et al., 2015; Abdollahi et al., 2020, respectively), the largest known population is constituted by blazars (see also Mirabal & Halpern, 2009; Hartman et al., 1999). In the most recent *Fermi*-LAT catalog (i.e., 4FGL), based on eight years of *Fermi*-LAT survey data, they form the vast majority of all associated sources ($\sim$93%, 3135 out of 3370 total). All these numbers also consider sources known as Blazars of Uncertain type (BCUs), which are blazars lacking a spectroscopic confirmation, constituting more than 25% of the entire 4FGL.

Recent optical spectroscopic campaigns have found that the largest fraction of both:

[1] https://fermi.gsfc.nasa.gov/science/resources/aosrd/

potential low-energy counterparts of UGSs, and classified BCUs, are BL Lacs (see e.g., Landoni et al., 2015b; Massaro et al., 2016; Klindt et al., 2017; Marchesi et al., 2018; Desai et al., 2019; Paiano et al., 2019). These results strongly indicate that BL Lacs are the most elusive counterparts of γ-ray sources with respect to other extragalactic classes.

Discovering more BL Lacs among UGSs has immediate scientific return both in building their γ-ray luminosity function (see e.g., Ajello et al., 2014), necessary to achieve a better understanding of the extragalactic γ-ray background (Ajello et al., 2015), and searching for signatures of the attenuation of the extragalactic background light in their γ-ray spectra (Domínguez et al., 2011; Ackermann et al., 2012). The identification of UGSs is also useful to select potential targets for future observations with the Cherenkov Telescope Array (Massaro et al., 2013; Arsioli et al., 2015); to obtain more stringent limits on the dark matter annihilation in sub-halos (Zechlin & Horns, 2012; Berlin & Hooper, 2014); to test new γ-ray detection algorithms (Abdollahi et al., 2020; Kerr, 2019) and finally, to search for new γ-ray source classes (Massaro et al., 2017; Bruni et al., 2018).

In the last decade many approaches have been used to search for UGS counterparts. These methods are mainly based on radio, both low- (i.e., $\sim$ 1 GHz Massaro et al., 2013; Nori et al., 2014; Giroletti et al., 2016; Mooney et al., 2019) and high-frequency observations (i.e., above 1 GHz Hovatta et al., 2012; Petrov et al., 2013; Schinzel et al., 2015), and/or infrared (IR) data (Massaro et al., 2011; D'Abrusco et al., 2012), and/or X-ray follow-up campaigns (Masetti et al., 2010; Paggi et al., 2013; Stroh & Falcone, 2013; Acero et al., 2013; Landi et al., 2015; Paiano et al., 2017b), as well as statistical algorithms (Ackermann et al., 2012; Doert & Errando, 2014; Salvetti et al., 2017), or optical polarimetry (Mandarakas et al., 2019; Liodakis & Blinov, 2019). Amongst these, the most powerful tools are radio follow up observations (Petrov et al., 2013; Nori et al., 2014; Schinzel et al., 2015; Giroletti et al., 2016; Schinzel et al., 2017) and statistical analysis of mid-IR colors (D'Abrusco et al., 2019). However, to ultimately confirm the blazar nature of the low energy counterparts proposed in these studies, optical spectroscopic observations are strictly necessary.

Thus since 2014, we started a spectroscopic follow-up campaign, mainly based on observations carried out at 4m class ground-based telescopes, to (i) confirm the blazar-like nature of candidate UGS counterparts selected on the basis of their mid-IR colors (Massaro et al., 2011); (ii) verify if BCUs were blazars and classify them according to the possible presence of features (or lack of them) in their optical spectra and (iii) observe any BL Lac whose redshift was still uncertain aiming to observe them in a low (i.e. quiescent) state (see e.g., Álvarez Crespo et al., 2016b).

3.2 Observing from the Southern Hemisphere: the optical spectroscopic campaign of unidentified gamma-ray sources carried out between 2014 and 2017

In this section, we present the spectroscopic observations of our campaign, focused in the southern hemisphere and acquired with the Southern Astrophysical Research Telescope (SOAR) between 2014-2017. Here we briefly describe our sample, observations, data reduction procedure, results, and conclusions of our spectroscopic observations.

3.2.1 Sample Description

The main aim of our campaign is to clarify, via optical spectroscopic observations, the nature of blazar-like sources lying within the positional uncertainty region of UGSs and BCUs, and listed in the latest release of the Fermi catalog. We selected the observed sources from the catalogs of WISE potential counterparts (D'Abrusco et al., 2013, 2019) based on their visibility during the available nights and with an airmass lower than 1.5 (Massaro et al., 2015b; Landoni et al., 2015b).

The sample presented in this section consists of 61 sources grouped in three categories: UGSs, BCUs and known blazars, as described below.

1. Thirty-three of our sources are blazar-like potential counterparts of UGSs selected with the WISE colors, all of them are listed in the 3FGL catalog with the exception of 1FGL J1129.2-0528.

2. Nearly half of our sample (27 out of 61) are BCUs, with counterparts in the X-rays and/or flat radio spectrum, all of them are included in the 3FGL catalog except the source 2FGL J1922.6-7454.

3. We pointed an additional source, the BZCAT object 5BZB J0814-1012 (3FGL J0814.1-1012), which is associated with the radio source NVSS J081411-101208 in 3FGL. This source already observed and classified by Álvarez Crespo et al. (2016c) was pointed because being a BL Lac we tried to get a redshift estimate hoping to observe it during a low flux state.

It is worth mentioning that 37 of our selected targets have Galactic latitude $|b| < 30°$, and 7 of them have $|b| < 10°$. All the sources are listed in Table 3.1, including its Fermi name, counterpart name and the observational logbook. For those we were able to estimate its redshift we reported it and for those we were not able we marked them with a quotation mark. Additionally we report its classification and finally show multifrequency notes for each objects to point up in their broad band detections.

3.2.2 Southern observations

The strategy for our follow up campaign consists in observing small samples of potential counterparts each observing run to minimize the impact on telescope schedules (Massaro et al., 2016).

All the spectra reported in this section were acquired at the Southern Astrophysical Research Telescope (SOAR) 4.1 m telescope, at Cerro Pachón, Chile. We performed both visitor and remote mode observations. We used an instrument configuration as described in Chapter 2. The observations were taken in a time span between December 2014 up to January 2017 as shown in Table 3.1.

For each source we acquired at least two exposures, I reduced the data with the procedure described in Chapter 2. Furthermore, we corrected the spectra by galactic extinction using the reddening law of Cardelli et al. (1989) and values of E_{B-V} computed by Schlegel et al. (1998). Finally, to highlight the spectroscopic features for visual inspection we normalised the spectra to the local continuum. In Figure 3.1 I report one example of the spectra and the correspondent finding charts, I refer the reader for the rest of sources (Peña-Herazo et al., 2017) while both the logbook and the results of our observations are reported in Table 3.1. In addition, we report the results of our spectroscopic observations in Table 3.1.

3.2.3 Results from the south hemisphere

All sources are listed in 3FGL with the only exceptions of UGS 1FGL J1129.2-0528 and the BCU 2FGL J1922.6-7454. We present below our results divided in the three categories of our sample.

Unidentified Gamma-ray Sources

Out of 33 UGSs in our sample, 20 of them show a BZB spectrum. We were not able to estimate the redshift for all of them with a with a single exception, WISE J012152.69-391544.2 which is the potential counterpart of 3FGL J0121.8-3917, with Ca II H & K lines visible at $\lambda\lambda_{obs} = 5438 - 5518$ Å and $EW_{obs} = 1.5 - 1.02$ Å leading to a redshift of $z = 0.390$ (see Table 3.1). The remaining 19 objects shows featureless blue spectra typical of a BZB.

Within the UGSs sample 7 blazar-like candidates have a quasar spectra but none of them has a radio counterpart in NVSS, SUMSS, FIRST (Condon et al.1998; Mauch et al.2003; Becker et al.1995; White et al.1997) and in the radio follow up performed by Petrov et al. (2013) and Schinzel et al.(2015). The lack of radio detections does not allow us to classify them as BZQs. We also found 6 objects with galaxy-like spectrum. QSOs and the galaxies could be considered contaminants of the selection procedures of UGSs counterparts (D'Abrusco et al., 2013; Massaro et al., 2013; Massaro et al., 2013).

We list all the UGS in Table 3.1 along with their classification and redshift estimates.

Blazar Candidates of Uncertain Type

In our sample there are 27 BCUs and for all of them we confirm a blazar nature thanks to our follow up spectroscopic observations. Within the sample we found two candidates with QSO spectra. The first one is the candidate WISE J080311.45-033554.5, counterpart of 3FGL J0803.3-0339, showing [OII]λ3727 emission line with EW_{obs} = 17 Å enabling us to estimate its redshift at z=0.365, while the second one is WISE J161717.91-584808.0 counterpart of 3FGL J1617.4-5846 that shows broad MgIIλ2798 and the blending of SiIII]λ1892 with CIII]λ1909, respectively, giving a $z = 1.423$.

The remaining 25 BCUs show a BZB spectra and for 6 of them it was also possible to estimate their redshifts or a lower limit of their redshift given the detection of interstellar absorption features usually seen in BL Lac spectra (Sbarufatti et al., 2006). In detail, for WISE J064933.60-313920.3 counterpart of 3FGL J0649.6-3138, and associated with the X-ray source 1RXS J064933.8-313914 for which we estimated a lower limit for its redshift of $z \geq 0.563$ using the Ca II H&K absorption lines. Meanwhile for the target J100850.54-313905.5 counterpart of 3FGL J1009.0-3137 we estimate its redshift at $z = 0.534$ based on the [OII]λ3727 emission line ($EW_{obs} = 1.4$ Å) and Ca II H&K absorption doublet at ($EW_{obs} = 0.7 - 0.4$ Å).

The third BCU is WISE J120317.88-392620.9, counterpart of 3FGL J1203.5-3925, for which we estimated a redshift of 0.227, based on the [OII]λ3727 emission (EW_{obs} = 3.2 Å), Ca II H&K absorption lines ($EW_{obs} = 3.3 - 2.0$ Å) and the [OIII] doublet emission line ($EW_{obs} = 2.0 - 4.2$ Å). The fourth BCU is the associated to 3FGL J1312.7-2349, WISE J131248.76-235047.3, we estimated the lower limit of its redshift at $z \geq 0.462$ showing the Mg II absorption lines ($EW_{obs} = 3.2 - 2.9$ Å) and the doublet of Ca II H&K absorption lines ($EW_{obs} = 0.6 - 0.7$ Å). Finally, for the BCU, WISE J195500.65-160338.4, counterpart of 3FGL J1955.0-1605, we estimated a lower limit for its redshift at $z \geq 0.630$ using the doublet of Mg II ($EW_{obs} = 2.0 - 1.6$ Å).

We found that WISE J110624.04-364658.9 associated with 3FGL J1106.4-3643 in the 3FGL/3LAC, is a high redshift BZB at $z \geq 1.084$, estimated from the multiplet of Fe II absorption lines and the Mg II doublet absorption lines ($EW_{obs} = 6.2 - 5.4$ Å). This is the second most distant BZB to date (Massaro et al. 2016).

Other targets

Finally, we report the observation of 3FGL J0814.1-1012 associated with the radio source NVSS J081411-101208 (a.k.a. WISE J081411.69-101210.2). We confirm its nature/classification as BZB but its spectrum does not have any spectroscopic feature that allows to estimate its redshift as occurred in previous observations (Álvarez Crespo et al. 2016c).

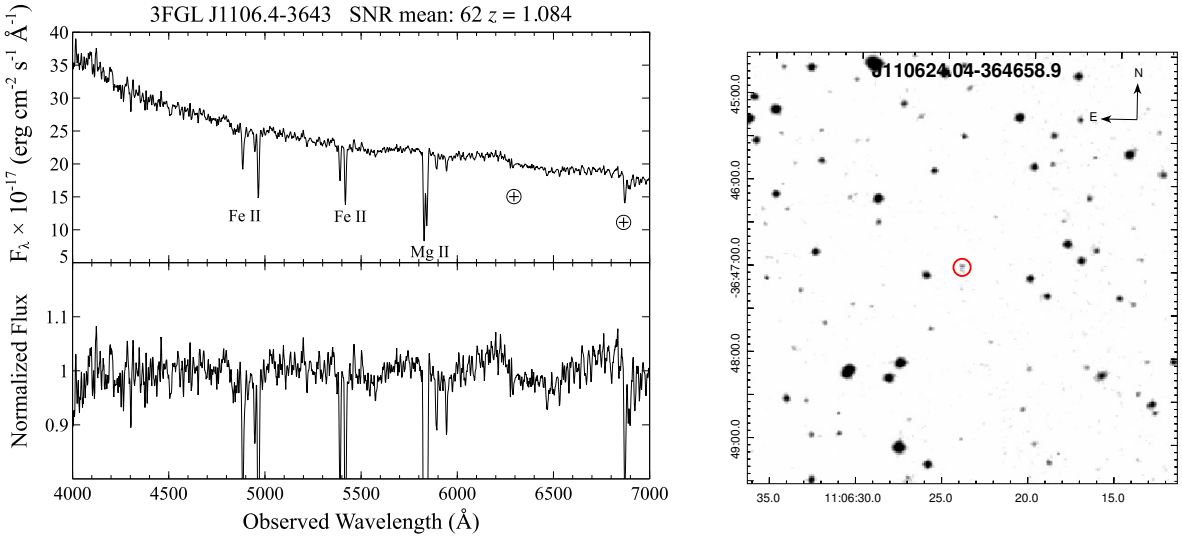

Figure 3.1: (Left panel) Optical spectrum of WISE J110624.04-364658.9 associated with 3FGL J1106.4-3643, in the upper part it is shown the Signal-to-Noise Ratio of the spectrum. (Right panel) The finding chart ($5' \times 5'$) retrieved from the Digital Sky Survey highlighting the location of the counterpart: WISE J110624.04-364658.9 (red circle).

3.2.4 Summary

We present the spectroscopic observations of 61 optical targets associated with Fermi-LAT detected sources. The observations were taken between 2014-2017 as part of our follow up optical campaign. Our sample consist of 33 blazar-like sources lying within the positional uncertainty regions of UGSs, selected on the basis of their IR colors, 27 BCUs and 1 known 3FGL BL Lac object. Results are summarized as follows.

- For the UGSs, we classified 20 candidates counterparts as BZBs. An estimate of redshift for WISE J012152.69-391544.2 potential counterpart of the source at 3FGL J0121.8 -3917 ($z = 0.390$). The remaining targets are thought to be contaminants of the WISE procedure used to search for potential counterparts (D'Abrusco et al., 2013; Massaro et al., 2013; Massaro et al., 2013), there are 7 QSOs, without radio information, and 6 galaxies.

- We confirm the blazar nature of all the 27 BCUs. Two of them are BZQs: WISE J080311.45 -033554.5 counterpart of 3FGL J0803.3 -0339 and WISE J161717.91 -584808.0 counterpart of 3FGL J1617.4 -5846 at $z = 0.365$ and $z = 1.414$, respectively. All the others are classified as BZBs with emission or absorption lines in their optical spectra with $EW < 5$ Å. For this subsample of BZBs we obtained 6 redshifts estimates.

We observed again 3FGL J0814.1-1012, previously observed and classified by Álvarez Crespo et al. (2016c). We confirm the blazar nature of its associated counterpart WISE J081411.69 -101210.2. The spectrum shows a featureless blue continuum as a classical BZB.

To summarize, we identified 50 new blazars, correspondent to an additional 20 % of those already classified and confirmed during our campaign to date. Finally, we also highlight the discovery of the BZB with the second most distant BL Lac known to date, 3FGL J1106.4-3643, with $z \geq 1.084$ estimated from the Mg II absorption lines.

3.3 Follow up spectroscopic observations with SOAR, OAGH and SDSS archive

The current section present an analysis of optical spectroscopic observations, both using archival, taken from the latest data release of the Sloan Digitized Sky Survey Data Release 14 (SDSS DR14; Abolfathi et al. 2018) and follow up observations carried out with SOAR and OAGH. We presented these results in Peña-Herazo et al. (2019). These analysis permitted us: i) confirm the nature of a selected sample of BCUs and ii) search for blazar-like potential candidates of UGSs listed in the *Fermi*-LAT 8-year Source List [2] (FL8Y), based on the first eighth science years of *Fermi*-LAT. The FL8Y list will be soon replaced by the 4FGL catalog. Thus our analysis will be timely used to associate *Fermi* sources in the next release of the *Fermi* source catalog.

3.3.1 Sample description

Sources analyzed here are divided in two main samples. The first lists all BCUs visible during the observing nights available to our group in 2018 at SOAR and OAGH telescopes, while the second lists all UGSs, lying in the SDSS footprint, having at least an optical source with a spectrum available. More details are provided below.

[2] https://fermi.gsfc.nasa.gov/ssc/data/access/lat/fl8y/

3.3.2 Observations

Newly acquired optical spectroscopic observations of BCUs

Here we report the results of pointed spectroscopic observations carried out in 2018 at SOAR and OAGH for which we only observed a BCUs. In Table 3.2 we report the log of all observations while in the following we provide all basic details of data acquisition and reduction procedures.

Optical spectroscopic observations of four sources were collected at Southern Astrophysical Research Telescope (SOAR) 4.1m telescope, at Cerro Pachón, Chile in remote observing mode on May 31^{st} of 2018. The observed targets are: NVSS J160005-252439, PKS 2043-682, PMN J2103-6232 and PMN J2211-7039. We used single, long slit mode of the Goodman High Throughput spectrograph (Clemens et al. 2004), I detail the used instrument configuration on Chapter 2.

Nine sources were observed with the 2.1 m telescope at OAGH in Cananea, Mexico, using the Boller & Chivens spectrograph between April 14^{th} and April 16^{th}, 2018. I present the used configuration on Chapter 2.

We acquired three different exposures for all our targets. Data reduction was then carried out using standard reduction procedures as showed on Chapter 2. All spectra presented in the current analysis were corrected by galactic extinction using the reddening law of Cardelli et al. (1989) and values of E_{B-V} computed by Schlegel et al. (1998) and reddening and extinction maps of Schlafly & Finkbeiner 2011. Finally, we performed box smoothing for visual representation and, to highlight spectroscopic features, we normalized the spectra to the local continuum.

Unidentified Gamma-ray Sources

We first selected a sample of UGSs focusing on searching BL Lac objects lying within their positional uncertainty regions. The same strategy, already successfully carried out in Álvarez Crespo et al. (2016a), helped us to find new BZBs that were and will probably be associate in the future releases of *Fermi* catalogs. To carry out the present search we used the latest releases of the SDSS archival observations (i.e., DR14) in combination with the latest list of *Fermi* sources, correspondent to the FL8Y, both unavailable when we performed our previous analyses.

Thus we selected all 357 UGSs lying in the footprint of the SDSS and then for all of them we searched for sources having an optical spectrum available. Our final sample of UGSs inspected lists 166 UGSs.

Blazar Candidates of Uncertain type

BCUs, as described in the *Fermi* catalogs, is a tentative classification for associated counterparts that i) shows a blazar-like multifrequency behavior or ii) are classified as Blazars of Uncertain type in the Roma-BZCAT. They are divided in three types (Ackermann et al., 2015), namely: BCUs I, those with a counterpart with available optical spectrum but without a good signal-to-noise ratio to classify them either as BZBs or BZQs; BCUs II, lacking optical spectrum in the literature but having an

estimate of the peak energy of their plausible synchrotron component; BCU III, blazar-like multifrequency emission and a flat radio spectrum but lacking an optical spectrum and for which it was not possible to estimate the synchrotron peak frequency.

Thirteen BCUs, previously associated with radio, infrared and/or X-ray counterparts have been pointed with SOAR and OAGH. All of them belong to the FL8Y list, with six of them in 3FGL and their selection was mainly driven by visibility and expected magnitude (i.e. they are all brighter than 18.5 mag in B band). Observation logs are reported in Table 3.2.

3.3.3 Results

Results of current analysis are reported below for each sample separately (i.e., UGSs first and BCUs later). We published Figures of spectra and finding charts of the UGSs potential counterparts in SDSS and those targets observed at OAGH and SOAR in (Peña-Herazo et al., 2019). Results are then summarized in Table 3.2, with spectral line measurements in Table 3.3.

Table 3.3: Spectral Line Measurements

Name	Line ID	EW Å	λ_{obs} Å	Type
CRATES J104630+544953	Ca II H&K	$7-10\pm2$	4966-4920	A
	[O III]	$4-6\pm3$	6192-6253	E
	G band	5 ± 1	5376	A
	Mg I	10 ± 1	6460	A
SDSS J111346.03+152842.9	Ca II H&K	$8-7\pm2$	4995-4953	A
	G band	90 ± 2	5418	A
	Hβ	13 ± 2	6123	A
	Mg I	7 ± 2	6515	A
VCS J1157+1638	Mg II	27 ± 6	5760	E
	Fe II 2964	7 ± 5	—	E
RFC J1231+3711	[O II]	8 ± 3	4550.0	E
	Ca II H&K	13 ± 4	4841-4794	A
	G band	7.2 ± 1	5244	A
AT20G J131938-004939	Mg II	60 ± 4	5298	E
	[Ne V]	$2-4\pm3$	6318-6478	E
	C II]	3 ± 2	4394	E
Q 1326-0516	Mg II	33 ± 7	4411	E
	Fe II 2964	3 ± 5	—	E
SDSS J150316.57+165117.7	Mg II	$2-1\pm1$	5512-5527	A
	Fe II 2600	$1-1\pm1$	5100-5126	A
	Fe II 2344	2 ± 1	4621	A
	Fe II 2374	1 ± 1	4681	A
RFC J1808+4520	Ca II H&K	$4-5\pm3$	4531-4493	A
	G band	4 ± 2	4916	A
	Hβ	19 ± 3	5552	A

Table 3.3: Spectral Line Measurements

Name	Line ID	EW Å	λ_{obs} Å	Type
	Na I	5 ± 3	6727	A
SDSS J223704.78+184055.9*	Ca II H&K	$2 - 3 \pm 1$	6842-6780	A
	G band	2 ± 1	7407	A

Column description: (1) Target Name; (2) Identification of the line; (3) Equivalent width in Å; (4) Observed wavelength in Å; (5) Line type: A for absorption and E for emission.
*For SDSS J223704.78+184055.9 we provide measurements of the tentative identification of the reported lines.

Searching for Gamma-ray BL Lac candidates using archival observations

To carry out this investigation we searched in the footprint of SDSS DR14 all sources having an optical spectrum and lying with the positional uncertainty of UGSs. The total number of UGSs lying in the SDSS footprint is 357, however only 166 of them have at least an optical source with a spectroscopic observation within the positional uncertainty region of *Fermi* . For only 18 out of 166 we found that one of the spectroscopic sources is classifiable as BZB. For the resting 148 UGSs we does not exclude the possibility of having a blazar within the *Fermi* positional uncertainty region.

All these spectroscopic identifications are based on the measurements of the EW of emission/absorption features found in the optical spectra or on the lack of them. We obtained a z estimate for SDSS J111346.03+152842.9 that appear to lie at $z = 0.2589$. Our result is based on the identification of Ca II H&K (EW=8-7 $\pm$2 Å), G band (EW=9 $\pm$2 Å), Hβ (EW=13 $\pm$2 Å) and Mg Iλ5174 (EW=7 $\pm$2 Å) absorption lines. However, the BZB SDSS J111346.03+152842.9 spectrum also shows spectral features of a foreground star. Additionally, we found an lower limit redshift estimation of SDSS J150316.57+165117.7 by identification of Mg II and Fe II multiplets of an intervening absorption system at $z = 0.972$. Finally, we find a tentative estimate of the redshift of SDSS J223704.78+184055.9 at $z = 0.724$ by the possible identification of Ca II H&K (EW=3-2 $\pm$1 Å) and G band (EW=2 $\pm$1 Å) absorption lines.

Additional detailed information for all 18 BZBs are available in Table 3.2 and Table 3.3 while their optical spectra were published in Peña-Herazo et al. (2019).

Since the SDSS has the same footprint of the FIRST survey, we confirm that all newly discovered BZBs have a radio counterpart, as expected for this radio-loud AGN population. We also confirm that all BZBs newly discovered have a classical double bumped SED. In addition all 18 targets have both IR colors of gamma-ray BL Lacs (Massaro & D'Abrusco 2016) but also those in the optical band are consistent with the BZB distribution (Massaro et al. 2012a).

To provide additional evidence that our newly discovered BZBs are potential counterparts of *Fermi* sources we also computed their *WISE* infrared colors. Association radius adopted to search the *WISE* counterpart of the optical SDSS source was set to $3\farcs3$ as reported in (D'Abrusco et al., 2013).

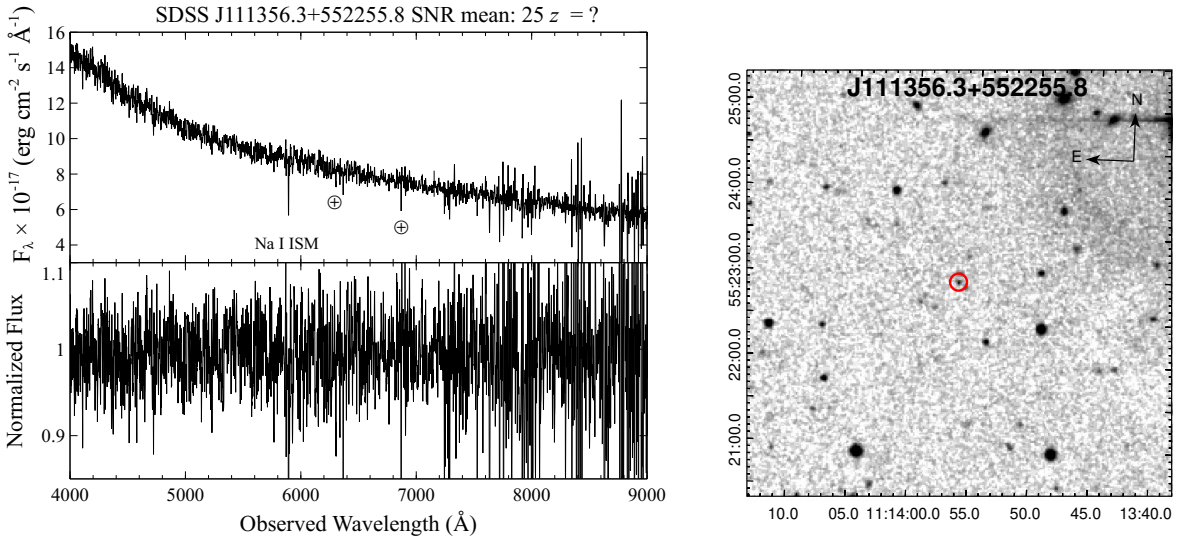

Figure 3.2: (Left panel) Optical spectrum of SDSS J111356.3+552255.8 potential candidate of the UGS FL8Y J1113.8+5524, in the upper part it is shown the Signal-to-Noise Ratio of the spectrum. (Right panel) The finding chart ($5' \times 5'$) retrieved from the Digitized Sky Survey (DSS) highlighting the location of the potential counterpart: SDSS J111356.3+552255.8 (red circle).

Motivated by the fact that *Fermi* blazars occupy a distinctive area in the WISE color-color diagram (Massaro et al. 2011), we verified that the location of the 18 newly identified BZBs, in the WISE color-color diagram $W1[3.4\mu m] - W2[4.6\mu m] - W3[12\mu m]$, is consistent with the well-known *WISE* Gamma-ray Strip (Massaro et al., 2012b). In Figure 3.3 we show that 17 out of 18 newly discovered BZBs, all UGS potential counterparts, clearly overlay with the *WISE* Gamma-ray Strip, having *WISE* colors consistent with those of BZBs listed the Roma-BZCAT associated in the 3FGL. The BZB SDSS J220652.9+221722.2 is not shown on the mid-IR color diagram since it lacks a *WISE* counterpart within $3''.3$. The location of the newly discovered BZBs suggests that infrared emission of these potential counterparts is dominated by non-thermal radiation, as expected for γ-ray BZBs, thus strengthening our results.

As additional test, we also compared the distribution of the angular separation between the position of the optical source and that of the *Fermi* UGS for all new BZBs and all BZBs, belonging to the Roma-BZCAT and associated in the 3LAC.

In Figure 3.4 we show the two distributions. It is worth noting that all 18 BZBs, lying within the positional uncertainty ellipses of UGSs, have angular separation within the 98th percentile of the previous distribution with the only exception of SDSS J172100.07+251249.7 for which this angular separation is $15.5'$.

Optical spectroscopic observations of Blazar Candidates of Uncertain type

Thanks to our optical spectra collected at SOAR and OAGH, we are also able to confirm the blazar nature of all 13 BCUs in our selected sample.

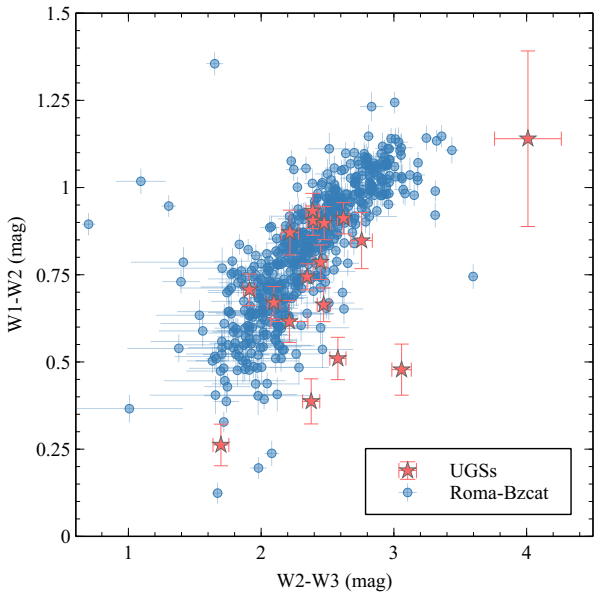

Figure 3.3: The comparison between the mid-IR WISE colors of the Fermi BZBs associated from the Roma-BZCAT and the newly discovered BZBs located within the positional uncertainty region of the selected UGSs.

In particular, three BCUs shows a clear quasar-like optical spectrum, leading to a BZQ classification, namely: VCS J1157+1638 counterpart of FL8Y J1157.5+1639, having a broad MgIIλ2798 (EW=27 $\pm$6 Å) emission line and FeIIλ2964 (EW=7 $\pm$5 Å) at a redshift of 1.058; AT20G J131938-004939 associated with FL8Y J1319.5-0046 showing MgIIλ2798 (EW=60 $\pm$4 Å), FeIIλ2964 (EW=5 $\pm$3 Å) emission lines and a redshift estimation of 0.890 and Q 1326-0516 counterpart of FL8Y J1329.4-0530 with an MgIIλ2798 (EW=33 $\pm$7 Å) and an FeIIλ2964 (EW=3 $\pm$5 Å) emission line at a redshift of 0.575.

The remaining 10 BCUs were indeed all classified as BZBs given their quasi-featureless spectra. We were able to estimate redshifts for 3 of them. In particular, CRATES J104630+544953 associated with FL8Y J1046.1+5449 lies at z=0.249 and shows Ca II H&K emission lines (EW=7-10 $\pm$2 Å) and [OIII] doublet emission lines (EW=4-6 $\pm$3 Å); RFC J1231+3711 counterpart of FL8Y J1231.1+3711 shows [OII] emission line (EW=8 $\pm$3 Å) and the absorption lines of Ca II H&K and G band leading to a redshift estimate of 0.219 and RFC J1808+3520 counterpart of FL8Y J1808.9+3522 for which the optical spectrum presents Ca II H&K (EW=5-4 $\pm$3 Å), G band (EW=4 $\pm$2 Å) and Hβ (EW=19 $\pm$3 Å) absorption lines allowing us to obtain a redshift estimate of 0.142.

Sources with redshift estimates were all acquired at OAGH and their redshift uncertainties are of the order of 0.004.

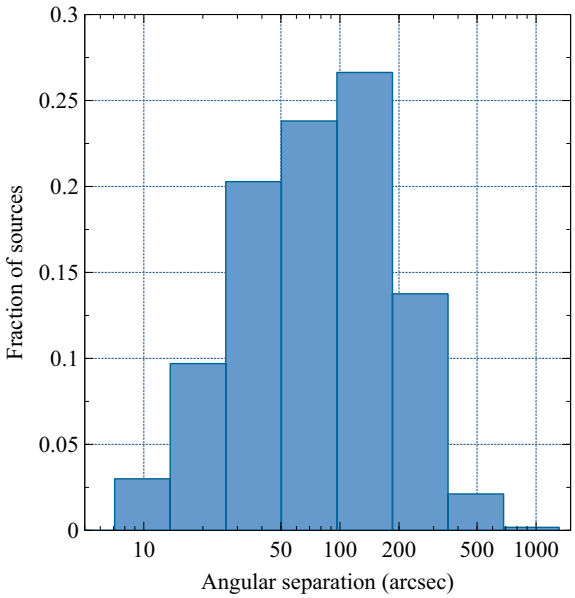

Figure 3.4: Distribution of the angular separation between *Fermi* -LAT and associate counterpart position of the Roma-BZCAT BZBs.

3.3.4 Summary

This work present a spectroscopic analysis of i) a selected sample of UGSs listed in FL8Y to search for blazar-like potential counterparts lying within their positional uncertainty regions along with ii) new observations acquired with SOAR and OAGH telescopes to confirm the nature of a selected sample of BCUs. In this section, I present a total of 31 optical spectra analyzed, consisting in i) data archive retrieval of 18 potential counterparts of UGSs and ii) pointed spectroscopic observations of 13 BCUs.

We highlight that previous results of our optical spectroscopic campaign were already extensively used to i) increase the number of sources listed in the Roma-BZCAT and ii) associate γ-ray sources in the lat releases of *Fermi*-LAT source catalogs.

Our results are summarized as follows:

- For the UGS sample, selected out the preliminary list of the forthcoming *Fermi*-LAT 4FGL catalog, we discovered 18 new BZBs out of 166 UGSs inspected, all lying in the SDSS DR14 footprint and within the γ-ray positional uncertainty regions at 95% level of confidence.

- We analyzed spectra of 13 BCUs observed in OAGH and SOAR telescope. Three of them shows quasar-like spectra, namely: VCS J1157+1638, AT20G J131938-004939 and Q 1326-0516, thus being BCU in the latest release of the *Fermi* catalog can be all classified as BZQs. The remaining 10 sources have all optical spectra featureless as generally occurs for BZBs, with only three exceptions for which we obtained a redshift estimate, namely: CRATES J104630+544953 at z=0.249; RFC J1231+3711 at $z = 0.219$; RFC J1808+3520 at $z = 0.142$.

In particular, within the sample of newly discovered BZBs we estimated the redshift of SDSS J111346.03+152842.9 at $z = 0.2589$ and for SDSS J223704.78+184055.9 we report a tentative redshift of $z = 0.724$ given the signal-to-noise ratio of the spectrum. Additionally, we obtained a lower limit estimate of the redshift for SDSS J150316.57+165117.7 at $z \geq 0.972$.

We also verified that mid-IR properties of these new BZBs are all in agreement with those of known and associated *Fermi* BZBs listed in Roma-BZCAT. Then seventeen out of 18 newly discovered BZBs have an angular separation within 98th percentile of the *Fermi* BZB distribution. These additional evidence strengthen our results that the new BZBs could be all potential counterparts of the UGSs.

The present analysis provides new spectroscopic identifications of potential counterparts of UGSs and BCUs. In particular we remark that most of BCUs analyzed here are BZBs supporting the trend that unclassified *Fermi* sources tend to be BZBs since BL Lacs are still the most elusive class of γ-ray sources.

Our optical spectroscopic follow up campaign is still ongoing with observing nights coming in the current and next semesters, expecting to release new results as soon as collected.

Finally we highlight that, while carrying out our analysis two sources presented here, namely the BCU FL8Y J1541.7+1413 associated with the source RFC J1541+1414 has been classified as a BL Lac at z =0.223 and the same potential counterpart of the UGS FL8Y J2244.6+2502, i.e., SDSS J224436.7+250342.6, was classified as a blazar at redshift z =0.65 (Paiano et al., 2019), in agreement with our results/classifications but providing redshift estimates thanks to the better spectroscopic observations available to the other group of colleagues.

3.4 The current status of the blazar hunt

In this section, I describe the overall impact of our optical campaign carried out since 2014 on the *Fermi*-LAT catalog releases highlighting the fraction of new associations obtained to date that were presented in Peña-Herazo et al., 2020, *submitted*. In our summary, we included results of 30 additional optical spectra, acquired for BCUs, and potential low-energy counterparts of UGSs and analyzed here. We observed the majority of them (22/30) in 2018 and 2019 using Blanco and OAN-SPM telescopes, while we collected the remaining from an archival search in the database of the Sloan Digital Sky Survey (SDSS) Data Release 15 (Aguado et al., 2019).

3.4.1 Blazar classifications

Since we are comparing *Fermi*-LAT catalogs with sources that could be included in future releases of the Roma-BZCAT (Massaro et al., 2009, 2015c), it is necessary to describe how sources are classified in these catalogs and the correspondences between the two.

Thus the for results of our spectroscopic campaign we adopted the Roma-BZCAT nomenclature. According to the Roma-BZCAT, sources observed during our campaign are classified mainly distinguishing between 3 types:

1. BL Lac objects, labelled as BZBs, are those sources with a featureless optical spectrum, or showing a blue continuum with absorption lines due to the host galaxy origin and eventually weak and narrow emission lines with equivalent width less than 5 Å.

2. Flat spectrum radio quasars, labelled as BZQs, presents an optical spectrum showing broad emission lines and dominant blazar characteristics.

3. BL Lac galaxy dominated sources (BZGs), sources usually reported as BL Lac objects in the literature, but having a spectral energy distribution dominated by the host galaxy emission overwhelming the nuclear one.

In addition some objects observed during our spectroscopic campaign were simply indicated as "quasars", labeled as QSO, since the lack of additional multifrequency observations, as the presence of a flat radio spectrum, did not allow us to firmly establish their blazar nature. All sources classified as BZQs, BZGs or labelled as quasars have always a firm redshift estimate while for BZBs, given their nature, details on the z measurements are specified.

Different labels are then used in the *Fermi*-LAT catalogs.

In the latest 4FGL release, BL Lac objects are indicated as BLLs while flat spectrum radio quasar as FSRQ. Then the *Fermi*-LAT catalogs have a class named as Blazar of Uncertain type (BCU) for all those sources that appear to share some blazar properties but lack an optical classification that confirms their nature. Additional sources are then indicated simply as AGN whereas the multifrequency observations available did not allow to proper identify a blazar-like nature. This is the same nomenclature adopted also in the 3FGL.

However, it is worth noting that in the 1FGL and 2FGL γ-ray sources associated with a known BL Lac or a known FSRQ were indicated as BZB and BZQ, respectively, even if they were not part of Roma-BZCAT. Such classification was then removed in the subsequent versions of the *Fermi*-LAT catalogs as it generated confusion. However, this implies that not all BZBs listed in both 1FGL and 2FGL respect the same classification criteria adopted in the Roma-BZCAT also used during our spectroscopic campaign. This explains why in Table 3.6 the first two lines reports BZB/BLL label for the *Fermi*-LAT class of each catalog.

Additionally, the BCU classification was adopted starting with the 3FGL in place of AGNs of uncertain type (AGUs) used in both 1FGL and 2FGL; the class of AGN remained unchanged through all the data releases. All details about the nomenclature adopted in different *Fermi*-LAT catalogs can be found therein. Thus all Roma-BZCAT sources classified as BZBs and BZQs are indicated as BLLs and FSRQs in the *Fermi*-LAT catalogs released after the 2FGL, respectively. A summary of the various classes used in the four Fermi-LAT data releases can be found in Table 3.8.

3.4.2 New optical spectra: sample selection and classification results

The strategy adopted during our optical spectroscopic campaign consists of observing small samples of targets each run to minimize the impact on telescope schedules and

mainly driven by visibility constraints.

The new spectra presented here are collected for targets selected from the following lists:

1. BCUs listed in 4FGL catalog that have an already assigned counterpart whose blazar nature is still uncertain;
2. radio and X-ray sources located within the γ-ray positional uncertainty of UGSs (Marchesini et al., 2020);
3. BL Lacs for which their optical spectrum is not available in the literature, or does not have a redshift estimate;
4. UGSs having a WISE source with blazar-like mid-IR colors lying within its positional uncertainty region, most of them being part of the WISE Blazar-like Radio-Loud Sources (WIBRaLS) and KDEBLLACS catalogs (D'Abrusco et al., 2019).

In particular, the WIBRaLS catalog lists sources with radio counterparts selected to have all mid-IR colors similar to those of *Fermi*-LAT detected blazars while, KDEBLLACS catalog, includes only BL Lac candidates selected using the Kernel Density Estimation (KDE) technique in the WISE W2-W3 *vs* W1-W2 color-color diagram.

The current sample of 30 new targets includes:

- Nineteen sources classified as BCUs in the 4FGL;
- three targets classified as UGSs in the preliminary version of the 4FGL (i.e., the FL8Y), all having a WISE blazar-like source lying within their γ-ray positional uncertainty region.
- Seven BL Lacs and one FSRQ, they were already reported in 4FGL as we provided their classification during the catalog's preparation. Our sample also includes 4FGL J1704.5-0527 and 4FGL J2115.2+1218, two known BL Lacs in the literature for which other groups published their spectra while our data analysis was in progress.

All our newly-observed BCUs are now classified as BZBs, four of them having also a redshift estimate, with the only exceptions of 4FGL J1640.9+1143 and 4FGL J1858.3+4321 that appeared to be BZGs. The 3 UGSs analyzed here all have a BZB lying within their γ-ray positional uncertainty region, in particular the one potentially associated with 4FGL J1637.5+3005 lies at z =0.0786. Then all BL Lacs were confirmed as BZBs, two with redshift estimates (i.e., 4FGL J1035.6+4409 at z =0.4438 and 4FGL J1814.0+3828 at z =0.2754) as well as the flat spectrum radio quasar 4FGL J1459.5+1527 being a BZQ at z =0.3711.

Table 3.4 reports all parameters and observational details about our selected sources. Then in Table 3.5 we show all results achieved on our source sample including emission/absorption ones detected and classification, while all figures of the new spectra are published in Peña-Herazo et al., 2020, *submitted* to A&A. It is worth mentioning that all sources not listed in Table 3.5 were classified as BZBs with unknown redshift.

3.4.3 Impact of optical spectroscopic observations on the *Fermi*-LAT source catalogs

Here we summarize all results achieved to date, distinguishing those obtained thanks to our optical spectroscopic campaign from those found in the literature. Our summary is presented separating each *Fermi*-LAT catalog release available to date to highlight the evolution of the impact of our campaign on *Fermi*-LAT associations. However, this also implies that sources listed in more than one *Fermi*-LAT catalog are counted in each of them.

In Appendix B we also report both a sample of summary lists including all details obtained thanks to our observations as well as those found in the literature search. Complete tables are available in Peña-Herazo et al., 2020.

Optical Spectroscopic Campaign

During our optical spectroscopic campaigns we analyzed 441 observations and we found 394 optical spectra that allowed us to clearly classify the target; this is our "clean" sample reported in Appendix B. These spectra include also those found in the SDSS and 6dF databases and analyzed as part of our campaign.

For the 47 optical spectra not used, 27 sources pointed during our observations revealed an "incorrect" target, as for example a star lying within the positional uncertainty region of a UGS, while additional seven spectra had a low signal-to-noise ratio (SNR) and thus are not reported in our summary table presented here. Our observations include also 13 targets pointed with more than one telescope.

In our "clean" sample, 237 sources out of 394 were previously unclassified and had no optical spectrum present in the literature. We observed 306 targets with ground based telescopes while 88 spectra were collected from archival observations of large spectroscopic surveys (i.e., SDSS and 6dF). In the clean sample, 121 of them lie in the northern hemisphere while the remaining 116 in the southern one. Facilities that were mostly used were OAN-SPM in the northern hemisphere and SOAR telescope at southern declinations.

During our campaign we also pointed a total of 128 Roma-BZCAT sources, mostly BL Lac candidates or sources with uncertain classification or lacking a z estimate to provide updated information in the next release of the blazar catalog. Then there are also 59 targets that, while we carried out our campaign, were also analyzed in other papers.

Results on the impact of our optical spectroscopic observations, carried out since the first release of the *Fermi*-LAT source catalog, on the association of γ-ray sources listed therein are all summarized as follows.

In Table 3.6 we report the number of *Fermi*-LAT sources observed in each catalog as classified therein. For example in the 2FGL we analyzed 76 spectra of sources listed therein as AGN or AGU.

Table 3.7 is simply devoted to summarize the fraction of uncertain sources, i.e., for example BCUs and UGSs in the 3FGL or similar in other catalogs, for which we provide a firm optical classification with respect to the total number reported in the original *Fermi*-LAT catalog. Since we started our campaign after the 2FGL release and

during the 3FGL preparation, the impact of our observations appear larger on these two catalogs where we were able to classify ∼25% of the uncertain AGNs and found potential blazar-like low-energy counterparts for 9% and 6% of UGSs listed therein.

In Table 3.8 we show for each sample of sources listed in all *Fermi*-LAT catalogs the classification we obtained. For example in the 3FGL we observed 103 sources listed therein as AGN or BCU for which their optical spectra clearly indicates them as BL Lacs and, as reported in parenthesis for the BZB column, 20 out of these 103 targets have also a firm redshift estimate. We also classified additional 14 AGNs or BCUs of the 3FGL as BZQ, plus 7 more simply as "quasars" since lacking radio spectral information and thus having numbers reported as 14[+7] in Table 3.8. Finally, 15 more AGNs or BCUs of the 3FGL were classified as BZGs, all with a firm z estimate and all for a total of 139 sources as indicated in Table 3.6.

Finally, Figure 3.5 shows the cumulative distributions of all confirmed blazars observed during our spectroscopic campaign in each published paper, and classified as BZBs or BZQs distinguishing between those observed and those discovered thanks to archival searches in major surveys (i.e., SDSS and 6dF).

Literature search

During our optical spectroscopic campaign, other teams worldwide were presenting optical spectra of sources listed in the *Fermi*-LAT catalogs as UGSs or BCUs. Thus, we were continuously trying to keep track of these additional analyses to avoid doubling targets and get a full overview provided to our colleagues of the *Fermi*-LAT collaboration for the next release of γ-ray source catalog. Thus here we report all information retrieved from the literature in the past years that met the same criteria adopted to classify sources in our campaign and those of the Roma-BZCAT.

In the literature we found a total of 123 sources, 67 analyzed from observations carried out in the northern hemisphere while 56 at lower declinations in the south. These observations includes (i) 23 known blazars listed in the latest release of the Roma-BZCAT and (ii) 19 targets collected from data available in the SDSS or in the 6dF surveys.

As in the previous section Table 3.9, as reported in Table 3.6, provides all information about the total number of sources analyzed for each *Fermi*-LAT catalog since the 1FGL release. It is quite evident that most of literature results reported here are focused on 3FGL sources. This was because observational campaigns carried out in parallel with us, for which we were able to retrieve data in the literature, started later, with the only exception being the observations analyzed by Shaw et al. (2013).

Then in Table 3.10 we show for each sample of sources listed in all *Fermi*-LAT catalogs the classification reported in the literature.

For literature results we did not report the comparison with the FL8Y, the intermediate catalog between the 3FGL and the 4FGL since as previously stated most of these results were focused on 3FGL sources, quite close to the FL8Y release. Nevertheless while during our optical spectroscopic campaign we observed some sources listed in the FL8Y catalog only, all sources found in the literature belong to one of the major releases (3FGL or 4FGL) and thus the comparison with the FL8Y it is not relevant.

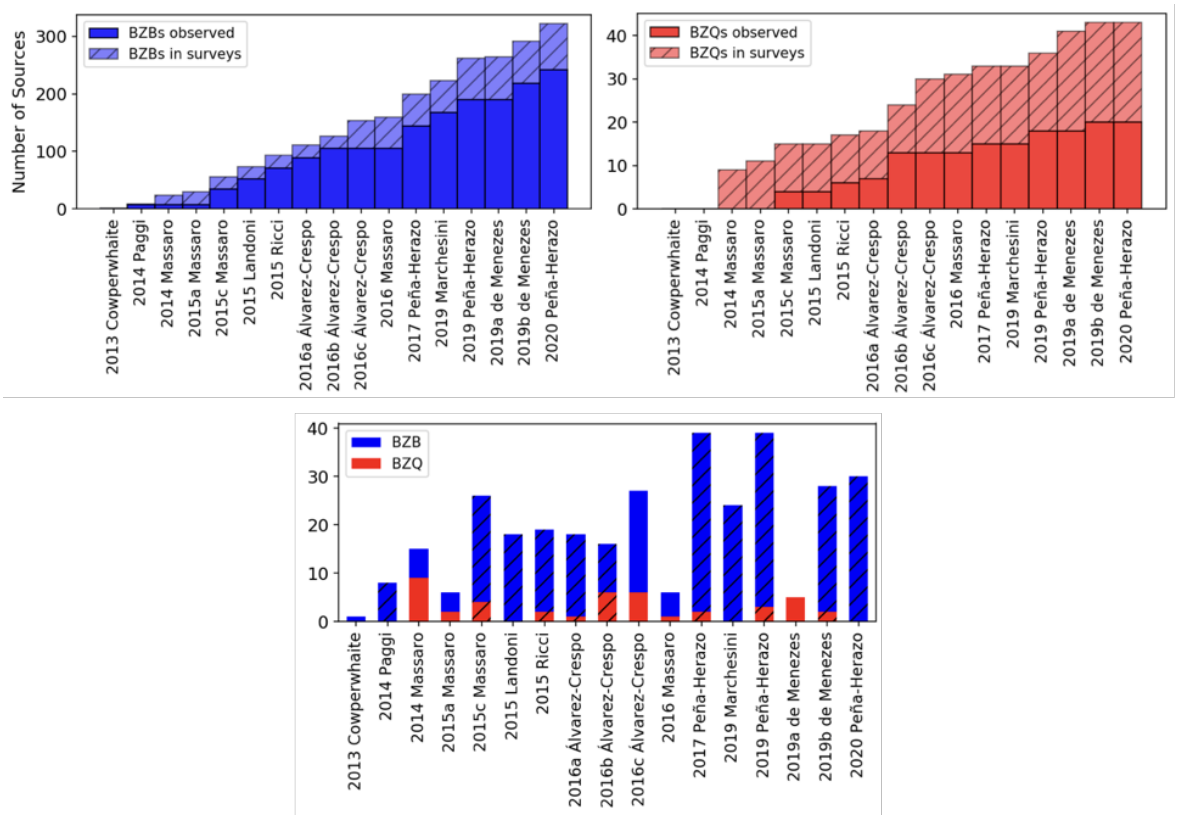

Figure 3.5: Cumulative distributions of all sources observed during our spectroscopic campaign (non-hatched bars) and classified as BZBs (*left panel* in blue) or BZQs (*right panel* in red) in addition to those found during our archival searches on spectroscopic surveys (hatched bars). *Lower panel*: number of sources reported in all articles of our optical campaign (hatched bars) and the articles dedicated to archival searches on spectroscopic surveys (non-hatched bars).

3.4.4 Comparing mid-IR color predictions with optical campaign and literature results

In this section we present the comparison between the predicted classification based on mid-IR colors with that ultimately provided by our optical spectroscopic observations. This comparison is presented distinguishing sources collected during our campaign as well as those found in the literature.

A large fraction of targets selected for our optical spectroscopic observations was based on the statistical analysis of mid-IR colors as presented in the WIBRaLS catalog (D'Abrusco et al., 2014), for which the second version, WIBRaLS2, has been recently released together with the KDEBLLACS (D'Abrusco et al., 2019). The main description of these two catalogs is summarized as follows.

- The WIBRaLS2 catalog contains 9541 candidate blazars, selected among WISE sources detected in all four W1, W2, W3 and W4 filters and whose colors are similar to those of confirmed gamma-ray emitting blazars. The selection is performed in the three-dimensional Principal Component (PC) space generated by the distribution of W1-W2, W2-W3 and W3-W4 colors for a sample of bona fide gamma-ray blazars (the locus). Differently from the direct color space, in the PC space the region occupied by the locus can be modeled with coaxial cylinders. This method also distinguishes among BZB-like, BZQ-like or MIXED candidates based on the WISE colors of the candidate, hereinafter labelled as WBZB, WBZQ and MIXED types, respectively, the latter since their colors are mainly consistent with both blazar classes. WISE-selected sources are further required to have a radio counterpart and to be radio-loud according to the q22 parameter (based on the ratio of the radio and W4 filter flux densities).

- The KDEBLLACS catalog includes 5579 BL Lac candidates selected among WISE sources that are not detected in the W4 band. The colors of these BL Lacs candidates are such as they are located within the region of the W1- W2 vs W2-W3 color-color diagram occupied by a set of confirmed, bona fide BL Lacs with WISE counterparts not detected in W4. The region of the color-color plane used to select KDEBLLACs sources is defined as the area enclosed by the 5% contour of the 2D density distribution of bona fide confirmed BLLacs, determined using the KDE method. As for the WIBRaLS, the final members of the KDEBLLACS catalog are selected to have a radio counterpart that is radio-sound according to the q12 parameter (based on the ratio of the radio and W3 filter flux densities).

Recently, we also characterized both catalogs by analyzing those sources with optical spectra available in SDSS DR15, finding that the efficiency of both catalogs in selecting blazars is $\sim 30\%$ (de Menezes et al., 2019).

Comparing our 394 sources with those listed in WIBRaLS we found 212 matches, 178 WBZBs, 22 WBZQs and 12 MIXED. Then in Table 3.11 we report how they were classified on the basis of our spectroscopic observations. In this table we adopted the same nomenclature of Table 3.8 to indicate those targets classified as quasars but lacking radio spectral information and thus are not qualified to be BZQ according to

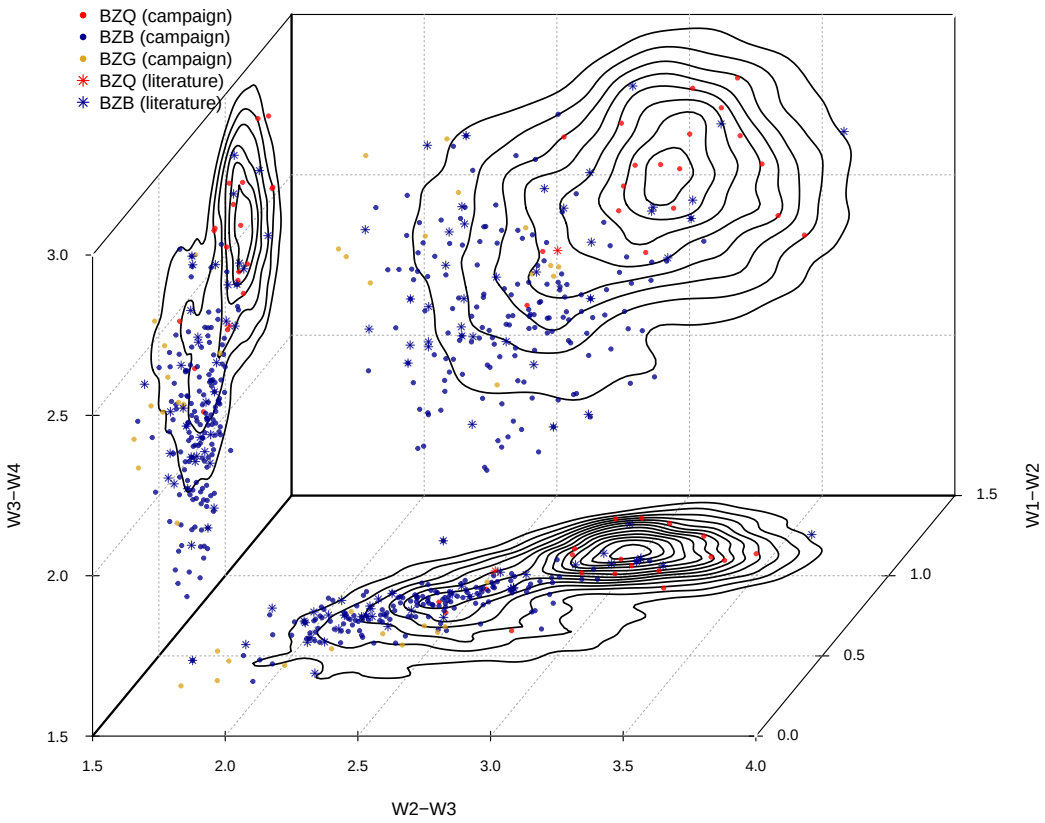

Figure 3.6: Projections on the three WISE color-color planes of spectroscopic sources discussed in this paper with counterparts in WIBRaLS. Red, blue and yellow points indicate, respectively, candidates classified as BZQ, BZB and BZG sources based on their optical spectra. Circles and stars are associated with sources observed in this campaign and sources for which spectra are available in the literature. The black lines on the three planes are the isodensity contours of the 2D projections of the 3D color distribution of locus sources (not plotted for clarity) used to define the WIBRaLS 3D model in the WISE colors space.

our criteria. We also present in Figure 3.6 the projections on the three WISE color-color planes, for the sources of this work that have a WIBRaLS counterpart.

Overall we found that only 8 sources out of 212 are classified as quasars. Then, we confirmed the nature of 161 out of 178 (i.e., 90%) of those targets expected to be BZBs, ∼70% of the WBZQs and the largest fraction of those indicated as MIXED in WIBRaLS2 are BZBs. It is worth noting that only 12 sources out of 212 are classified as BZGs and they were all expected to be BZBs according to their mid-IR colors in WIBRaLS2.

On the other hand, there are 43 sources out of 394 listed in KDEBLLACS, thus all expected to be BZBs and for which our spectroscopic observations confirmed 40 as BZBs, with only 3 better classified as BZGs.

This comparison strongly supports both the reliability of methods based on mid-IR

colors to select candidate counterparts for UGSs and that there is a high chance to confirm the blazar-like nature of BCUs, most likely to be classified as BZBs.

A similar situation occurs for literature results where comparing WIBRaLS2 with sources analyzed by other groups we found 37 matches out of 123 targets (see Table 3.12). All WIBRaLS2 sources were confirmed as BZBs with only one exception: 3FGL J0644.3-6713 that is a BZQ. Then in the KDEBLLACS catalog there are indeed 35 out of 123 sources listed among those classified in the literature and again all of them are BZBs.

3.4.5 Summary and Conclusions

In this work we summarized all results achieved to date thanks to the optical spectroscopic campaign we carried out to unveil the nature of those *Fermi*-LAT sources classified as BCUs and to potentially identify blazar-like sources lying within the positional uncertainty regions of UGSs.

Since the beginning of our campaign in 2014 we analyzed 394 unique targets confirming the blazar-like nature of 371 of them. These are classified as 300 BZBs (38 with a firm redshift estimate), 40 BZQs, and 31 BZGs. Additionally, there are 23 sources for which the lack of radio spectral information prevented us from labeling them as BZQs thus are simply indicated as quasars.

We observed 122 targets in the northern hemisphere mostly thanks to the OAN-SPM facility and 116 targets in the southern one predominantly through observations with the SOAR telescope. We observed 306 targets out of 394 using ground-based telescopes while 88 spectra were collected from archival observations of large spectroscopic surveys. The selection of our targets was mainly based on mid-IR colors since 212 out of 394 also belong to the WIBRaLS2 catalog and 43 to the KDEBLLACS (D'Abrusco et al., 2019) and the expected blazar classification reported therein was also mainly confirmed by our followup observations. All these results also include 30 new spectra presented in this work for which all details on the data reduction and analysis are available in Section 2.

Here we also described results found in an extensive literature search carried out in parallel during our campaign to avoid observing targets already classified by other groups. For all literature results we found a total of 123 sources, 67 lying in the northern hemisphere while 56 in the southern one. These observations include (i) 1 BZG, (ii) 4 BZQs and 1 quasar, while all remaining sources were classified as BZBs, 34 with a firm redshift estimate. For these total 123 sources, only in 19 cases were spectra analyzed from archival observations available thanks to spectroscopic surveys. A significant fraction of them (i.e., $\sim$65%) has also a mid-IR counterpart in one of the two main catalogs used to select targets for our campaign, namely 37 in WIBRaLS2 and 35 in KDEBLLACS. All these sources are classified as BZBs with only one exception, thus mainly confirming the expected classification reported therein and based on WISE colors.

Finally, we conclude that $\sim$20% of blazars currently listed in the 4FGL are classified thanks to our optical spectroscopic campaign and additional $\sim$7% arise from literature results. Moreover the largest fraction of them are BL Lac objects thus confirming that

this is the most elusive class of extragalactic γ-ray sources. Our observational campaign is still ongoing and while preparing this work additional 62 spectra have been already collected. Considering new observing runs already awarded to our group and taking into account the efficiency on how we acquired data to date, we expect to release results for additional $\sim$500 targets by around 2022.

3.5 The Fourth Fermi-LAT Active Galactic Nuclei catalog

The Fourth Fermi-LAT Active Galactic Nuclei catalog (4LAC) (Ajello et al., 2020) derives from the 4FGL catalog, based on 8 years of *Fermi*-LAT data. It contains 2863 with galactic latitude $|b| > 10\,\mathrm{deg}$ classified as AGN. Blazars represents 98% of 4LAC AGNs, and are divided in: 655 FSRQs, 1067 BL Lacs, and 1077 BCUs. It includes also other 64 AGNs, classified as: 38 radio galaxies, 9 NLSy1s, 5 radio galaxies, 2 SSRQs, and 10 other AGNs.

The classification of the sources as AGN from the 4FGL catalog, is based on their optical classification, other spectral band information and literature classification is used to refine these classification.

In this section I describe my contribution on the elaboration of the 4LAC catalog. I performed an extensive search on the literature to corroborate the redshift of blazars in the 4LAC. I checked those sources that are classified there in as BLL, FSRQ, and AGN. I search their counterparts on NED looking for spectroscopic classification information, i.e., if there was an image of their spectrum.

The performed literature search consisted to check:

- 885 BCUs in the list FL8Y that lie out of the SDSS footprint, for 47 of them I found some information about their classification, collecting their spectra references.
- 114 sources in the list FL8Y that are classified as AGN, BLL or FSRQ, and lie out of the SDSS but are not present in the BZCAT and he found that only 13 of them have a classification and/or a spectrum available, keeping track of the spectrum reference.
- BCUs that lie in the SDSS footprint, finding a total of 242 sources.
- Sources classified as BLL or FSRQ but out of BZCAT and in the SDSS footprint 31 sources, I found spectra and have notes/comments for 18 of them that appear to be blazar-like all the others have an unknown origin for the classification and going to the BCU sample.
- The type of redshift for sources classified as BCU, BLL, FSRQ. Finding 17 sources with photometric redshift and 65 with spectroscopic redshift.

The outcome of these search were valuable for the construction of the 4LAC as part of the *Fermi*-LAT collaboration. We publish these results in Ajello et al. (2020). There

we presented 999 sources with robust redshift estimations, and 656 sources based on photometric estimations or bad SNR ratio optical spectra. We reported redshifts for all FSRQs and for 36% BL Lacs listed on 4LAC.

3.6 What's next in the Roma-BZCAT v6.0

The Roma-BZCAT[3] catalog has been extensively used in the preparation of the *Fermi*-LAT catalog. It is based on previously published catalogs and literature data (Massaro et al., 2009, 2015a).

This catalog relies on the following selection criteria:

- Existence of an optical spectrum and its optical classification.
- Detection at 1.4 or 0.843 GHz and 5 GHz with $\alpha < 0.5$ (Condon et al., 1998; White et al., 1997; Mauch et al., 2003).
- Radio morphology with dominant core and a one-sided jet or compact.
- X-ray luminosity $L_X \gtrsim 10^{43}$erg s$-$1.

These selection criteria make the Roma-BzCAT the largest homogeneous catalog of blazars nowadays. They introduced new label on their classification of blazars as BZBs to identify BL Lac type sources; BZQs, for FSRQs; BZG, for sources reported to be BL Lac but showing host galaxy feature in their spectrum; and BZU, blazars of uncertain type, for sources that shows blazar-like broad band blazar characteristics. On its first version (Massaro et al., 2009) it listed 2728 with 1558 % FSRQs, 925 BZBs and 245 BZUs . On their fifth version are reported 1909 BZQs, 1151 BZBs, 274 BZGs, and 227 BZUs (Massaro et al., 2015a).

We are working on the next version of the Roma-BZCAT, which is extensively using the results obtained in thesis.

[3] http://www.asdc.asi.it/bzcat

Table 3.1: Observing Log and Summary of Results

Fermi Name	WISE Counterpart	R.A. (J2000) hh:mm:ss	Dec. (J2000) dd:mm:ss	Obs. Date yyy-mm-dd	Exp. Time (s)	S/N	z	Class	Notes
UGSs									
3FGL J0121.8-3917	J012152.69-391544.2	01:21:52.70	-39:15:44.21	2016-08-02	900	41	0.390 ± 0.001	bzb	N,w,g
3FGL J0156.5-2423	J015624.54-242003.7	01:56:24.55	-24:20:03.77	2015-08-23	600	52	?	bzb	c,w,x
3FGL J0200.3-4108	J020020.94-410935.7	02:00:20.95	-41:09:35.70	2015-08-26	600	38	?	bzb	w,x
3FGL J0312.7-2222	J031235.70-222117.2	03:12:35.71	-22:21:17.21	2017-01-31	1200	71	?	bzb	N,w
3FGL J0340.4-2423	J034050.11-242254.6	03:40:50.11	-24:22:54.66	2015-08-23	600	41	0.683 ± 0.002	qso	w
3FGL J0351.0-2816	J035051.32-281632.8	03:50:51.33	-28:16:32.81	2016-08-29	1800	45	?	bzb	N,w
3FGL J0414.9-0840	J041433.10-084206.8	04:14:33.10	-08:42:06.86	2016-09-11	1200	30	?	bzb	w, N
3FGL J0420.4-6013	J042011.02-601505.5	04:20:11.03	-60:15:05.51	2015-08-23	600	38	?	bzb	w,x
3FGL J0437.7-7330	J043837.07-732921.6	04:38:37.07	-73:29:21.60	2016-08-30	600	24	0.150 ± 0.001	gal	S,w,M,x
3FGL J0704.3-4828	J070421.81-482647.5	07:04:21.82	-48:26:47.59	2016-12-22	1800	20	?	bzb	w,x
3FGL J0721.5-0221	J072113.90-022055.0	07:21:13.90	-02:20:55.07	2014-12-17	1800	28	?	bzb	N,w,x
3FGL J0747.5-4927	J074724.74-492633.1	07:47:24.74	-49:26:33.18	2016-12-30	1800	36	?	bzb	S,w
3FGL J0826.3-6400	J082627.86-640415.4	08:26:27.87	-64:04:15.45	2017-01-30	1800	51	?	bzb	S,w,x
3FGL J1013.4-4008	J101319.30-400550.4	10:13:19.50	-40:05:49.20	2017-01-30	2400	100	?	bzb	S,N,w
3FGL J1033.0-5945	J103332.15-503528.8	10:33:32.16	-50:35:28.82	2016-12-22	1200	27	?	bzb	w,x
3FGL J1100.2-2044	J110028.22-205000.7	11:00:28.32	-20:50:05.60	2017-01-30	1000	33	0.239 ± 0.001	gal	N,w,s
3FGL J1132.0-4736	J113209.26-473853.3	11:32:09.26	-47:38:53.31	2017-01-30	600	41	0.210 ± 0.001	gal	S,w,M,x
3FGL J1325.2-5411	J132457.35-541503.2	13:24:57.36	-54:15:03.29	2016-08-02	900	20	0.218 ± 0.001	gal	w
3FGL J1946.4-5403	J194633.62-540236.4	19:46:33.63	-54:02:36.43	2015-06-23	900	35	0.460 ± 0.002	qso	w
3FGL J2009.2-1458	J200838.59-150453.2	20:08:38.60	-15:04:53.27	2015-08-23	600	10	0.990 ± 0.004	qso	N,w
3FGL J2030.5-1439	J203027.91-143917.1	20:30:27.91	-14:39:17.17	2016-08-02	1200	25	0.234 ± 0.001	qso	N,w,s
3FGL J2112.5-3044	J211217.41-304655.3	21:12:17.41	-30:46:55.33	2015-08-18	900	26	0.216 ± 0.001	gal	w,x
3FGL J2144.6-5640	J214429.57-563849.0	21:44:29.57	-56:38:49.08	2016-08-02	1200	25	?	bzb	w,x
3FGL J2150.5-1754	J215046.60-174954.1	21:50:46.61	-17:49:54.18	2015-08-26	600	55	0.186 ± 0.001	gal	N,w
3FGL J2209.8-0450	J220941.69-045110.3	22:09:41.70	-04:51:10.33	2015-08-23	600	54	?	bzb	F,N,w,s
3FGL J2237.5-8326	J224201.61-832744.4	22:42:01.62	-83:27:44.45	2015-08-18	900	50	0.202 ± 0.001	qso	w
3FGL J2244.6+2503	J224436.66+250343.1	22:44:36.67	+25:03:43.20	2015-08-18	600	36	?	bzb	N,w,s
3FGL J2300.1-3547	J230053.29-355051.0	23:00:53.30	-35:50:51.08	2016-12-30	1200	49	0.753 ± 0.001	qso	w
3FGL J2321.6-1619	J232136.98-161928.3	23:21:36.98	-16:19:28.32	2015-08-23	600	47	?	bzb	N,w
3FGL J2337.2-8425	J233627.96-842652.1	23:36:27.97	-84:26:52.17	2015-08-18	600	22	?	bzb	w
3FGL J2351.9-7601	J235116.13-760015.5	23:51:16.13	-76:00:15.53	2015-08-26	600	40	?	bzb	S,w,x
3FGL J2358.6-1809	J235836.83-180717.4	23:58:36.84	-18:07:17.48	2015-08-23	600	51	?	bzb	N,w,x
1FGL J1129.2-0528	J112914.05-052856.3	11:29:14.06	-05:28:56.36	2015-05-20	1350	34	0.920 ± 0.001	qso	F,N,w,s
BCUs and AGUs									
3FGL J0127.2+0325	J012713.94+032300.6	01:27:13.95	+03:23:00.64	2016-12-22	1800	44	?	bzb	N,w,s,x
3FGL J0310.4-5015	J031034.72-501631.1	03:10:34.72	-50:16:31.13	2014-12-17	2100	62	?	bzb	S,w,X,x
3FGL J0439.9-1859	J043949.73-190101.5	04:39:49.73	-19:01:01.57	2014-12-17	2100	57	?	bzb	Pm,w,x
3FGL J0626.6-4259	J062636.71-425805.9	06:26:36.71	-42:58:05.92	2017-01-30	900	45	?	bzb	w,X
3FGL J0649.6-3138	J064933.60-313920.3	06:49:33.60	-31:39:20.34	2014-12-18	1050	55	≥ 0.563	bzb	w,X,x
3FGL J0703.4-3914	J070312.65-391418.8	07:03:12.66	-39:14:18.89	2014-12-17	1800	49	?	bzb	w, S,N,A,X,x
3FGL J0803.3-0339	J080311.45-033554.5	08:03:11.45	-03:35:54.57	2014-12-18	900	45	0.365 ± 0.001	bzq	Pm,V,T N,w,x
3FGL J0827.2-0711	J082706.16-070845.9	08:27:06.17	-07:08:45.93	2015-05-19	300	52	?	bzb	Pm,N,w,M,X
3FGL J0858.1-3130	J085802.90-313038.3	08:58:02.91	-31:30:38.31	2014-12-18	1050	25	?	bzb	w,X
3FGL J0947.1-2542	J094709.52-254059.9	09:47:09.53	-25:40:59.97	2014-12-18	600	95	?	bzb	N,w,6,X,x
3FGL J1009.0-3137	J100850.54-313905.5	10:08:50.55	-31:39:05.50	2015-05-19	1350	98	0.534 ± 0.001	bzb	Pm,T,S,N,c,w
3FGL J1106.4-3643	J110624.04-364658.9	11:06:24.04	-36:46:58.96	2015-05-21	1500	62	1.084 ± 0.001	bzb	Pm,N,S,A,c,w
3FGL J1125.0-2101	J112508.62-210105.9	11:25:08.63	-21:01:05.98	2015-05-19	1200	103	?	bzb	Pm,N,c,w,X,
3FGL J1203.5-3925	J120317.88-392620.9	12:03:17.89	-39:26:20.96	2015-05-20	900	63	0.227 ± 0.001	bzb	Pm,S,N,c,w
3FGL J1218.8-4827	J121902.26-482627.9	12:19:02.27	-48:26:27.98	2015-05-21	1800	84	?	bzb	Pm,S,c,w
3FGL J1307.6-4300	J130737.98-425938.9	13:07:37.98	-42:59:38.97	2015-05-19	600	115	?	bzb	w,X,x
3FGL J1312.7-2349	J131248.76-235047.3	13:12:48.76	-23:50:47.38	2015-05-19	1800	63	≥ 0.462	bzb	N,w
3FGL J1512.2-2255	J151212.75-225508.4	15:12:12.76	-22:55:08.47	2015-05-21	2700	67	?	bzb	w,X,x
3FGL J1518.0-2732	J151803.59-273131.1	15:18:03.60	-27:31:31.13	2015-05-20	150	67	?	bzb	Pm,T,N,A,c,w,M,g
3FGL J1539.8-1128	J153941.19-112835.3	15:39:41.20	-11:28:35.36	2015-05-20	600	107	?	bzb	Pm,N,w,6,g,X,
3FGL J1547.1-2801	J154712.13-280221.5	15:47:12.13	-28:02:21.57	2015-05-20	1350	54	?	bzb	w,X
3FGL J1617.4-5846	J161717.91-584808.0	16:17:17.91	-58:48:08.07	2015-05-20	900	115	1.414 ± 0.001	bzq	Pm,A,w,X
3FGL J1637.6-3449	NVSS J163750-344915	16:37:50.99	-34:49:15.40	2015-05-19	300	62	?	bzb	N,A,X
3FGL J1656.8-2010	J165655.14-201056.2	16:56:55.15	-20:10:56.30	2015-05-21	1800	43	?	bzb	w,X
3FGL J1955.0-1605	J195500.65-160338.4	19:55:00.66	-16:03:38.41	2015-05-19	1200	65	≥ 0.630	bzb	w,N,6,g,X
3FGL J2024.4-0848	J202429.37-084804.6	20:24:29.37	-08:48:04.66	2015-05-19	1800	43	?	bzb	N,w,6,g,X
2FGL J1922.6-7454	J192243.02-745349.5	19:22:43.02	-74:53:49.60	2015-08-26	600	31	?	bzb	S,w,X
Known Blazars									
3FGL J0814.1-1012	J081411.69-101210.2	08:14:11.69	-10:12:10.25	2014-12-18	600	93	?	bzb	N,A,6,w,x

Column description: (1) 3FGL name; (2) Associated counterpart; (3) R.A. (Equinox J200); (4) Dec. (Equinox J200); (5) Observation date; (6) Exposure time; (7) Signal-to-noise ratio; (8) redshift, question marks indicate unknown z; (9) Source classification; (10) Multifrequency notes: V, VLA Low-frequency Sky Survey Discrete Source Catalog (VLSS) (Cohen et al. 2007); Pm, Parkes-MIT-NRAO Surveys (PMN) (Wright et al., 1994); T , Texas Survey of Radio Sources (TEXAS) (Douglas et al. 1996); c, Combined Radio All-Sky Targeted Eight-GHz Survey (CRATES) (Healey et al. 2007); N, NRAO VLA Sky Survey (NVSS) (Condon et al. 1998); F, VLA Faint Images of The Radio Sky at 20 cm (FIRST) (Becker et al. 1995); w, WISE all-sky survey in the Allwise Source catalog Two (WISE) (Wright et al., 2010); M, Two Micron All Sky Survey (2MASS) (Skrutskie et al. 2006); s, Sloan Digital Sky Survey Data Release 9 (SDSS DR9) (Ahn et al. 2012); 6, Six-degree-field Galaxy Redshift Survey (6dFGS) (Jones et al. 2004; Jones et al.2009); g, GALaxy Evolution eXplorer All-Sky Survey Source Catalog (GALEX) (Seibert et al. 2012); X, ROSAT Bright Source Catalog ROSAT (RBSC) (Voges et al. 1999); X, ROSAT Faint Source Catalog (RFSC) (Voges et al. 2000); x, XMM-Newton Slew Survey (XMMSL) (Saxton et al. 2008; Warwick et al. 2012); x, Deep *Swift* X-Ray Telescope Point Source Catalog (1SXPS) (Evans et al. 2014); x, Chandra Source Catalog (CSC) (Evans et al. 2010).

Table 3.2: Observing Log and Summary of Results

Fermi Name	Name	R.A. (J2000) hh:mm:ss	Dec. (J2000) dd:mm:ss	WISE Counterpart	Obs. Date yyy-mm-dd	Telescope	S/N	Exp. Time (s)	z	Class
BCUs										
FL8Y J1046.1+5449	CRATES J104630+544953	10:46:28.80	+54:49:44.39	J104628.24+544944.8	2018-04-16	OAGH	4	1800	0.249	BZB
FL8Y J1129.4+3033	WISE J112937.30+303634.4	11:29:37.30	+30:36:34.45	J112937.30+303634.4	2018-04-14	OAGH	6	1800	?	BZB
FL8Y J1157.5+1639	VCS J1157+1638	11:57:34.84	+16:38:59.65	J115734.83+163859.6	2018-04-14	OAGH	16	1800	1.058	BZQ
FL8Y J1231.1+3711	RFC J1231+3711	12:31:24.10	+37:11:02.04	J123124.08+371102.2	2018-04-14	OAGH	5	1800	0.219	BZB
FL8Y J1319.5-0046	AT20G J131938-004939	13:19:38.84	-00:49:39.29	J131938.76-004939.9	2018-04-16	OAGH	24	1800	0.890	BZQ
FL8Y J1329.4-0530	Q 1326-0516	13:29:28.61	-05:31:36.12	J132928.62-053135.7	2018-04-16	OAGH	61	1200	0.575	BZQ
FL8Y J1331.7-0647	WISE J133146.84-064633.1	13:31:46.85	-06:46:33.17	J133146.84-064633.1	2018-04-01	OAGH	9	1800	?	BZB
FL8Y J1541.7+1413	RFC J1541+1414	15:41:50.10	+14:14:37.58	J154150.09+141437.6	2018-04-16	OAGH	9	1200	?	BZB
FL8Y J1559.8-2525	NVSS J160005-252439	16:00:05.40	-25:24:39.46	J160005.35-252439.7	2018-05-31	SOAR	4	900	?	BZB
FL8Y J1808.9+3522	RFC J1808+3520	18:08:49.69	+35:20:42.68	J180849.69+352042.7	2018-04-16	OAGH	18	1200	0.142	BZB
FL8Y J2048.6-6804	PKS 2043-682	20:48:23.83	-68:04:51.70	J204823.99-680451.9	2018-05-31	SOAR	14	800	?	BZB
FL8Y J2103.8-6233	PMN J2103-6232	21:03:38.39	-62:32:25.92	J210338.38-623225.8	2018-05-31	SOAR	22	400	?	BZB
3FGL J2212.3-7039	PMN J2211-7039	22:11:56.23	-70:39:14.82	J221156.23-703914.8	2018-05-31	SOAR	5	800	?	BZB
UGSs										
FL8Y J0024.1+2401	J002406.10+240438.3	00:24:06.10	+24:04:38.39	J002406.10+240438.6	2015-09-21	SDSS	9	3600	?	BZB
FL8Y J0112.1-0320	J011205.78-031753.6	01:12:05.79	-03:17:53.63	J011205.78-031753.7	2014-11-19	SDSS	5	7201	?	BZB
FL8Y J0829.7+5106	J082948.08+510827.9	08:29:48.08	+51:08:27.96	J082948.08+510827.6	2010-01-13	SDSS	17	3601	?	BZB
FL8Y J1113.9+1527	J111346.03+152842.9	11:13:46.03	+15:28:42.96	J111345.94+152843.9	2005-01-09	SDSS	5	3300	0.2589	BZB
FL8Y J1113.8+5524	J111356.3+552255.8	11:13:56.31	+55:22:55.85	J111356.24+552255.3	2014-01-02	SDSS	25	4500	?	BZB
FL8Y J1137.2+0534	J113737.76+053016.5	11:37:37.77	+05:30:16.56	J113737.76+053016.5	2012-01-20	SDSS	16	5405	?	BZB
FL8Y J1243.6+1727	J124351.76+172644.3	12:43:51.76	+17:26:44.34	J124351.76+172644.4	2012-06-12	SDSS	12	2702	?	BZB
FL8Y J1258.4+6552	J125733.06+655100.2	12:57:33.07	+65:51:00.25	J125733.04+655059.9	2014-03-08	SDSS	19	4500	?	BZB
FL8Y J1503.3+1651	J150316.57+165117.7	15:03:16.58	+16:51:17.78	J150316.56+165117.6	2012-04-22	SDSS	13	2702	≥ 0.972	BZB
FL8Y J1511.4+0549	J151100.45+054920.8	15:11:00.45	+05:49:20.82	J151100.44+054920.5	2011-04-01	SDSS	8	5405	?	BZB
FL8Y J1516.3+4353	J151631.37+434949.5	15:16:31.37	+43:49:49.58	J151631.37+434949.7	2012-05-25	SDSS	12	3603	?	BZB
FL8Y J1544.9+3218	J154433.19+322149.1	15:44:33.19	+32:21:49.14	J154433.19+322148.6	2011-07-05	SDSS	27	3603	?	BZB
FL8Y J1721.3+2529	J172100.07+251249.7	17:21:00.08	+25:12:49.79	J172100.05+251249.7	2011-05-28	SDSS	13	7207	?	BZB
FL8Y J2207.1+2222	J220652.9+221722.2	22:06:52.90	+22:17:22.20		2014-10-24	SDSS	4	4500	?	BZB
FL8Y J2207.1+2222	J220704.10+222231.4	22:07:04.11	+22:22:31.40	J220704.11+222231.5	2014-10-25	SDSS	11	4500	?	BZB
FL8Y J2228.5+2211	J222839.49+221125	22:28:39.49	+22:11:25.01	J222839.49+221125.0	2014-10-30	SDSS	17	4500	?	BZB
FL8Y J2236.9+1840	J223704.78+184055.9	22:37:04.78	+18:40:55.99	J223704.83+184055.5	2015-06-22	SDSS	10	4500	0.724?	BZB
FL8Y J2244.6+2502	J224436.7+250342.6	22:44:36.70	+25:03:42.62	J224436.66+250343.1	2015-10-14	SDSS	28	5401	?	BZB

Column description: (1) *Fermi*-LAT 8-year Source List Name; (2) Associated counterpart; (3) R.A. (Equinox J200); (4) Dec. (Equinox J200); (5) WISE counterpart; (6) Observation date; (7) Telescope; (8) Signal-to-noise ratio; (9) Exposure time; (10) Redshift, question marks indicate unknown z; (11) Source classification.

Table 3.4: Summary of the new optical spectra analyzed and presented here.

4FGL name	4FGL class	4FGL counterpart	WISE name	R.A. (J2000)	Dec. (J2000)	Facility	Obs. Date dd/mm/yy	Exposure (sec)
J0836.9+5833	bcu	NVSS J083705+583151	J083706.00+583152.9	08:37:06.01	+58:31:52.931	SDSS DR15	–	–
J0914.8+5846	bll	SDSS J091451.54+584438.1	J091451.57+584438.1	09:14:51.58	+58:44:38.111	SDSS DR15	–	–
J1019.3+5625	ugs		J101919.15+562428.8	10:19:19.16	+56:24:28.818	SDSS DR15	–	–
J1035.6+4409	bll	7C 1032+4424	J103532.12+440931.4	10:35:32.13	+44:09:31.481	SDSS DR15	–	–
J1226.0+5622	bll	SDSS J122602.81+562254.6	J122602.82+562254.9	12:26:02.83	+56:22:54.920	SDSS DR15	–	–
J1238.1-4541	bcu	PMN J1238-4541	J123806.03-454129.6	12:38:06.04	-45:41:29.640	Blanco	12/06/2019	2x600
J1403.4+4319	bll	NVSS J140319+432018	J140319.46+432020.1	14:03:19.46	+43:20:20.121	SDSS DR15	–	–
J1454.7+5237	bll	87GB 145311.3+524904	J145445.32+523655.4	14:54:45.32	+52:36:55.475	SDSS DR15	–	–
J1459.5+1527	fsrq	MG1 J145921+1526	J145922.16+152654.9	14:59:22.17	+15:26:54.907	OAN	03/07/2019	3x600
J1545.0-6642	ugs		J154458.88-664146.9	15:44:58.89	-66:41:46.925	Blanco	12/06/2019	3x600
J1545.8-2336	bcu	J1545-2339	J154546.58-233928.4	15:45:46.59	-23:39:28.418	Blanco	12/06/2019	2x600
J1600.3-5811	bcu	MRC 1556-580	J160012.36-581102.8	16:00:12.37	-58:11:02.851	Blanco	12/06/2019	3x400
J1637.5+3005	ugs		J163738.24+300506.4	16:37:38.24	+30:05:06.475	OAN	04/07/2019	3x900
J1640.9+1143	bcu	TXS 1638+118	J164058.89+114404.2	16:40:58.90	+11:44:04.226	OAN	05/07/2019	2x1200
J1647.1+6149	bcu	RX J1647.3+6153	J164723.42+615347.5	16:47:23.42	+61:53:47.582	OAN	03/07/2019	3x900
J1704.5-0527	bll	NVSS J170433-052839	J170433.83-052840.7	17:04:33.84	-05:28:40.788	Blanco	12/06/2019	2x1200
J1705.4+5436	bcu	NVSS J170520+543700	J170520.54+543659.8	17:05:20.55	+54:36:59.842	OAN	06/07/2019	3x900
J1706.8+3004	bcu	87GB 170454.3+300758	J170650.43+300412.5	17:06:50.44	+30:04:12.594	SDSS DR15	–	–
J1744.4+1851	bcu	1RXS J174420.1+185215	J174419.81+185217.9	17:44:19.81	+18:52:17.978	OAN	07/07/2018	3x900
J1810.7+5335	bcu	2MASS J18103800+5335016	J181037.98+533501.5	18:10:37.99	+53:35:01.531	OAN	07/07/2019	3x900
J1814.0+3828	bcu	2MASS J18140339+3828107	J181403.43+382810.1	18:14:03.44	+38:28:10.156	OAN	06/07/2019	3x900
J1838.4-6023	bcu	2MASS J18382063-6025224	J183820.63-602522.6	18:38:20.64	-60:25:22.602	Blanco	12/06/2019	3x300
J1858.3+4321	bcu	NVSS J185813+432452	J185813.43+432451.9	18:58:13.43	+43:24:51.938	OAN	04/08/2018	3x1200
J1929.4+6146	bcu	TXS 1928+616	J192935.09+614629.4	19:29:35.10	+61:46:29.425	OAN	07/07/2019	3x1200
J2043.7+0000	bcu	2MASS J20435020+0001280	J204350.15+000127.8	20:43:50.16	+00:01:27.885	OAN	02/07/2019	3x1200
J2046.8-4258	bcu	MRSS 285-029065	J204644.01-425713.2	20:46:44.01	-42:57:13.236	Blanco	12/06/2019	2x400
J2115.2+1218	bcu	NVSS J211522+121802	J211522.00+121802.6	21:15:22.00	+12:18:02.660	OAN	04/07/2019	3x900
J2141.4+2947	bcu	87GB 213913.0+293303	J214123.89+294706.2	21:41:23.90	+29:47:06.286	OAN	05/07/2019	3x900
J2208.2+0350	bll	SDSS J220812.70+035304.6	J220812.70+035304.5	22:08:12.70	+03:53:04.537	OAN	06/07/2019	3x900
J2235.3+1818	bcu	2MASS J22352860+1816356	J223528.60+181635.5	22:35:28.61	+18:16:35.550	OAN	07/07/2019	3x900

Note: col. (1) 4FGL name; (2) *Fermi*-LAT class as listed in 4FGL; (3) assigned counterpart in the 4FGL with the exceptions of UGSs; (4) pointed WISE counterpart; (5) right ascension and (6) declination of the WISE target; (7) telescope used to carry out the spectroscopic observation or queried survey; (8) observing dates and (9) exposure times in seconds.

Table 3.5: Summary of the new optical spectra analyzed and presented here.

4FGL name	WISE name	Class	z	Line ID	EW (Å)	Ca break (Å)	λ_{obs} (Å)	Type
J1035.6+4409	J103532.12+440931.4	bzg	0.4438	[O II]	10	0.25	5380	E
				H	6		5730	A
				K	7		5680	A
J1459.5+1527	J145922.16+152654.9	bzb	0.3711	[O II]	5	0.06	5110	E
				H	3		5441	A
				K	3		5391	A
J1545.8-2336	J154546.58-233928.4	bzb	0.1204	Mg I	6	–	5800	A
				Na I	4		6602	A
J1637.5+3005	J163738.24+300506.4	bzb	0.0786	[O II]	10	0.25	4019	E
				K	5		4243	A
				H	8		4280	A
				G	6		4644	A
				[O III]	3		5401	E
				Mg I	3		5581	A
J1640.9+1143	J164058.89+114404.2	bzg	0.0799	K	8	0.35	4248	A
				H	6		4285	A
				G	5		4649	A
				Hβ	3		5250	A
				Mg I	13		5586	A
				Na I	10		6365	A
J1647.1+6149	J164723.42+615347.5	bzb	0.347	K	3	0.11	5298	A
				H	4		5349	A
				G	5		5798	A
J1814.0+3828	J181403.43+382810.1	bzb	0.2754	K	6	0.23	5017	A
				H	5		5059	A
				G	5		5492	A
J1838.4-6023	J183820.63-602522.6	bzb	0.120	Hβ	3	–	5447	A
				Mg I	4		5795	A
				Na I	3		6602	A
J1858.3+4321	J185813.43+432451.9	bzg	0.1356	[O II]	5	0.26	4233	E
				K	3		4468	A
				H	3		4506	A
				G	6		4888	A
				Na I	4		6692	A
J1929.4+6146	J192935.09+614629.4	bzb	0.2117	[O II]	1	0.17	4516	E
				K	5		4767	A
				H	4		4808	A
				G	5		5215	A
				Mg I	3		6271	A
J2115.2+1218	J211522.00+121802.6	bzb	>0.498	Mg II	2	–	4188	A
				Mg II	4		4199	A

Note: col. (1) 4FGL name; (2) pointed WISE counterpart; (3) the classification provided by our analysis and based on collected spectra; (4) a redshift estimate only for sources showing emission/absorption lines; (5) emission/absorption line identified; (6) correspondent equivalent width (EW); (7) Ca II break intensity; (8) observed wavelength of the emission/absorption line listed in col. (5); (9) type of spectral feature/line: E = emission while A = absorption.

Table 3.6: γ-ray classification of targets observed during our spectroscopic campaign as reported in each *Fermi*-LAT catalog.

Fermi-LAT class	1FGL	2FGL	3FGL	4FGL	FL8Y
BZB/BLL	32	55	80	212	1
BZQ/FSRQ	5	10	10	36	0
AGN/AGU/BCU	10	76	139	86	10
UGS /UNK	58	52	57	13	15
Total	105	193	286	350*	26

Note: col. (1) lists the *Fermi*-LAT class, in particular BZB and BZQ were mainly used for 1FGL and 2FGL together with AGU classification, then they were removed in the latest releases of the *Fermi*-LAT catalogs. The UNK class for sources with unknown nature that were all counted together with UGSs in our summary; col. (2,3,4,5) the number of sources classified according to col. (1) listed in each *Fermi*-LAT catalog.
(*) The total number of 4FGL sources is 350 instead of 347 since we observed three targets lying within the positional uncertain regions of three sources associated to one pulsar and two radio galaxies. Results of our campaign confirmed the 4FGL classification and in particular for the pulsar we only found a quasar within its γ-ray positional uncertainty ellipse.

Table 3.7: Fractions of *Fermi*-LAT sources with uncertain nature (i.e., AGUs, BCUs and UGSs) analyzed during our campaign and computed with respect to the total number in each *Fermi*-LAT catalog.

Fermi-LAT class	1FGL	2FGL	3FGL	4FGL
AGN/AGU/BCU	0.08	0.27	0.24	0.06
UGS/UNK	0.09	0.09	0.06	0.01

Note: col. (1) lists the *Fermi*-LAT class, in particular AGU classification was used only in 1FGL and 2FGL being then replace by the BCUs since the release of the 3FGL. The class UNK for sources with unknown nature that were all counted together with UGSs in our summary; col. (2,3,4,5) report the fraction of sources in each class computed over the whole number of sources belonging to that class listed in each *Fermi*-LAT catalog.

Table 3.8: Classification results achieved thanks to our optical spectroscopic campaign split with respect to sources listed in each *Fermi*-LAT catalog.

Fermi-LAT class	BZB	BZQ	BZG
in 1FGL			
BZB	32(1)	-	-
BZQ	1	4	-
AGN/AGU	7(1)	1	2
UGS	48(2)	2[+5]	3
in 2FGL			
BZB	54(3)	-	1
BZQ	3	7	-
AGN/AGU	54(6)	13[+2]	7
UGS	36(4)	3[+12]	1
in 3FGL			
BLL	79(3)	-	1
FSRQ	-	9[+1]	-
AGN/BCU	103(20)	14[+7]	15
UGS	40(5)	4[+12]	1
in 4FGL			
BLL	193(18)	1	18
FSRQ	2(2)	30[+4]	-
AGN/BCU	66(23)	1[+10]	9
UGS/UNK	8(1)	-[+5]	-
in FL8Y			
BLL	1	-	-
FSRQ	-	-	-
AGN/BCU	6(5)	3	1
UGS	15(3)	-	-

Note: col. (1) lists the *Fermi*-LAT class according to labels reported in each *Fermi*-LAT catalog; col. (2,3,4) indicates the number of BZBs, BZQs and BZGs classified thanks to our observations, respectively. Number in parenthesis for col. (2) corresponding to BZB classification indicates those BL Lacs having a firm z estimate, while that in col. (3) for BZQs indicate additional sources classified as quasars for which information about their radio spectral shape were not found.

Table 3.9: γ-ray classification of sources analyzed in the literature as reported in each *Fermi*-LAT catalog.

Fermi-LAT class	1FGL	2FGL	3FGL	4FGL
BZB/BLL	9	11	14	53
BZQ/FSRQ	1	-	-	5
AGN/AGU/BCU	6	23	58	53
UGS/UNK	22	25	51	7
Total	38	60*	123	118

Note: col. (1) lists the *Fermi*-LAT class, in particular BZBs and BZQs were mainly used for 1FGL and 2FGL together with AGU classification, then they were removed in the latest releases of the *Fermi*-LAT catalogs where it was introduce the class UNK for sources with unknown nature that were all counted together with UGSs in our summary; col. (2,3,4,5,6) the number of sources classified according to col. (1) listed in each *Fermi*-LAT catalog. (*) in the 2FGL the total number of sources is 60 instead of 59 since in the literature we found that one 2FGL source classified as pulsar later classified as BCU in both the 3FGL and the 4FGL.

Table 3.10: Classification results collected from the literature distinguishing sources belonging to each *Fermi*-LAT catalog.

Fermi-LAT class	BZB	BZQ	BZG
in 1FGL			
BZB	9(3)	-	-
BZQ	-	-[+1]	-
AGN/AGU	6(2)	-	-
UGS	22(5)	-	-
in 2FGL			
BZB	11(4)	-	-
BZQ	-	-	-
AGN/AGU	19(3)	3	1
UGS	23(8)	1[+1]	-
in 3FGL			
BLL	14(4)	-	-
FSRQ	-	-	-
AGU/BCU	53(8)	4	1
UGS	50(22)	-[+1]	-
in 4FGL			
BLL	53(15)	-	-
FSRQ	4(1)	1	-
AGU/BCU	49(15)	3	1
UGS/UNK	6(1)	-[+1]	-

Note: col. (1) lists the *Fermi*-LAT class according to labels reported in each *Fermi*-LAT catalog; col. (2,3,4) indicates the number of BZBs, BZQs and BZGs classified as in literature, respectively. Number in parenthesis for col. (2) corresponding to BZB classification indicates those BL Lacs having a firm z estimate, while that in col. (3) for BZQs indicate additional sources classified as quasars for which information about their radio spectral shape were not found.

Table 3.11: Comparison between the expected classification provided in WIBRaLS2 catalog with that obtained with our optical spectroscopic campaign.

WIBRALS Type	BZB	BZQ	BZG	Total
WBZB	5	-	-	5
	32	-	1	33
	78	3	4	85
	46	- [+2]	7	55
WBZQ	-	- [+1]	-	1
	1	5 [+1]	-	7
	1	6 [+1]	-	8
	-	5 [+1]	-	6
MIXED	-	-	-	-
	4	- [+1]	-	5
	4	2 [+1]	-	7
	-	-	-	-

Note: col. (1) indicates the class/type as listed in the WIBRaLS2 catalog; col.; col. (2,3,4) classification results provided by our optical spectroscopic observations (nomenclature is the same adopted in Table 3.10); col. (5) total number of sources observed for each type and subclass.

Table 3.12: Comparison between the expected classification provided in WIBRaLS2 catalog with that obtained from our literature search.

WIBRALS Type	BZB	BZQ	Total
WBZB	0	-	1
	6	-	6
	10	-	10
	13	-	12
WBZQ	1	-	1
	3	-	3
	1	-	1
	1	-	1
MIXED	-	-	-
	1	-	1
	1	1	2
	-	-	-

Note: col. (1) indicates the class/type as listed in the WIBRaLS2 catalog; col. (2,3,4) classification results found during our literature search (nomenclature is the same adopted in Table 3.10); col. (5) total number of sources observed for each type and subclass.

Chapter 4

The 1st release of the Turin-SyCAT: a multifrequency catalog of Seyfert galaxies

In this chapter, I describe all catalogs and samples of Seyfert galaxies used to carry out Seyfert galaxies' original selection included in the Turin-SyCAT, together with all selection criteria adopted. Section 4.3 is then devoted to the catalog description and cross-matches with multifrequency databases. Results on the characterization of the Seyfert galaxy population achieved thanks to the 1^{st} release are then presented in Section 4.4. Finally, I dedicate Section 5.5 to our summary, conclusions, and future perspectives. I report then all tables in Appendix C as well as in the published papers.

4.1 Introducing the Turin-SyCAT

In the literature, several catalogs or samples of Seyfert galaxies already exists. One of the most statistically robust sample, selected on the basis of homogeneous criteria, is certainly the one based on the Palomar spectroscopic survey of nearby galaxies (Ho et al., 1997, 2003), but unfortunately is listed only 52 Seyfert galaxies. Other Seyfert galaxy catalogs/samples present in the literature are: (1) that of Lipovetskij et al. (1987); Lipovetsky et al. (1988), composed of 959 sources, most of the Seyfert known at that time, selected via the UV excess method drawn by the First Byurakan Survey (Markarian et al., 1989); (2) the 49 Seyfert galaxies selected out of the CfA spectroscopic survey (Huchra & Burg, 1992); (3) Seyfert galaxies selected using far-IR colors (de Grijp et al., 1992) or (4) those listed in the Maiolino & Rieke (1995) sample based on the Revised Shapley-Ames catalog (Sandage & Tammann, 1987); (5) Seyfert galaxies present in the BASS survey (Koss et al., 2017); (6) more than 16000 Seyfert galaxies listed in the catalog of quasars and active nuclei of Veron-Cetty & Veron (1989); Véron-Cetty & Véron (2006, 2010) compiled including those AGN lists collected from an extensive literature search based on surveys as 2dF/2QZ (Croom et al., 2004), SDSS DR-3 (Fukugita et al., 1996; Abazajian et al., 2005), as well as compact radio sources in the ICRF2 (Fey et al., 2015), VLBA (Beasley et al., 2002; Fomalont et al., 2003), the large quasar astrometric catalog (Souchay et al., 2009) and

X-ray discovered AGNs (Treister et al., 2005).

However, all these catalogs/samples are characterized either by having a relatively small number of sources (i.e., including less than 100 objects) and/or being highly contaminated by different AGN classes as radio galaxies or quasars. Nevertheless, in many cases, sources listed in these samples lack optical spectroscopic redshifts, and Seyfert classification is not based on multifrequency criteria. Thus, trying to tackle and solve some of these problems and to obtain a precise characterization of the whole Seyfert population, we present here the 1^{st} release of a homogeneous and statistically "clean" (i.e., with accurate selection) Seyfert catalog: the Turin-SyCAT. This multi-frequency catalog, with information mainly gathered from radio, optical, infrared, and X-ray surveys, will permit to investigate (i) on trends or correlations between different parameters/observed quantities and (ii) study the large scale environment of Seyfert galaxies.

4.2 Be or not to be a Seyfert galaxy: multifrequency selection criteria

We selected Seyfert galaxies for this 1^{st} release of the Turin-SyCAT out of the following five main surveys and/or catalogs.

- The 3^{rd} release of the Palermo BAT source catalog (hereinafter 3PBC)[1], including all hard X-ray sources detected by the BAT instrument on board of the SWIFT satellite within the first 66 months of mission (see e.g., Segreto et al., 2010; Cusumano et al., 2010).

- The BAT 105 months survey (hereinafter BAT105)[2] carried out again using the data collected by the BAT instrument but reduced with a different procedure with respect to that of the 3PBC and by a different group (Oh et al., 2018).

- The Seyfert Catalog[3] created by Lipovetskij et al. (1987) (hereinafter LipCAT).

- The 13^{th} edition of the VeronCAT (Véron-Cetty & Véron, 2010).

- All objects associated with a hard X-ray source and classified as Seyfert galaxy that has been observed during the optical spectroscopic campaign targeting low energy counterparts of both SWIFT-BAT and INTEGRAL unidentified sources (see e.g., Masetti et al., 2004, 2006, 2010).

[1] http://bat.ifc.inaf.it/bat_catalog_web/66m_bat_catalog.html
[2] https://swift.gsfc.nasa.gov/results/bs105mon/
[3] http://vizier.u-strasbg.fr/viz-bin/VizieR?-source=VII/173

4.2.1 Initial selection

The main goal is to create a statistically clean and homogeneous catalog of Seyfert galaxies, to investigate their multifrequency behavior using a sample having a negligible fraction of contaminants. Thus, we adopted the following minimum requirements to include a source in the Turin-SyCAT.

We inspected all sources belonging to samples previously listed, and we included only those selected according to the following criteria:

1. A literature paper where it is possible to verify its published optical spectrum. This is to guarantee its classification, at least distinguishing between type 1 and type 2 Seyfert galaxies and firm redshift estimate. The reference for the spectrum inspected to check both redshift and classification is reported in Appendix.

2. Radio luminosity lower than 10^{40} erg s^{-1} whenever has a radio counterpart belonging to one of the major radio surveys, namely: NVSS, FIRST and SUMSS.

3. A mid-IR counterpart listed in the AllWISE Source catalog.

4. The ratio between $L_{3.4\mu m}$ and 10^{11} $L_{\odot}$ is lower than 100 to guarantee we are not selecting nearby quasars since this ratio implies that the mid-IR emission is of the same order of the stellar population of the host galaxy[4].

Each step of the selection process is also summarized in the flow chart available in Figure 4.1.

We remark that to extract Seyfert galaxies from the SWIFT-BAT based catalogs, we searched for optical spectral images in the literature, while for the LipCAT and the VeronCAT we restricted our search to the SDSS footprint and used its database to collect spectral images uniformly.

The angular separation adopted to search for a radio counterpart in these major surveys are 11″, 4″, and 8″for the NVSS, FIRST, and SUMSS, respectively. Previous analyses indicate that the probability of spurious associations at these angular separations is almost negligible (see, e.g., D'Abrusco et al., 2012, 2019). If the source does not have a potential radio counterpart within the angular separation previously mentioned we assumed its radio power being within our threshold since a flux density of 100 mJy at 1.4 GHz from a source lying at redshift 0.5 is $\sim 10^{39}$ erg s^{-1}, all our sources have $z < 0.5$.

Then, we chose an angular separation of 3.″3, statistically derived and successfully adopted in our previous analyses (Massaro et al., 2012b; D'Abrusco et al., 2013; Massaro et al., 2015c) for all crossmatches between WISE coordinates and the position in the original catalog/survey. This corresponds to a chance of spurious associations

[4]We are aware of the fact that such ratio should have been evaluated using optical magnitudes, but they are not available uniformly as the mid-IR ones for all sources listed in the Turin-SyCAT.

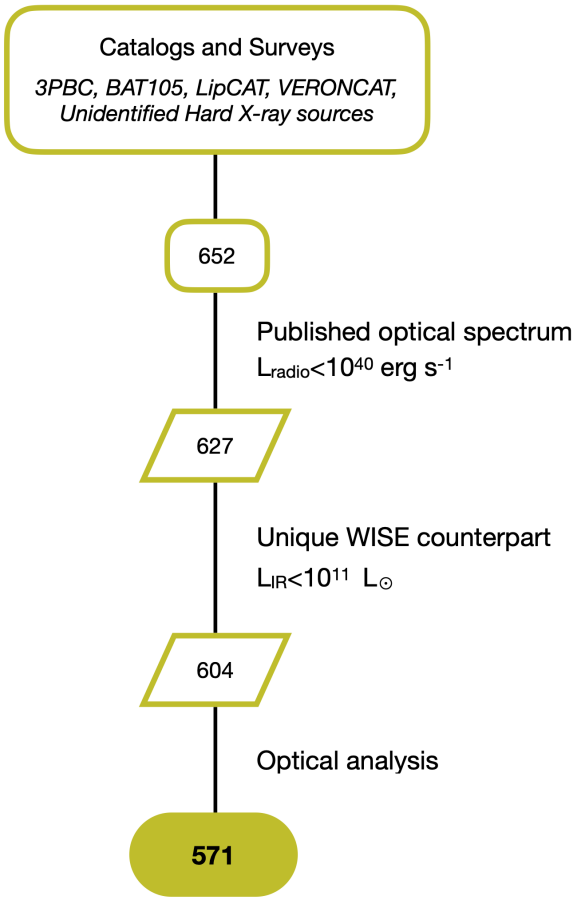

Figure 4.1: The flow chart highlighting all steps and thresholds applied to select the final sample of Seyfert galaxies belonging to the 1^{st} release of the Turin-SyCAT.

lower than 1% (Massaro et al., 2011; Massaro et al., 2013). This crossmatch allows us to assign to all Seyfert galaxies coordinates of their mid-IR counterparts so to have their positions uniformly estimated. Hereinafter WISE coordinates will be used for all other crossmatches.

All numbers related to the initial sample of Seyfert galaxies extracted from each starting catalog are summarized in Table 4.1 and described as follows.

- The 3PBC lists a total of 1593 hard X-ray sources with 534 unidentified sources and having 356 of those associated with a low energy counterpart classified as Seyfert 1 and 164 as Seyfert 2. When inspecting this catalog, we only extracted a total of 222 Seyfert galaxies that met our criteria.

- The BAT105 catalog includes a total of 1632 BAT detected sources, whereas those with an unknown nature are only 243. It lists 379 Sources classified as Seyfert 1 and 448 as type 2. Out of this catalog, we only selected a total of 73 Seyfert galaxies that were also not included in the previous sample.

- Inspecting the Seyfert Catalog created by Lipovetskij et al. (1987) we restricted its original list only to those sources lying in the SDSS footprint to (i) have the chance to verify our radio luminosity criterion immediately, since the SDSS has the same footprint of the FIRST, and (ii) have a good probability of getting the image of the optical spectrum available in the archive without the necessity of searching it in the literature as carried out for the previous samples. This catalog lists a total of 959 Seyfert galaxies were only 321 where in the SDSS footprint and out of which we selected 70 Seyfert galaxies matching our criteria, previously highlighted. Again none of the selected Seyfert was included in previous selections.

- We also adopted a similar cut for extracting Seyfert galaxies out of the VERONCAT. This catalogs list a total of 168941 sources where 17389 are classified as Seyfert 1 galaxies and 6186 as type 2 in addition to other sources listed as Seyfert but lacking a firm classification that we did not consider. As previously carried out, to increase the chance of finding the image of the spectrum we restricted our search to VERONCAT Seyferts in the SDSS footprint, and we only looked those associated with a ROSAT counterpart lacking a radio counterpart in the FIRST within an angular separation of $5''$ for a total of 369 targets. The number of Seyferts extracted from this catalog, including all cuts, is 158.

- We then searched for Seyfert galaxies out of the sample of unidentified hard X-ray sources in both the SWIFT-BAT and the INTEGRAL catalog that have been targets of the optical spectroscopic campaign carried out in the last decade (see also Masetti et al., 2012, 2013). In their samples, we were able to find an additional 80 Seyfert galaxies. These samples are less homogeneous than the previous ones, but follow up spectroscopic observations complement the selection based on the 3PBC and the BAT105, thus motivating our choice of including them.

We remark that for each sample listed above, with the only exception of the last one, the number of selected Seyfert galaxies is significantly lower than the original one. The main reasons of this discrepancy are due to the fact that (i) we are classifying as Seyfert galaxies only those sources with radio power lower than 10^{40} erg s^{-1}, thus applying a multifrequency criterion and (ii) we found a significant number of sources lacking a published optical spectrum for which we could not verify the z estimate and its proper classification. We noticed that the Seyfert classification adopted, for example, in the SWIFT-BAT catalogs, both 3PBC and BAT105, is often misleading since it is based only on the optical properties of the hard X-ray counterpart; there are many radio galaxies, even belonging to the Third Cambridge Catalog (3C; Edge et al., 1959) or the Fourth Cambridge catalog (4C; Gower et al., 1967; Pilkington & Scott, 1965) erroneously classified as Seyferts but for which the whole multifrequency behavior is completely different.

The total number of Seyfert galaxies selected out the previous surveys/samples and according to the radio and mid-IR properties is 603.

Table 4.1: Number of sources in the starting catalogs/samples for the initial Seyfert galaxy selection.

Catalog	Total sources	Seyfert galaxies	Targets selected
3PBC	1593	520	222
BAT105	1632	827	73
LipCAT	959	321*	70
VERONCAT	168941	23575+	158
Unidentified Hard X-ray sources	-	-	80

(*): This number of sources is limited to those lying in the SDSS footprint.
(+): this source number refers to those objects listed in the VERONCAT but lying in the SDSS footprint, with an X-ray counterpart in the RBSC and no radio counterpart in the FIRST, as described in Section 4.2.

4.2.2 Optical classification

We then provided our own optical spectroscopic classification on the basis of the following criteria, outlined by Khachikian & Weedman (1974), since optical spectra for all sources were retrieved from the literature. We selected only those sources for which at least three co-authors agree on the same Seyfert galaxy classification, so restricting our final sample to 571 objects.

Both Seyfert classes, see Figure 4.2, show the presence of narrow emission lines (widths $\sim 10^2$ km s^{-1}) in their optical spectra interpreted as due to low density (n_e $\sim 10^3$-10^6cm^{-3}) gas clouds photoionized by the central source (Koski, 1978; Ferland & Netzer, 1983; Stasińska, 1984). Broad (widths up to 10^4 km s^{-1}) lines, due to permitted transition, are visible only in Seyfert 1 where the absence of broad forbidden emission lines indicates relatively high density (i.e., $n_e > 10^9$ cm^{-3}) gas clouds.

In addition to all these optical emission lines, weak absorption features due to late-type giant stars in the host galaxy are also observed in both type 1 and type 2 Seyfert spectra; absorption lines are relatively weak because the starlight is diluted by the non-stellar "featureless continuum". Indeed, the AGN continuum is usually so weak in Seyfert 2 galaxies that it is quite difficult to isolate it from the stellar continuum unambiguously (Storchi-Bergmann et al., 1998; Contini & Viegas, 2000).

It is worth noting that narrow-line spectra are clearly distinguishable from the HII-region spectra seen in normal galaxies, as the Seyfert spectra show a wide range in ionization level, which is typical of a gas ionized by a source where the input continuum spectrum falls off slowly (relative to a Wien law) at ionizing wavelengths and on the basis of the data collected up to date it was not possible to distinguish Seyfert galaxies from low luminosity active galaxies classified as LINERs.

The final number of Seyfert galaxies listed in this 1^{st} release of the Turin-SyCAT is 571, distinguished in 412 type 1 and 159 type 2.

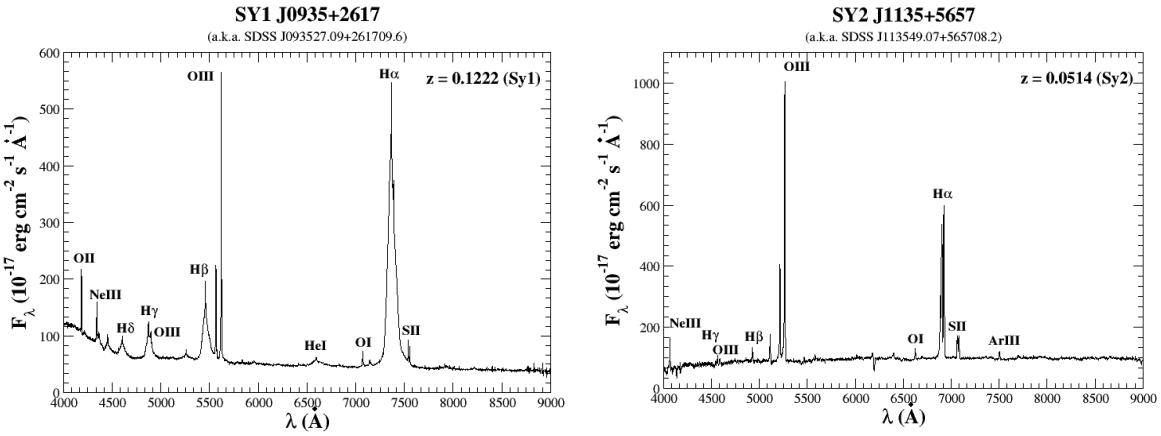

Figure 4.2: Left panel) The optical spectrum of a classical type 1 Seyfert galaxy, namely SY1 J0935+2617 (a.k.a. SDSS J093527.09+261709.6) listed in the Turin-SyCAT where broad emission lines are clearly seen in the range $4000 - 9000$ Å and marked in the figure. Right panel) Same of left panel but for a typical type 2 Seyfert galaxy, i.e. SY2 J1135+5657 (a.k.a. SDSS J113549.08+565708.2), lacking broad emission lines. The main spectral emission and/or absorption features are marked in both figures thus providing clear examples of those spectra searched in the literature to prepare the Turin-SyCAT.

4.3 The Turin-SyCAT

In the current release of the Turin-SyCAT, we only distinguished between type 1 and type 2 Seyfert galaxies since we do not have spectral data for all to refine this classification. Then we labeled all sources listed therein a prefix Sy1 or Sy2 and the coordinates in the format J0000+0000 to have a unique name to identify them. For only 24 sources out of 571, our optical classification was different from the one reported in the literature; in any case, they are reported in the catalog table available in the Appendix. We also highlight that narrow-line Seyfert 1 galaxies (Osterbrock & Pogge, 1985) were labeled in this catalog release as Sy1.

The redshift distribution of all 571 Seyferts is shown in Figure 4.4, where Seyfert galaxies classified as type 1 are shown in black stars while those classified as type 2 in yellow circles. This color code is adopted for all other figures and plots reported hereinafter. In Figure 4.3 it is quite evident the lack of type 2 Seyfert galaxies above z =0.1 as well as the fact that at $z > 0.04$ the fraction of type 2 over type 1 Seyfert drastically drops suggesting that samples and catalogs used to create the Turin-SyCAT could be incomplete. The sky distribution, computed using the Aitoff projection, of all 571 Turin-SyCAT sources is then reported in Figure 4.4 where a larger fraction of sources (378) lie in the northern hemisphere where it is to easier to get access to optical telescopes to perform source identifications (Green et al., 1986; Colless et al., 2001; Jones et al., 2004; Aguado et al., 2019).

All Seyfert galaxies in the current list are detected in all four WISE bands, with the only exception of SY1 J0629-1355 lacking a mid-IR counterpart at 22μm (i.e., in W4).

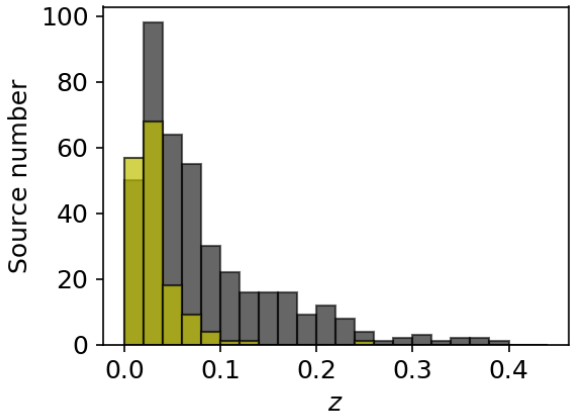

Figure 4.3: The redshift distribution of all Seyfert galaxies included in the 1^{st} release of the Turin-SyCAT. Seyfert galaxies classified as type 1 are shown in black while those classified as type 2 in yellow. It is worth noting that type 2 Seyfert are basically not selected at z >0.1 and considered samples/catalogs used to extract Turin-SyCAT could be incomplete above z ∼0.04.

In the near IR (i.e., 2MASS, automatically associated in the AllWISE catalog), we have 563 sources detected in J band, 562 in the H band, and 564 in Ks out of a total of 571. The number of Seyfert galaxies within the SDSS footprint is 259 out of 571, and all of them have a unique crossmatch within 1″, where we also considered two associations at larger angular separations, namely: SY2 J1225+1239 selected from the 3PBC having the SDSS counterpart at 1.″51 from its WISE position and SY2 J1001+5540, from the LipCAT, lying at 3.″27, respectively.

Once we obtain uniform coordinates for all sources in Turin-SyCAT thanks to their WISE counterparts we crossmatched, again, our catalog with both 3PBC and 4^{th} Fourth IBIS/ISGRI Soft Gamma-Ray Survey Catalog[5] (IBISCAT4 Bird et al., 2007) and BAT105 as well as with the ROSAT Bright and Faint Source catalog (RBSC and FRSC Voges et al., 1999, 2000, respectively).

In the hard X-ray sky, we found that 303 out of 571 Seyfert galaxies lie within the positional uncertainty of 3PBC sources as reported in the catalog, actually 120 more sources than those originally found when starting our selection from the 3PBC itself. A significant fraction of these sources were added thanks to the optical spectroscopic campaign of unidentified hard X-ray sources, while a few more were included in the Turin-SyCAT since they belong to other catalogs inspected as BAT105. To carry out these crossmatches, we adopted a conservative positional uncertainty for WISE coordinates of 1″, quite larger than that reported in the AllWISE catalog (Wright et al., 2010), but our results are not affected significantly by this choice. All matches are also unique, as expected by the low sky density of the hard X-ray sources. Then for the IBISCAT4, we found only 119 matches out of 571 Seyfert galaxies. In this case, as for the 3PBC crossmatch, we used the positional uncertainty reported in the

[5]https://heasarc.gsfc.nasa.gov/W3Browse/integral/ibiscat4.html

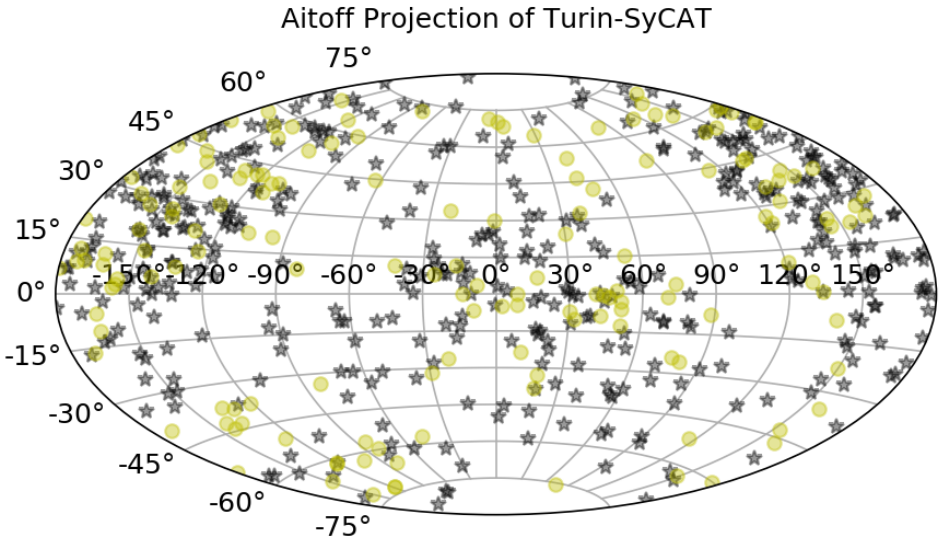

Figure 4.4: The sky distribution of all 571 Seyfert galaxies listed in the Turin-SyCAT, in the Aitoff projection.

IBISCAT4.

Crossmatching with the BAT105 we obtain 331 out of 571 unique matches, again larger number than the one previously reported due to many sources listed in the 3PBC that are also detected in BAT105 as well as many targets included in the lists of unidentified hard X-ray sources (Masetti et al., 2004, 2006, 2009, 2010, 2012, 2013). In this case, we initially performed the crossmatch using assigned counterpart coordinates, as listed in the catalog. Then we also computed all positional uncertainties adopting the formula reported in Oh et al. (2018), and we found an additional of 12 Seyfert galaxies lying within the positional error circle. For six out of 12 matches, namely: SY2 J0209-1010, SY1 J1212+0659, SY1 J1444+8600, SY2 J1606-7252, SY2 J1643+3948 and SY1 J2355+2530 the angular separation between the SYCAT source and the BAT105 assigned counterpart is larger than 30″and thus were not considered. Then five out of the remaining six were added to the previous 331 bringing the number of BAT105 unique matches to 336 out of 571, while SY1 J0919+5521 was excluded since the nearby SY2 J0919+5527 is the associated counterpart of SWIFT J0919.2+5528. It is worth noting that more than 95% of these crossmatches have an angular separation smaller than 6″, and those at larger distances were also included given the associated counterpart name listed in BAT105.

Finally, we carried out the crossmatch with the ROSAT Bright Source Catalog and the ROSAT Faint Source Catalog (Voges et al., 1999, 2000) finding that 281 Seyferts out of 571 have a soft X-ray counterpart, unique match, within the positional uncertainty reported therein for the X-ray coordinates and 1″for the AllWISE coordinates as previously considered.

4.4 Characterizing the Seyfert galaxy population

4.4.1 Infrared properties

We compared the mid-IR colors of type 1 and type 2 Seyfert galaxies listed in this 1^{st} release of the Turin-SyCAT as shown in Figure 4.5 since all selected sources have a WISE counterpart detected in all four WISE bands with only one exception (see Section 4.2 for additional details).

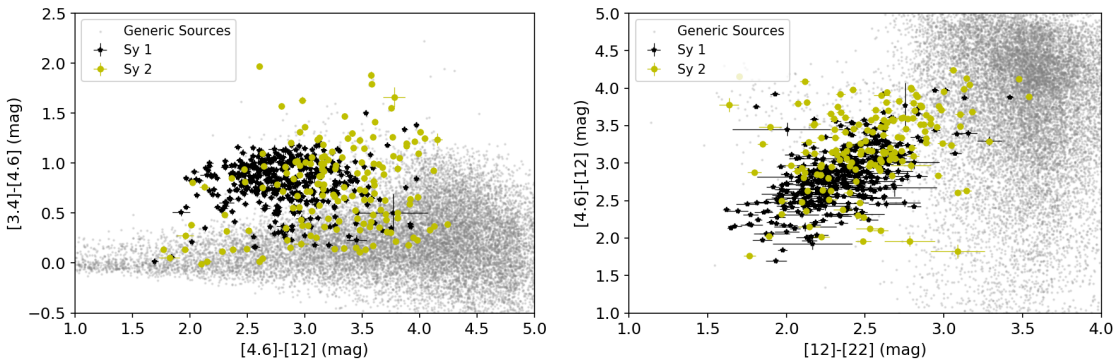

Figure 4.5: The color-color diagrams based on the WISE magnitudes comparing Seyfert galaxies of type 1 (black) and type 2 (yellow) with generic mid-IR sources selected in a random region of the sky (see Massaro et al., 2011; Massaro et al., 2013,?; Massaro et al., 2016, for a similar analysis). Seyfert galaxies of type 2 appear to be redder than those of type 1 and quite separated in the w1-w2 vs w2-w3 color-color plot in the left lower.

The distribution of the W1-W2 color appears to be more concentrated for the Seyfert galaxies of type 1, while that of type 2 covers a broader range. No neat differences are visible in both WISE color diagrams, with the only exception that overall Seyfert 2 galaxies tend to be redder than Seyfert 1. More than 90% of Seyfert 1 galaxies and ∼50% of type 2 ones have the mid-IR color $W1 - W2 > 0.5$, the same criterion used to distinguish and select AGNs from other sources (Ashby et al., 2009) while adopting a more conservative threshold (higher selection efficiency) ∼75% of Seyfert 1 galaxies and ∼40% of Seyfert 2 show $W1 - W2 > 0.8$ (Stern et al., 2012), respectively. Given the recent and extensive use of these mid-IR color-color diagrams to select γ-ray blazar-like candidates that could be potential counterpart of unidentified γ-ray sources (Massaro et al., 2012b; D'Abrusco et al., 2013; Massaro et al., 2013; Massaro & D'Abrusco, 2016) and targets of optical campaigns (Paggi et al., 2014; Massaro et al., 2014, 2015b; Landoni et al., 2015b; Álvarez Crespo et al., 2016c; Marchesini et al., 2016; Peña-Herazo et al., 2017; Paiano et al., 2017b; Marchesi et al., 2018; Marchesini et al., 2019; Paiano et al., 2019; Peña-Herazo et al., 2019) we also compare the mid-IR colors of Seyferts with those of both BL Lac objects and flat spectrum radio quasars, labeled as BZBs and BZQs respectively, listed in the latest release of Roma-BZCAT (Massaro et al., 2009, 2015a) and associated with a Fermi source in the Fourth Fermi-LAT Source catalog (Abdollahi et al., 2020). This comparison is shown in Figure 4.6,

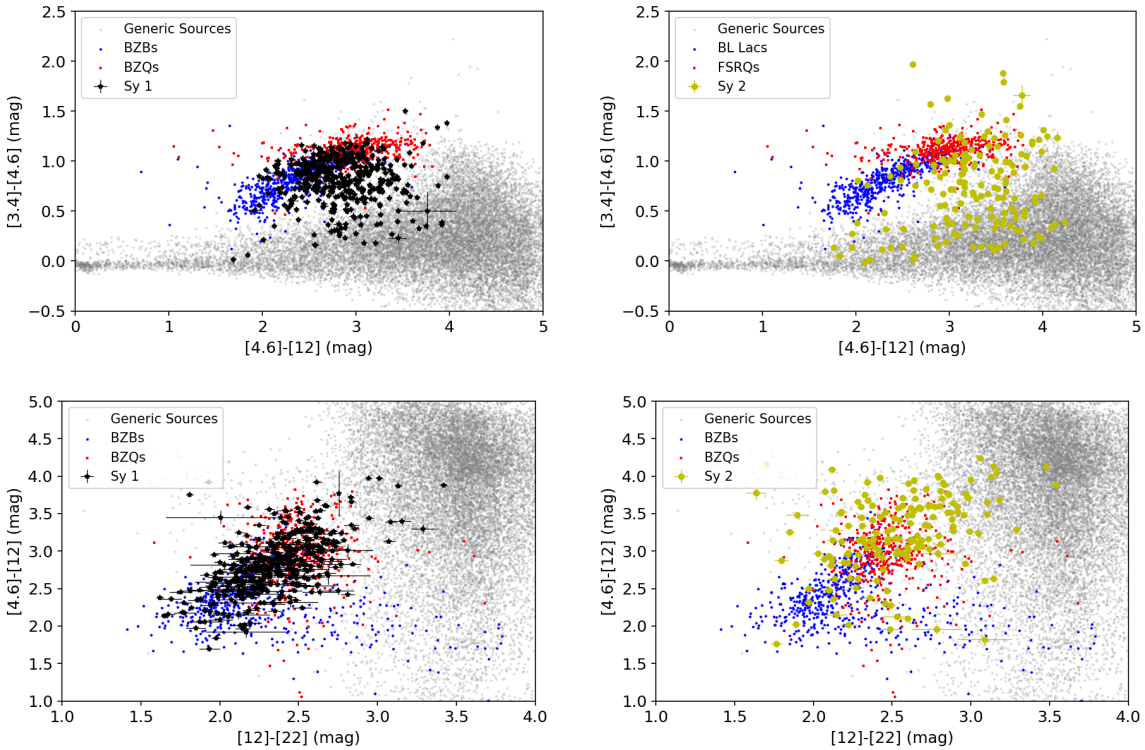

Figure 4.6: The comparison between the mid-IR colors of Seyfert galaxies listed in the Turin-SyCAT and the γ-ray blazars of the Roma-BZCAT. Seyfert 1 galaxies tend to be more similar to blazars in their mid-IR emission, in particular when compared with BZQs that have the same infrared and optical properties of normal quasars, while Seyfert 2 galaxies show mid-IR properties similar to BZQs only in the W2-W3 vs W3-W4 diagram.

where it is clear that in the W1-W2 vs. W2-W3 diagrams Seyfert 1 galaxies appear to lie in the middle between BZBs and BZQs having a fraction fo them with similar colors while type 2 Seyferts have mid-IR colors well distinct from blazars. On the other hand, in the W2-W3 vs. W3-W4 plane, Seyfert galaxies of type 1 are more similar to BZQs, and the same situation occurs for type 2 Seyferts. It is worth highlighting that even if there is a fraction of Seyfert galaxies showing mid-IR colors similar to known γ-ray blazars, as previously highlighted in de Menezes et al. (2019), these sources do not contaminate the selection of γ significantly-ray blazar candidates since this is also based on the radio-loudness parameter (see D'Abrusco et al., 2014, for more details).

For Turin-SyCAT sources having a counterpart in the 2MASS, we also show their near-IR properties in Figure 4.7. As in the previous color-color diagrams, Seyfert 2 galaxies are redder than type 1 sources, but even if well distinct from background sources, they show quite similar properties.

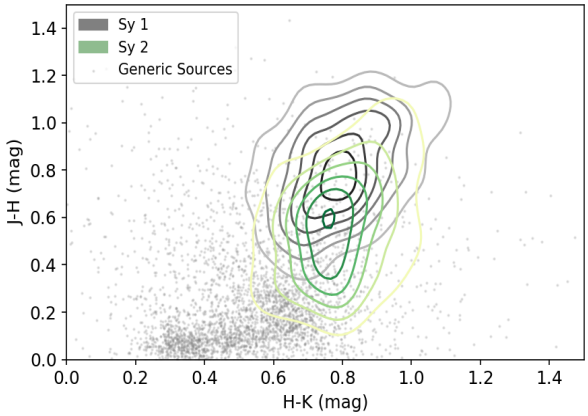

Figure 4.7: The color-color diagrams based on the 2MASS magnitudes comparing contours of Seyfert galaxies of type 1 (grey-to-black) and type 2 (yellow-to-green) with generic sources selected in a random region of the sky (see , for a similar analysis). While Seyfert galaxies occupy a well distinct region from that of generic infrared sources their near-IR properties are quite similar. Isodensity contours are computed using KDE (see e.g., D'Abrusco et al., 2019).

4.4.2 Optical colors

Given the significant number of Seyfert galaxies lying in the SDSS footprint selected for the 1^{st} release of the Turin-SyCAT (see Section 4.2), we also investigated their optical colors in comparison with their mid and near IR ones as shown in Figure 4.8. The $u - r$ color separate quite well the two Seyfert galaxy populations, as expected given their spectral properties, with Seyfert 1 being bluer than type 2 sources.

All sources listed in the Turin-SyCAT at declinations above ∼-33°, thus being in the footprint of Pan-STARRS, within 1″.5, in this survey, for a total of 494. We inspected all their colors, but we did not find any additional information rather than those that can be already obtainable with the red SDSS bands. However, consistently with the mid-IR luminosities, all the R band optical luminosities computed using the Pan-STARRS measurements lie in the range between 10^8 and 10^{11} $L_\odot$ with only two exceptions, namely: SY1 J1404+4327 and SY1 J1821+6420 being one order of magnitude brighter. It is worth noting that for all Seyfert galaxies lying both in the Pan-STARRS and SDSS footprints, their R band magnitudes are consistent within 2σ uncertainty.

4.4.3 The IR – hard X-ray connection

We also carried out an analysis to compare the mid-IR properties of Sefyert galaxies with their hard X-ray ones. First, we computed the distribution of ratios between their flux at 12μm and 22μm, respectively (i.e., F_{12} and F_{22}), with that measured in the hard X-rays (i.e., F_{HX}) between 15 keV and 150 keV, for which we adopted the measurements reported in the 3PBC (see Figure 4.9). Investigating the connection between the hard X-ray and the mid-IR emission in Seyfert galaxies is crucial since

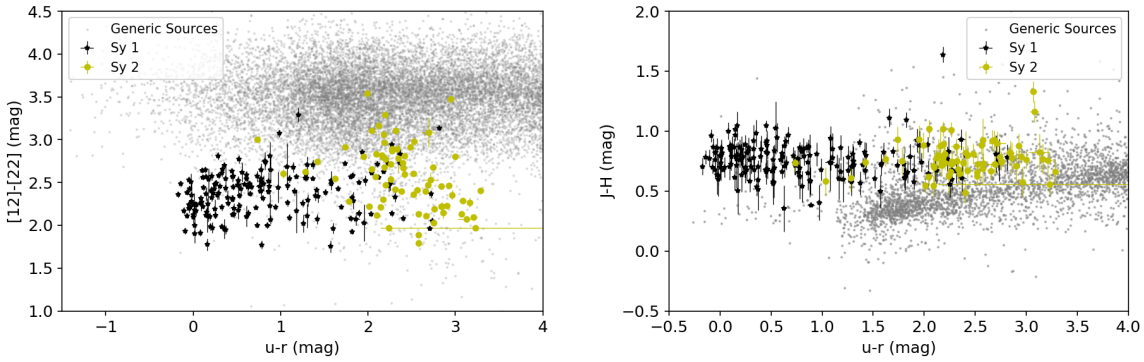

Figure 4.8: The comparison between the optical and the mid (left panel) and near (right panel) infrared colors for both Seyfert galaxies of type 1 (black in both plots) and type 2 (yellow in both diagrams). Seyfert galaxies are well separated in two distinct regions of both plots when considering the $u-r$ color. These color-color diagrams are drawn only for those Seyferts lying in the SDSS footprint (see Section 4.2.)

high energy emission measures an intrinsic radiated luminosity above ten keV while WISE 12μm and 22μm is related to the reprocessed radiation from the dust of all energy absorbed from the optical and UV wavelengths. We did not find any significant difference in both the distributions of the infrared-to-hard X-ray fluxes between Seyfert 1 and Seyfert 2 galaxies, according to the Kolmogorov-Smirnov test the null hypothesis that the two distributions are the same cannot be rejected.

On the other hand, we discovered two significant trends when comparing the mid-IR fluxes with those in the hard X-rays bands, as shown in Figure 4.10. In log-log scales, the correlation between F_{12} and F_{HX} has a linear correlation coefficient of 0.63 (slope of 0.95) for Seyfert 1 galaxies and 0.47 (slope of 0.85) for Seyfert 2, respectively. In both cases, there is a negligible chance probability. Similar values for the correlation between F_{22} and F_{HX} being 0.61 (with a slope of 0.99) for type 1 Seyferts and 0.45 (slope of 0.80) for Seyferts 2, with again p-chance always less than 10^{-6}. Considering both classes together, given their similar mid-IR to hard X-ray ratios, we found a correlation coefficient of 0.57 and 0.55 (slopes of 0.93 and 0.95), for the hard X-ray flux F_{HX} correlating with F_{12} and F_{22}, respectively. Carrying out this analysis, we also compared the hard X-ray photon index Γ_{HX} with all mid-IR colors, but we did not find any significant trend and the distribution of Γ_{HX} appear to be the same when comparing type 1 and type 2 Seyfert galaxies.

On the other hand, we also found a correlation between the mid-IR flux computed at 3.4μm and F_{HX} (correlation coefficient equal to 0.67) as for other mid-IR fluxes, but only a mild trend (correlation coefficient equal to 0.45) is indeed present when comparing near IR fluxes computed from 2MASS magnitudes and F_{HX}, both with negligible p-chances.

We remark that the underlying reason to choose to show only results related to the 3PBC catalog with respect to BAT105 and IBISCAT4 samples is that the former does not have positional uncertainty reported therein. Thus we could expect some incorrect

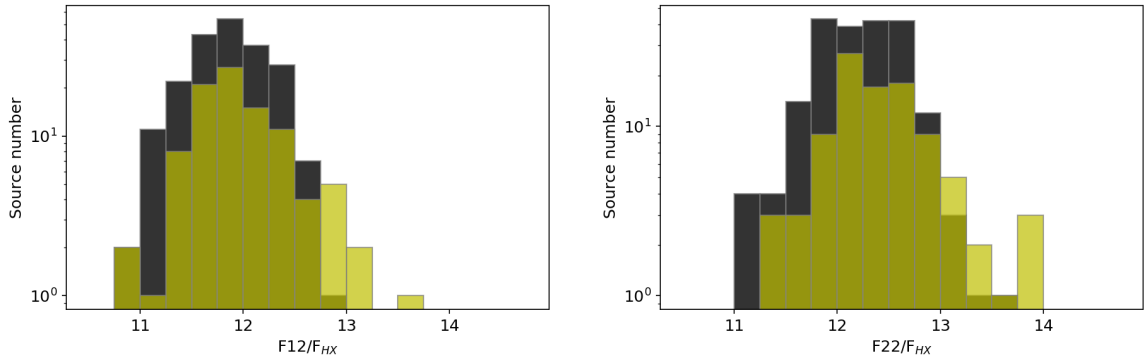

Figure 4.9: The distributions of the ratios between the integrated flux in the WISE band centered at the nominal wavelength of 12μm (top panel) and 22μm (bottom panel), respectively, over the integrated flux in the hard X-ray band F_{HX} between 15 and 150 keV collected for all Seyfert galaxies with a counterpart in the 3PBC and selected to belong to the Turin-SyCAT. There is no neat difference between the distributions of type 1 and type 2 Seyfert galaxies appearing in black and yellow, respectively.

associations while the latter has fewer counterparts that the 3PBC. However, results are not different when using hard X-ray fluxes reported in the BAT105 and IBISCAT.

As an additional test, we also crossmatched our SYCAT sources with the Point Source catalog of the Infrared Astronomical Satellite (IRAS)[6] using all elliptical positional uncertainty regions listed therein. We found that 45 Seyfert 1 and 55 Seyfert 2 galaxies have a unique IRAS counterpart at 60μm, while these numbers increase up to 59 and 66 sources detected at 100μm, respectively. Then we searched for a trend between the flux at 60μm, and 100μm (i.e., F_{60} and F_{100}, respectively) and that measured in the hard X-ray from the 3PBC as previously performed for WISE. As shown in Figure 4.11, no neat trend or correlation was found. This is in agreement with our previous results since cold dust, mostly responsible for the star formation in SYCAT sources it is not expected to be linked directly with the central AGN. While relatively hot dust emitting in the mid-IR, being mostly associated with the dusty torus surrounding the central black hole appears to be connected with the hard X-ray radiation.

4.5 Summary, conclusions and future perspectives

The main goal of the analysis presented here is to create an extremely homogeneous catalog of Seyfert galaxies based on an extensive literature search and considering multifrequency selection criteria mainly drawn on the basis of their radio, infrared and optical properties. Despite the fact that several catalogs and samples used to prepare the Turin-SyCAT are based on hard X-ray observations, our selection criteria are completely unbiased with respect to the high energy emission.

Our initial selection is based on the following 5 catalogs/samples: (i) the 3^{rd} release

[6]https://heasarc.gsfc.nasa.gov/W3Browse/iras/iraspsc.html

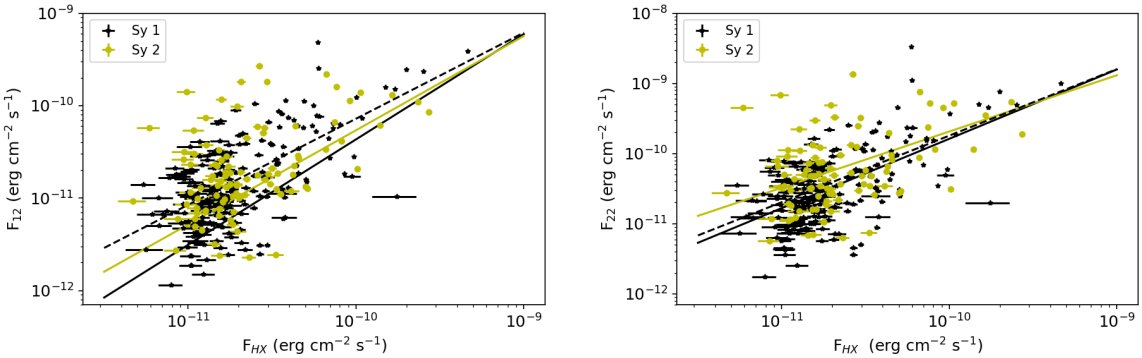

Figure 4.10: Left panel) The correlation found between the W3 integrated flux and that in the hard X-ray band from the 3PBC, for both Seyfert 1 and 2 galaxies (marked in black and yellow, respectively). The dashed line corresponds to the regression line computed for the whole sample while the straight black and yellow lines mark that for type 1 and type 2 Seyfert galaxies, respectively. Correlation coefficients are reported in Section 4.4 while p-chance are negligible being all lower than 10^{-6}. Right panel) Same of left plot but computed using the mid-IR flux at 22μm.

of the Palermo BAT source catalog (Cusumano et al., 2010), (ii) the BAT 105 months survey (Oh et al., 2018) carried out again using the data collected by the SWIFT-BAT instrument; (iii) The Seyfert Catalog created by Lipovetskij et al. (1987); (iv) Seyfert galaxies listed in the 13^{th} edition of the VeronCAT (Véron-Cetty & Véron, 2010) and (v) all unidentified hard X-ray sources, observed with SWIFT-BAT and INTEGRAL satellites, that were targets of optical spectroscopic campaigns aimed to search their low energy counterparts of unidentified sources (Masetti et al., 2004, 2006, 2009, 2010, 2012; Parisi et al., 2012; Masetti et al., 2013; Rojas et al., 2017; Marchesini et al., 2019).

Adopting our thresholds while applying our selection criteria (see Section 4.3 for all details), we built the 1^{st} release of the Turin-SyCAT, listing 571 Seyfert galaxies. Then, thanks to all crossmatches performed with existing databases; we also carried out a multifrequency analysis of the Seyfert galaxy population. All sources listed in the Turin-SyCAT have a published spectrum that allowed us to firmly establish their redshifts and their optical spectroscopic classification, they all have an associated mid-IR counterpart in the AllWISE catalog, and then they all have radio luminosity when associated with a radio counterpart in one of the major surveys (i.e., NVSS, FIRST and SUMSS) less than 10^{40} erg s^{-1} and mid-IR luminosity computed at 3.4μm lower than 10^{11} L$_{\odot}$. References for their redshifts and for their spectra used to classify the source and for a literature comparison are all reported in the Appendix.

Results of the multifrequency characterization for all Seyfert galaxies listed in the Turin-SyCAT can be summarized as follows.

- We selected 571 Seyfert galaxies with homogeneous properties at radio, infrared and optical energies. All Seyfert belonging to the Turin-SyCAT have a published spectrum that we inspected to determine their classification, distinguishing between type 1 and type 2, and their redshifts.

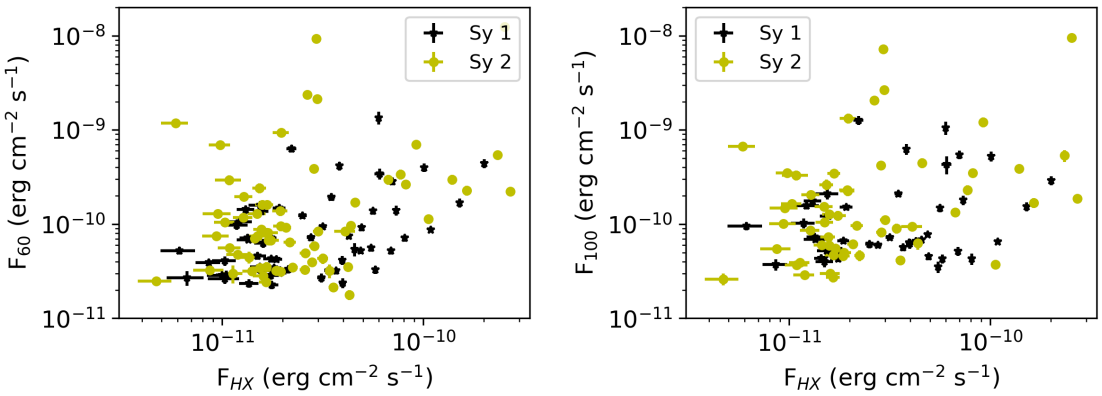

Figure 4.11: Left panel) The scatter plot for the integrated flux at 60μm collected from the IRAS Point source catalog (i.e., F_{60}) and that in the hard X-ray band (i.e., F_{HX}) as listed in the 3PBC, for both Seyfert 1 and 2 galaxies (marked in black and yellow, respectively, as shown in previous figures). No neat trend/correlation appear evident. Right panel) Same of left plot but computed using the far-IR flux at 100μm (i.e., F_{100}).

- We found that mid-IR colors of type 1 Seyfert galaxies are more concentrated in the W1-W2 vs. W2-W3 color-color diagram with respect to those of Seyfert 2 galaxies.

- Type 1 Seyfert galaxies could have mid-IR colors similar to blazars, but being radio quiet they are barely selected in catalogs of γ-ray blazar candidates. Seyfert 2 galaxies have mid-IR colors similar to quasars but clearly distinct from those of BL Lac objects.

- For those Turin-SyCAT sources with a counterpart in the SDSS footprint, we also highlight that, in agreement with their spectral properties, type 1 and 2 Seyfert galaxies have a neat distinction when using the u-r color.

Comparing the mid-IR properties of those Seyfert galaxies belonging to the 3PBC with their hard-X-ray emissions, we discovered a tight correlation between the mid-IR flux (in both W3 and W4 bands) and that above 15 keV for both classes of Seyfert galaxies. The ratio between these two integrated fluxes is also remarkably similar for both Seyfert classes.

The correlation is also present when considering the mid-IR flux at 3.4μm but has less significance when using the near IR fluxes collected thanks to the 2MASS crossmatches. All these correlations are in agreement with expectations of the unification scenario of Seyfert galaxy of type 1 and type 2, where the fraction of luminosity absorbed by dusty components should be the same for both Seyfert types and their differences are mainly related to their our viewing direction. In addition, we did not find any trend between far-IR fluxes and hard X-ray ones for all SyCAT sources with a

counterpart in the IRAS Point Source Catalog (193 out of 517). In agreement with the fact that relatively "cold" dust emitting at longer wavelengths than those observed by WISE, it is not directly related to the central AGN and the dusty torus obscuring it. We plan to carry out a further investigation of the mid-IR vs. hard X-ray connection using the Combined Atlas of Sources with Spitzer IRS Spectra (CASSIS[7], Lebouteiller et al., 2011, 2015) since a significant fraction of SyCAT sources (i.e., ∼30%, being 157 out of 571) have mid-IR spectra already available.

It is worth mentioning that similar tests of the unification scenario were carried out in the past by Mulchaey et al. (1994) for a sample of 116 Seyfert galaxies. They found that distributions of [O III] λ5007, infrared, and hard X-ray continuum are similar for Seyfert type 1 and 2. They also discovered a correlation between the ultraviolet continuum and emission-line fluxes in type 1 Seyferts, but not for type 2, consistent with the idea that the central engine is responsible for powering the line emission, all properties are consistent with those expected in the dusty torus model.

As future perspectives, correlations between the mid-IR flux and the hard X-ray one could be used to search for heavily obscured Seyfert galaxies, among unidentified hard X-ray sources seen by SWIFT-BAT and INTEGRAL. Having strong dust absorption could not emit significantly in the optical energy range but could show similar mid-IR to hard X-ray flux ratios as the Seyferts listed in our Turin-SyCAT. We also expect to investigate the large scale environments of Seyfert galaxies (Dultzin-Hacyan et al., 1999; Koulouridis et al., 2006b; Villarroel & Korn, 2014; Jiang et al., 2016) using sources listed in Turin-SyCAT adopting the same statistical procedures described in Massaro et al. (2019, 2020) as an additional test for the unification scenario.

Finally, it is worth highlighting that we are already working to the 2^{nd} release of the Turin-SyCAT, planned for the end of 2021, to increase the number of Seyfert galaxies listed therein.

[7] cassis.sirtf.com

Chapter 5

On the large-scale environment of Seyfert galaxies, up to Mpc scale

In this chapter I study the Mega parsec scale of Seyfert galaxies based on the Turin-SyCAT samples using the so-called cosmological overdensities method. This chapter is organized as follows: in Section 5.2 we describe the main properties and selection criteria of all catalogs and samples used to perform our analysis. Section 5.3 is then devoted to a basic description of the statistical method adopted to investigate the large-scale environment of Seyfert galaxies. Results of our study are then presented in Section 5.4, this also include a comparison with radio galaxies in the same redshift range. Section 5.5 is finally dedicated to our summary, conclusions and future perspectives. All tables with the results of our statistical analysis are reported in the Appendix.

5.1 Where Seyfert galaxies live, grow and die: the state-of-art

In 1974 when Khachikian and Weedman proposed to classify Seyfert galaxies based on features in their optical spectra distinguishing between type 1 and type 2 on the relative width of their Balmer or forbidden emission lines, where type 2 Seyferts are those with similar relative width of Hβ to the [OIII] lines (see also Khachikian & Weedman, 1971; Weedman, 1977; Ho, 2008).

Seyfert galaxies are also X-ray sources with luminosities $L_{2-10keV} \sim 10^{38-43}$ erg/s (see e.g., Panessa et al., 2006, for recent work on *XMM-Newton* and *Chandra* satellites, and references therein) with soft X-ray spectra showing a power law continuum with a high energy cut-off (see, e.g. Mushotzky et al., 1980; Haardt & Maraschi, 1991; Singh et al., 2011) and a "soft excess" which origin is due to "unresolved" X-ray emission lines (Fabian et al., 1986; Walter & Fink, 1993; Gliozzi & Williams, 2020) while, around 6 keV, they generally show the Fe Kα fluorescent emission line (Nandra & Pounds, 1994; Matt et al., 1996; Patrick et al., 2012).

According to the unification scenario of AGNs (Antonucci & Miller, 1985; Antonucci, 1993), differences between type 1 and 2 Seyfert galaxies are due to the orien-

tation of the dusty torus obscuring the central "engine" respect to the line-of-sight.

However, several discoveries as (i) changing look Seyfert galaxies (e.g., Collin-Souffrin et al., 1973; Aretxaga et al., 1999), (ii) type 2 Seyferts without X-ray absorption features (Pappa et al., 2001), (iii) rare Seyfert galaxies lacking features correspondent to broad line region (BLR; Panessa & Bassani, 2002; Shi et al., 2010); (iv) the presence of multiple absorbers in the BLR necessary to explain X-ray variability (Elvis et al., 2004; Lamer et al., 2003) and (v) different properties of their host galaxy (Maiolino & Rieke, 1995; Malkan et al., 1998; Villarroel et al., 2017) are currently challenging the unification scenario, casting doubts on the interpretation of type 1 and type 2 sources viewed at different angles.

Moreover the role of the environment where Seyfert galaxies live is still under debate.

Several works tackle the study of the environment of Seyfert galaxies finding conflicting results. A significant excess in the number of "companion galaxies" compared with non-active galaxies was initially found (Petrosian, 1982; Dahari, 1984; MacKenty, 1989; Laurikainen & Salo, 1995; Rafanelli et al., 1995; Salvato & Rafanelli, 1997) then not confirmed by subsequent studies (De Robertis et al., 1998; Schmitt, 2001). These differences can be attributed to Seyfert and control sample selection, the definition of neighbors and environment, and cosmological biases, to name a few (Sabater et al., 2013). Additional analyses pointed out that a richer environment of Seyfert 2 galaxies (see e.g., Dultzin-Hacyan et al., 1999) lead to an sequence of co-evolution between their central supermassive black hole and host galaxies (see also Krongold et al., 2002; Koulouridis et al., 2006a, 2016; Hopkins et al., 2008; Koulouridis et al., 2013).

Then it was found a statistically significant difference between the richness of environments of Seyfert 1 and 2 galaxies, the latter living where there is an higher galaxy density (Laurikainen & Salo, 1995; Malkan et al., 1998; Dultzin-Hacyan et al., 1999; Koulouridis et al., 2006a; Jiang et al., 2016; Villarroel & Korn, 2014; Gordon et al., 2017). However, also in this case Tran (2001, 2003) found conflicting results using a sample that excludes type 2 without a detected broad component in polarized spectra. Koulouridis et al. (2016) found that Seyfert 2 galaxies with detected hidden broad line region, at $z < 0.04$, are more likely to have a close companion (200 h^{-1} kpc) compared with the control sample, probably due to a higher frequency of mergers.

Additional studies were also carried out on type 1 and type 2 AGNs, even if not specifically classified as Seyfert galaxies. Villarroel & Korn (2014), investigating AGN pairs at scales smaller than ∼350 kpc, found that (i) the closer companion of a type 2 AGN is generally also optically classifiable as type 2 and (ii) surrounding galaxies of type 2 sources are bluer than those of type 1, the latter claim interpreted as due to more star formation coupled with less dust and metallicity.

Main aim of the study presented here is to tackle the investigation of the large-scale environment of Seyfert galaxies up to Mpc scales to provide an additional test of the unification scenario of active galaxies.

The main advantage of the analysis carried out is the possibility to use an extremely homogeneous and statistically "clean" (i.e. with accurate selection) Seyfert catalog: the 1^{st} release of Turin-SyCAT (Peña-Herazo et al., 2020a), with larger number of sources, all spectroscopically classified, with respect to literature analyses. This implies that

the contamination by different AGN classes is quite limited as well as lack optical spectroscopic redshifts and Seyfert classification is well constrained. Nevertheless it will allow us to investigate the Seyfert environments with respect to several source parameters. This multifrequency catalog of Seyfert galaxies, with information gathered and combined from radio, optical, infrared and X-ray surveys, already permitted us to investigate trends or correlations between different parameters/observed quantities (Peña-Herazo et al., 2020a).

5.2 Sample Selection

We used several samples and catalogs while carrying out the analysis of the large-scale environments of Seyfert galaxies. Here we only report their basic description for completeness, while more details are available in the literature.

We recently published the 1^{st} release of the Turin-SyCAT catalog whereas all Seyfert galaxies listed therein were selected on the basis of an extensive literature search and considering multifrequency criteria. We visually inspected all spectra available for all selected sources and applied several thresholds to their radio, infrared and optical properties.This catalog includes 571 Seyfert galaxies distinguished in 412 type 1 and 159 type 2 sources.

This catalog is based on sources classified as Seyfert galaxies in (i) the 3^{rd} release of the Palermo BAT source catalog (hereinafter 3PBC)[1] (Cusumano et al., 2010); (ii) the BAT 105 months survey (hereinafter BAT105)[2] carried out using the data collected by the Burst Alert Telescope instrument on board of SWIFT satellite (Oh et al., 2018); (iii) the Seyfert Catalog[3] created by (Lipovetskij et al., 1987) (hereinafter LipCAT); (iv) the 13^{th} edition of the VeronCAT (Véron-Cetty & Véron, 2006, 2010) and (v) selected among those discovered during the optical campaign to search for counterparts of unidentified hard x-ray sources (Masetti et al., 2004, 2006, 2009, 2010).

All SyCAT sources have a published optical spectrum, $L_{radio} < 10^{40}$ erg s^{-1}, and unique wise counterpart with $L_{IR} < 10^{11}$ $L_{\odot}$ to guarantee we are not selecting nearby quasars. Then we restricted the analysis only to the SDSS footprint thus considering 212 Seyfert galaxies (i.e., 142 of type 1 and 70 of type 2) in the 1^{st} release of the Turin-SyCAT out of 571 listed therein to carry out our environmental study.

Results on the environments of Sefyert galaxies is compared with that of radio galaxies (RGs) in the same redshift range, i.e., $0.02 \leq z_{\rm src} \leq 0.15$, to achieve this aim we thus used the following two catalogs both limited to the SDSS footprint.

The first catalog is a combination of FRICAT and sFRICAT both described in Capetti et al. (2017a). FRICAT sources are selected on the basis of their classical FR I radio morphology and have a radio structure extended beyond a distance of 30 kpc (Fanaroff & Riley, 1974), measured from the optical position of their host galaxy. On the other hand, the 14 sFRICAT radio galaxies show indeed extended emission, with similar morphology at 1.4 GHz, but between 10 and 30 kpc but limited to $z_{\rm src} = 0.05$

[1] http://bat.ifc.inaf.it/bat_catalog_web/66m_bat_catalog.html
[2] https://swift.gsfc.nasa.gov/results/bs105mon/
[3] http://vizier.u-strasbg.fr/viz-bin/VizieR?-source=VII/173

(see Capetti et al., 2017a, for details). All these radio galaxies are hosted in red early-type galaxies and spectroscopically classified as low excitation radio galaxies (LERGs; Hine & Longair, 1979; Laing et al., 1994) for a total of 209 radio sources.

The second sample is the FRIICAT (Capetti et al., 2017b), listing 105 edge-brightened radio sources (FR II type) within the same redshift range of the previous catalog. About ∼90% of the FR IIs listed in the FRIICAT are spectroscopically classified as LERGs, being hosted red early-type galaxies as occurs for FR Is. The remaining ∼10% shows optical spectra typical of high excitation radio galaxies (HERGs) and host galaxies bluer in the optical band and redder in the infrared than FR II LERGs.

HERGs were excluded from the comparison sample thus restricted only to LERGs independently by their radio morphology.

Thanks to their selection criteria both RG catalogs are not contaminated by compact radio objects, as compact steep spectrum sources and FR 0s (Baldi et al., 2015, 2018), which show a different cosmological evolution, with respect to FR Is and FR IIs and could potentially lie in different environments.

In a few cases we also compare the environmental behavior of Seyfert galaxies with that of a catalog of quiescent elliptical galaxies (hereinafter ELL). This has been selected out of all sources listed in the Galaxy Zoo[4] data release 1 (Lintott et al., 2008).

Elliptical galaxies have a single counterpart in the SDSS data release 9 within 5″all with SDSS flags: *spType*, *spClass* equal to GALAXY and *subclass* NULL, an elliptical classification with at least 45 votes, according to the Galaxy Zoo analysis and with spectroscopic $z_{\rm src}$ smaller than 0.15. In addition we selected only elliptical galaxies with a clean photometry (i.e., SDSS flags *q_mode*=1 and Q>2) and classified as *galaxies* (i.e., SDSS flag *cl* equal to 3) and lacking a radio counterpart within 5″ so to avoid a possible radio galaxy contamination.

5.3 Statistical analysis

Our analysis on the large-scale environment of Sefyert galaxies is based on the definition of cosmological neighbors and cosmological overdensities according to the method described in Massaro et al. (2019, 2020) and also adopted in Capetti et al. (2020).

Cosmological neighbors are all optical sources lying within the 2 Mpc radius computed at $z_{\rm src}$ of the central Seyfert galaxy with all the SDSS magnitude flags indicating a galaxy-type object (i.e., *uc*=*rc*=*gc*=*ic*=*zc*=3), and having a spectroscopic redshift z with $\Delta z = |z_{\rm src} - z| \leq 0.005$, corresponding to the maximum velocity dispersion in groups and clusters of galaxies (see e.g., Moore et al., 1993; Eke et al., 2004; Berlind et al., 2006). The number of cosmological neighbors lying within 500 kpc, 1 Mpc and 2 Mpc distance from the central Seyfert galaxy, being an estimate of the environmental richness, is labelled as N_{cn}^{500}, N_{cn}^{1000} and N_{cn}^{2000}, respectively.

Then we indicate the presence of a cosmological overdensity when the number of cosmological neighbors within 500 kpc is higher than the 95% quantile of the N_{cn}^{500} distribution measured for a sample of mock sources located in random positions of the sky. At redshifts above 0.1 we imposed to have at least two cosmological neighbors

[4]https://www.galaxyzoo.org

within 1 Mpc in addition to the previous criterion on N_{cn}^{500} given the lower number of spectroscopic sources in the SDSS. The entire procedure adopted to set this threshold is described in Massaro et al. (2019), this was chosen in bin of $z_{\rm src}$ of size 0.01 to compare sources at same redshifts.

It is worth highlighting that the procedure based on cosmological overdensities avoids bias and artifacts due to the assumed cosmology, by adopting an adaptive threshold as function of redshift bin $z_{\rm src}$ having size of 0.01 in our analysis.

5.3.1 Cosmological Artifacts

Here I highlight the importance of using threshold on the number of cosmological neighbors changing with redshift $z_{\rm src}$. For this reason, we present an example of one Radio Galaxy, SDSS J160722.95+135316.4 at $z_{\rm src} = 0.034$. For all cosmological neighbors we computed the absolute R magnitude. Then we calculated their apparent magnitudes if the radio galaxy would be redshifts 0.05, 0.10, and 0.15, instead of its original redshift. For each of those redshift we computed the radii of the circles of 500 kpc, 1 Mpc, and 2 Mpc. I show this example In Figure 5.1, with the locations of cosmological neighbors marked with red symbols and dashed lines the distances of 1 Mpc and 2 Mpc, respectively. It is evident that the number of cosmological neighbors decreases with z. The cosmological neighbors within 500 kpc decrease from $\rm N_{cn}^{500} = 10$ at $z_{\rm src} = 0.034$, to $\rm N_{cn}^{500}$ =3 at $z_{\rm src} = 0.05$, $\rm N_{cn}^{500}$ =2 at $z_{\rm src} = 0.10$ and zero at $z_{\rm src} = 0.15$. Similarly with $\rm N_{cn}^{2000}$, with values of 47 at 0.034 and 20, 4, 1 at $z_{\rm src} = 0.05, 0.100.15$, respectively.

Finally, we reported here in Table 5.1 all environmental parameters estimated for each Seyfert galaxy considered in our sample.

5.4 The large-scale environments of Seyfert galaxies

We first remark that to carry out this environmental analysis it is strictly necessary to compare the behavior of different source classes in redshift bins to avoid cosmological bias and artifacts. Thus we initially show, in Figure 5.2, the projected distance d_{proj}, computed between from the central Seyfert galaxy and the average values of coordinates of cosmological neighbors, as function of the redshift difference between the Seyfert galaxy and the average redshift of cosmological neighbors within 2Mpc.

We did not find any difference between the two Seyfert galaxy populations and moreover we did nothing also when comparing Seyferts with LERGs and quiescent elliptical galaxies. This implies that Seyfert galaxies appear to be located close to the center of their large-scale environments. Thus to complete this comparison and to highlight the richness of their environments, we show in Figure 5.3 the medians of the number of cosmological neighbors, i.e. $\bar{N}_{cn}^{500}$, located within 500 kpc from the central source as a function of redshift for both types of Seyferts and in comparison with LERGs.

As previously pointed out, also in this case, we found that the richness of large-scale environments in both types of Seyfert galaxies is (i) remarkably similar between the

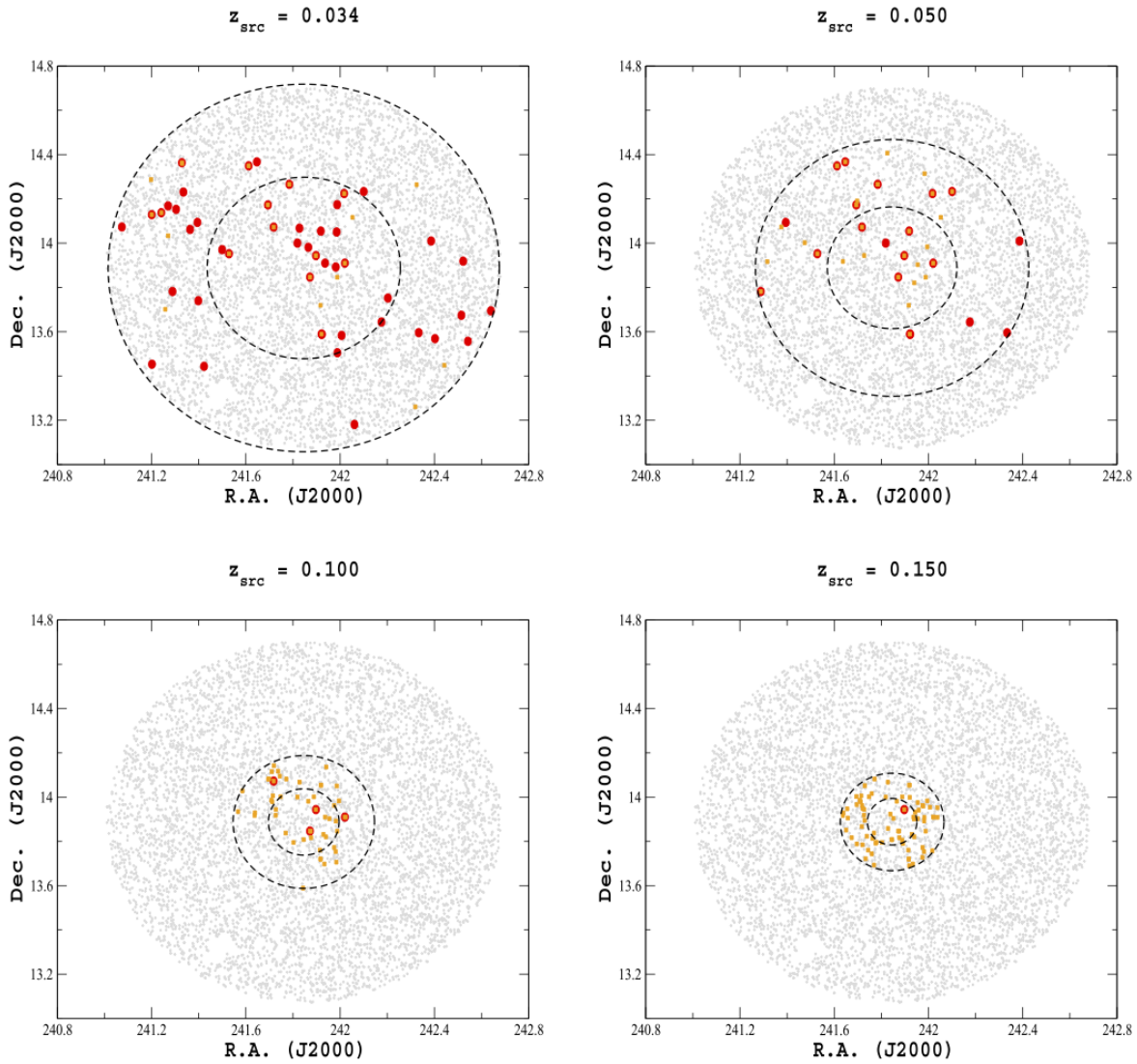

Figure 5.1: *Upper left panel:* SDSS J160722.95+135316.4 at its original redshift $z_{\rm src} = 0.034$. Dashed black lines are the radii at 1 Mpc and 2 Mpc distances from the central RG, respectively. Cosmological neighbors are shown in red circles, and orange squares are optical galaxies with $m \leq m_{src} = 2$, showing how the noise increases at higher redshift. Other panels show the location of the cosmological neighbors and optical galaxies if the central source would be located at $z_{\rm src} = 0.05, 0.10$, and 0.15. On these three panels, cosmological neighbors' m_r was re-scaled to the different redshift examples using M_r. Are shown only the cosmological neighbors with a re-escalated apparent magnitude brighter than 17.8 mag. From Massaro et al. (2020).

two types and (ii) does not change significantly with redshift. The former result is consistent with the unification scenario of AGNs since the large-scale environment is expected to be independent by orientation effects. However the latter claim is quite interesting because due to cosmological effects you could expect that $\bar{N}_{cn}^{500}$ is decreasing with $z_{\rm src}$, as occurs for LERGs in the same plot, but the lack of this behavior could

Table 5.1: Environmental parameters for Seyfert galaxies (first 10 lines)

SyCAT name	$z_{\rm src}$	$\Delta\, z_{cn}$ (1e-3)	d^{cn}_{proj} (kpc)	N^{500}_{cn}	N^{1000}_{cn}	N^{2000}_{cn}	ζ_{cn}	$< z_{cn} >$	σ_z (1e-3)	d^{cn}_{m} (kpc)
SY1J0008+1450	0.045	2.10	258.12	0.0	0.0	2.0	0.0	0.043	1.56	1300.94
SY2J0034-0002	0.042	0.0	0.0	0.0	0.0	0.0	0.0	0.0	0.0	0.0
SY1J0047+1442	0.040	0.10	413.38	1.0	2.0	6.0	0.5	0.040	1.78	1099.73
SY1J0114-0116	0.120	1.72	222.78	1.0	1.0	1.0	1.0	0.120	0.0	222.78
SY1J0206+0017	0.042	0.62	757.14	0.0	3.0	3.0	0.0	0.043	0.73	785.26
SY1J0214+0044	0.026	0.54	290.43	2.0	2.0	2.0	1.0	0.027	0.3	295.76
SY2J0252-0829	0.0168	0.91	376.22	1.0	1.0	1.0	1.0	0.018	0.0	376.23
SY2J0303-0106	0.0136	0.0	0.0	0.0	0.0	0.0	0.0	0.0	0.0	0.0
SY1J0310-0049	0.08	0.42	96.94	3.0	3.0	3.0	1.0	0.080	0.21	131.4
SY2J0315+4202	0.0237	0.0	0.0	0.0	0.0	0.0	0.0	0.0	0.0	0.0

Col. (1): SyCAT name.
Col. (2): source redshift.
Col. (3): Absolute value of the redshift difference between the Seyfert galaxy and the average redshift of cosmological neighbors within 2Mpc.
Col. (4): Physical distance between the central Seyfert galaxy and the average position of the cosmological neighbors within 2 Mpc. This is computed at the $z_{\rm src}$ of the central Seyfert galaxy.
Col. (5,6,7): Number of cosmological neighbors within 500, 1000 ad 2000 kpc, respectively, estimated at the $z_{\rm src}$ of the central radio galaxy.
Col. (8): The concentration parameter ζ_{cn}.
Col. (9): The average redshift of the cosmological neighbors in 2 Mpc.
Col. (10): The standard deviation of the redshift distribution for the cosmological neighbors within 2 Mpc.
Col. (11): Average distance of the cosmological neighbors within 2 Mpc.

be strongly dependent by the limited number of Seyfert galaxies in our sample above redshift 0.1, where there are no type 2 Seyfert galaxies and those of type one are only 29 out of 142.

In the same Figure 5.3 we are also able to compare the behavior of $\bar{N}^{500}_{cn}$ between Seyfert galaxies and LERGs, and here it is quite clear how Seyfert galaxies tend to live in poor groups while radio galaxies are mostly located in richer environments. In particular N^{500}_{cn} is only greater than 10 for 2 type 1 and 3 type 2 Seyfert galaxies in the entire Turin-SyCAT. This difference between radio galaxies and Seyfert galaxies can be ascribed to their host galaxies since while the former are generally located in elliptical galaxies these tend to live in richer large-scale environments than spiral galaxies that are the host galaxy of the Seyfert populations (see e.g., Biviano, 2000). Similar results were obtained when comparing N^{1000}_{cn} and N^{2000}_{cn} as occurred in previous analyses (Massaro et al., 2019, 2020).

We also investigated additional parameters that characterize the environments at Mpc scale of Seyfert galaxies in comparison with that of radio galaxies, optically classified as LERGs. In Figure 5.4 we show the concentration parameter, ζ_{cn}, as function of $z_{\rm src}$, where ζ_{cn} is defined as the ratio of the number of cosmological neighbors lying within 500 kpc and those located within 1 Mpc. This parameter allows us to test if Seyfert galaxies tend to lie close to the center of their large-scale environments or in the outskirt of a group/cluster of galaxies around them. The large fraction of Seyfert galaxies have low values of ζ_{cn} in agreement with their low richness with respect to LERGs, while those located in regions with higher concentration of cosmological neighbors be-

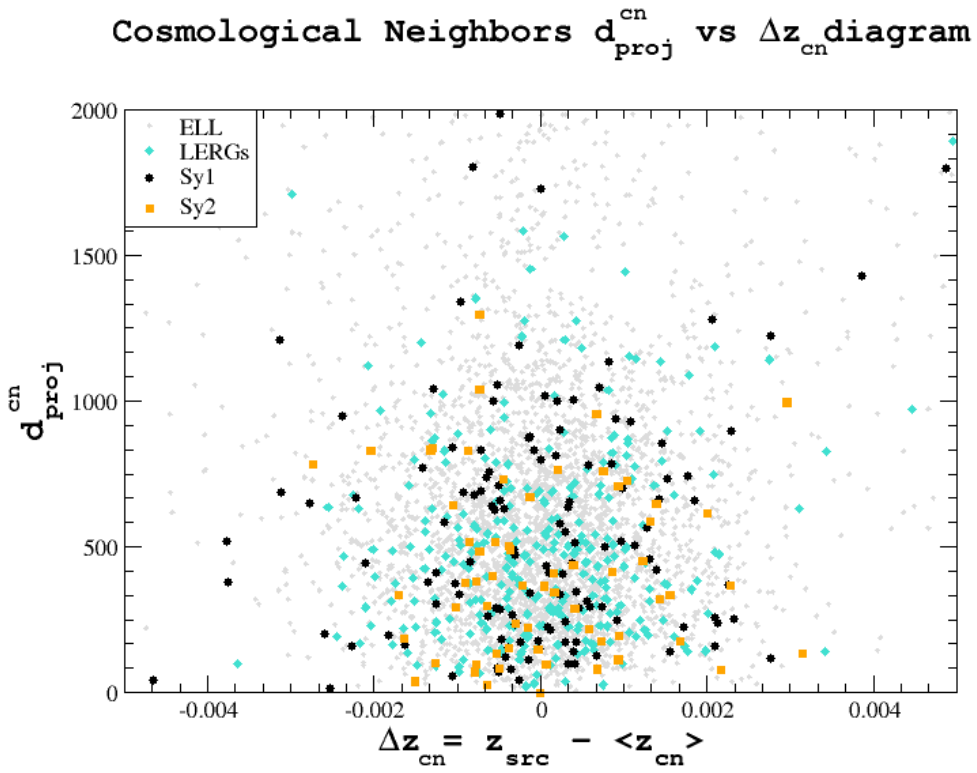

Figure 5.2: The physical distance in kpc between the central source (type 1 or type 2 Seyfert, radio or elliptical galaxy, in black, orange, cyan and grey, respectively, same color code adopted in all figures hereinafter) and the average position of the cosmological neighbors within 2 Mpc. This is computed at the $z_{\rm src}$ of the central source. There are no neat differences in the behavior of type 1 and type 2 Seyfert galaxies between them and in comparison with radio galaxies.

have as LERGs. In Figure 5.5 we compare the standard deviation σ_z of the redshift distribution of all cosmological neighbors within 2 Mpc, a proxy for the estimate of the velocity dispersion of the large-scale environments, and N_{cn}^{2000}. As in previous cases here the behavior of Seyfert galaxies is the same between their subclasses and appear similar to that of radio galaxies. It is worth noting that the main difference resides in the number of cosmological neighbors used to compute σ_z that for Seyfert galaxies is rather small and often restricted to one or two nearby companions.

In Figure 5.6 we report σ_z as function fo redshift and absolute magnitude in the r band, M_r, of the central Seyfert galaxy and no neat trends is evident as well as the comparison between the two types of Seyferts as well as with LERGs is remarkably similar. The difference in both the $z_{\rm src}$ and in the M_r distributions between Seyfert galaxies and radio galaxies is basically due to a selection effect where the former population are simply less powerful and located at lower redshifts than the latter.

Then we also show in Figure 5.7 the average projected distance d_m^{cn} of the cosmological neighbors within 2 Mpc again as function of $z_{\rm src}$ and again no difference between

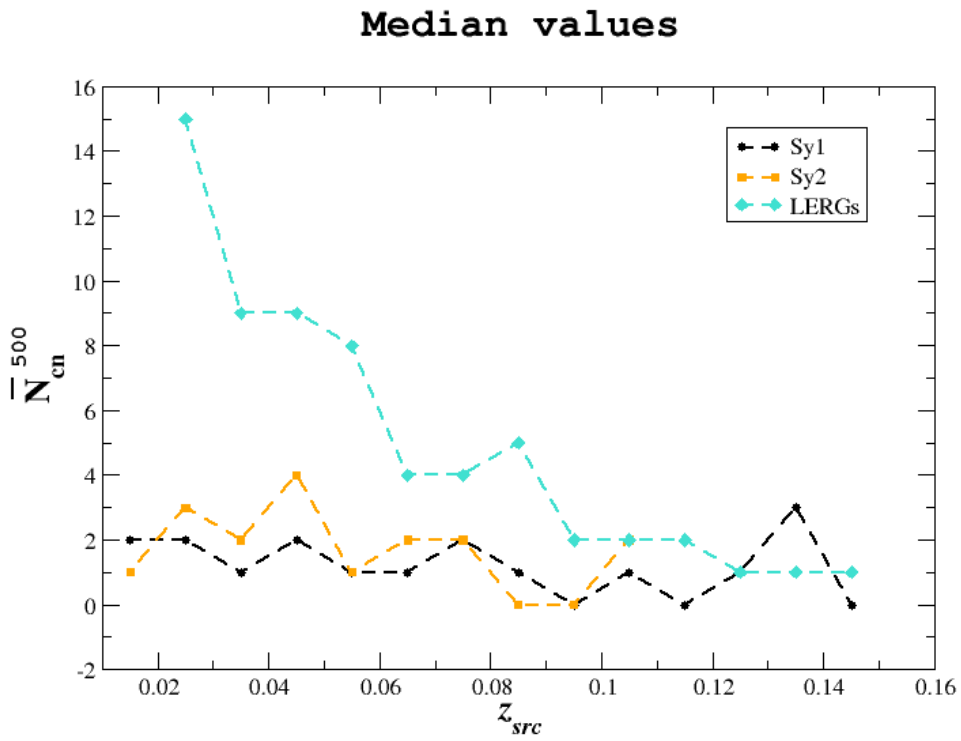

Figure 5.3: Medians of N_{cn}^{500} type 1 and type 2 Seyfert galaxies (black circles and orange squares) and LERGs (cyan diamonds) per redshift bins of 0.01 size. As shown the large-scale environment is consistent between the two types of Seyfert galaxies but appear richer in LERGs showing all medians distributed systematically above those of Seyfert galaxies. Elliptical galaxies have a behavior similar to that of radio galaxies (Massaro et al., 2020).

the two distributions are evident.

Finally, we also investigated the distribution of the Σ_5 parameter, i.e. the 5-th nearest neighbor density (see e.g., Baldry et al., 2006), comparing both Seyfert galaxies and LERGs. The Σ_5 parameter is defined as the ratio between the source number 5 and the projected area $\pi\, r_5^2$, where r_5 is the projected distance between the central Seyfert/radio galaxy and the 5-th nearest neighbor. As extensively discussed in the literature, this parameter can be used as beacon to trace the dark matter halo density (Sabater et al., 2013; Worpel et al., 2013) and it also appears to be related with its halo mass (Haas et al., 2012).

According to our previous analyses (Massaro et al. 2019) to compute Σ_5 we considered as the fifth closest *candidate elliptical galaxy* being defined out of all optical sources, lying within the 2 Mpc distance from the central source, estimated at $z_{\rm src}$, and having $u-r$ and the $g-z$ SDSS colors consistent with those of the ELL sample within $\Delta\, z$<0.005. This color-color selection is based on the iso-density contours, computed adopting the Kernel density Estimation (KDE: see e g., Richards et al., 2004;

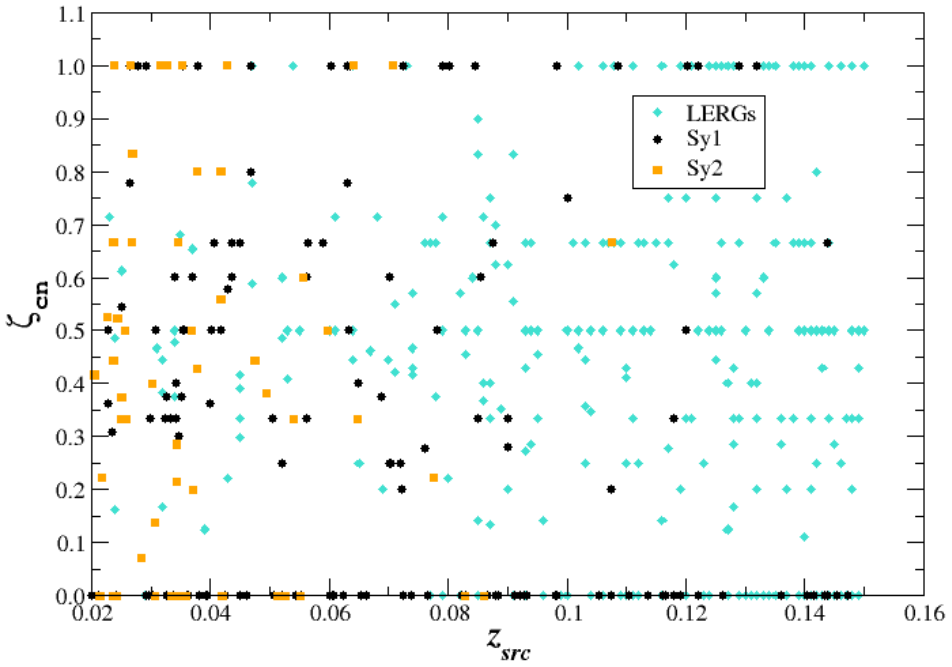

Figure 5.4: The concentration parameter ζ_{cn} as function of redshift $z_{\rm src}$ for both Seyfert and radio galaxies. No trend between these two parameters is evident thus we can claim that there is no cosmological evolution of the concentration parameter, however it seems that Seyfert galaxies tend to have lower values of ζ_{cn} in agreement witht he fact that they inhabit poorer large-scale environments than radio galaxies. Values of ζ_{cn} in the first bin (i.e., close to zero) are simply due to the lack of cosmological neighbors within 500 kpc distance from the central source.

D'Abrusco et al., 2009; Massaro et al., 2013), at 90% a level of confidence. Source selected as *candidate elliptical galaxies* do not necessarily have spectroscopic redshifts, they have only the same colors of elliptical galaxies at $z_{\rm src}$.

Finally, in Figure 5.8 we show the normalized distribution of the Σ_5 parameter where Seyfert 2 galaxies shows larger values than type 1 Seyferts, with LERG distribution peaking between the two types. However, this difference could be ascribed to the different redshift distribution of type 1 and type 2 Seyfert galaxies and the lack of the latter ones at high redshifts (i.e., $z_{\rm src}$ >0.1), since this parameter is affected by the Malmquist bias.

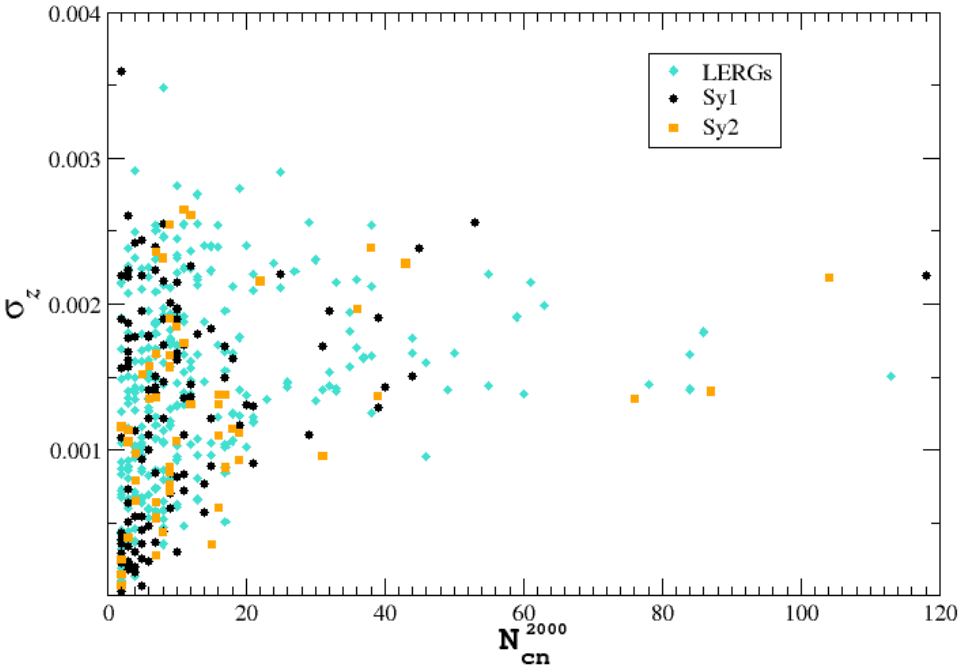

Figure 5.5: Comparison between the standard deviation of the redshift distribution of the cosmological neighbors, σ_z , and the number of cosmological neighbors within 2 Mpc, N_{cn}^{2000}. As in previous plots no differences are found between type 1 and type 2 Seyfert galaxies as well as in comparison with LERGs.

5.5 Summary and conclusions

The study of the environment of AGNs is still an open question, with works leading to conflicting results. Jiang et al. (2016), investigating low-redshift (i.e., z <0.09) SDSS sources, found that type 2 AGNs tend to inhabit richer environment at scales of 100 h^{-1} kpc than type 1 while their large-scale environment ($\sim 1h^{-1}$ Mpc) become quite similar. They also proved that type 2 and normal galaxies reside in similar environments. On the other hand, a recent analysis carried out with the Galaxy and Mass Assembly (GAMA) by Gordon et al. (2017) concluded that there are no differences in the environment of type 1 and type 2 AGNs in AGN-galaxy pairs, with the exception of pairs closer than 20 kpc h^{-1} where there is an excess of type 2 active galaxies. Then at large-scales ($\sim$ 2 h^{-1} Mpc) Strand et al. (2008) found that type 2 AGNs have more companions comparing a sample of local AGNs.

Some studies of the environment of Seyfert galaxies an excess of Seyfert 2 compared with Seyfert 1 galaxies (Laurikainen & Salo, 1995; Malkan et al., 1998; Dultzin-Hacyan et al., 1999; Koulouridis et al., 2006a; Jiang et al., 2016; Villarroel & Korn, 2014; Gordon et al., 2017) . These results are in conflict when compared with other works that find

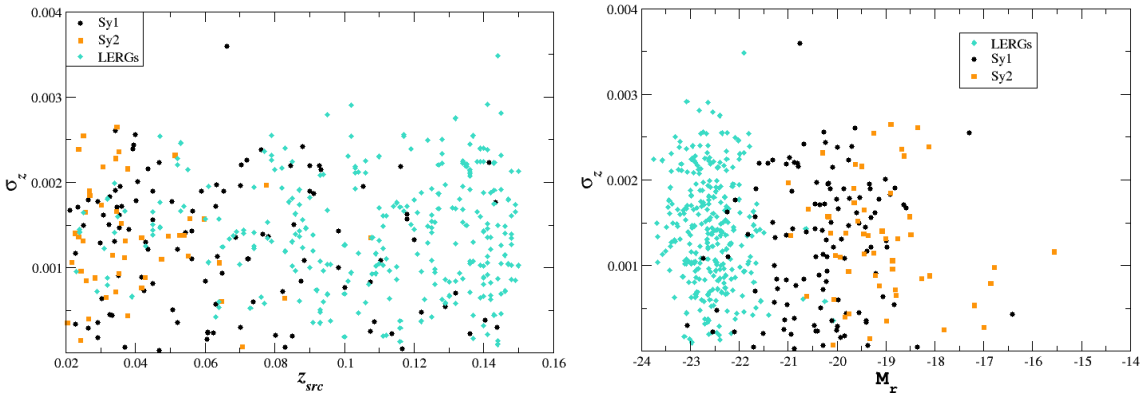

Figure 5.6: The scatter plot of σ_z as function of the absolute magnitude $z_{\rm src}$ (left panel) and M_r (right panel) of the central source for both type of Seyfert galaxies and in comparison with LERGs. No neat trend or correlation is found between these two parameters and the separation in the right plot between Seyfert and radio galaxies is mainly due to their redshift distribution.

no significant difference in the environment of both types of Seyfert galaxies (Schmitt, 2001; Tran, 2001, 2003). These differences can be due to different environment scales, tracing different aspects, or different redshift distributions, or due to sample selection biases.

We carried out a statistical investigation of the large-scale environments of Seyfert galaxies up to Mpc scales. Our analysis is based on the 1^{st} release of the Turin-SyCAT (Peña-Herazo et al., 2020a), an extremely homogeneous and statistically "clean" (i.e. with accurate selection) catalog of Seyfert galaxies, here restricted to those lying in the SDSS footprint.

The method adopted here is based on the cosmological overdensities as recently and successfully carried out to compare the behavior of the large-scale environments of radio galaxies. This is based on the spatial distribution of the cosmological neighbors, optical sources lying within 2 Mpc from the Seyfert galaxy having all SDSS magnitude flags indicating a galaxy-type object and having a spectroscopic redshift z with $\Delta\, z = |z_{\rm src} - z| \leq 0.005$

It is worth mentioning that, as performed in previous analyses on radio galaxies, also here we investigated the large-scale environments in bins of redshift, to avoid cosmological biases and artifacts (Massaro et al., 2019, 2020).

Our results can be summarized as follows.

- Type 1 and type 2 Seyfert galaxies inhabit the same large-scale environments with no neat differences in terms of spatial distribution and richness of surrounding galaxies.

- Comparing the large-scale environments of Seyfert and radio galaxies we found that the former class have higher spatial density of surrounding galaxies. All other parameters related to the large-scale environments of both classes appear

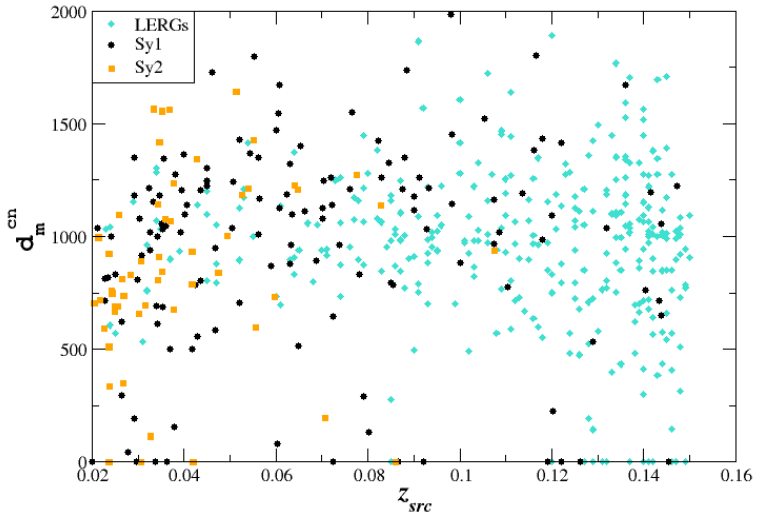

Figure 5.7: The comparison between the average projected distance d_m^{cn} of the distribution of cosmological neighbors vs. the redshift $z_{\rm src}$ of the central source, either Seyfert or radio galaxy. No clear trend was found between these parameters.

to be quire similar.

- We found no dependence of the concentration parameter, ζ_{cn}, as function of redshift $z_{\rm src}$.
- We showed a difference on the distribution of the fifth nearest neighbor density, Σ_5. We attribute this difference to the difference on redshift distribution between type 1 and 2 Seyfert galaxies.

The differences found by Koulouridis et al. (2006a) in the large-scale environment ($<= 1$ h^{-1} Mpc), when comparing both type of Seyfert galaxies ($0.004 \leq z \leq 0.036$) is attributed to the morphological type of their host galaxies differences rather than related to the nuclear activity. In constrast, we show no that there is no difference on the large scale environment of Seyfert 1 and 2 galaxies, up to redshift $z_{\rm src} \leq 0.15$.

We conclude that in agreement with the predictions of the unification scenario type 1 and type 2 Seyfert galaxies live in the same large-scale environments thus confirming that their differences could be mainly ascribed to a different orientation of the central nucleus with respect to the line of sight. Then the richer environments of radio galaxies with respect to that of Seyfert is in agreement with the expectations of their host galaxies, i.e., elliptical vs spirals (Xanthopoulos, 1996; Malkan et al., 1998; Best & Heckman, 2012; Miraghaei & Best, 2017).

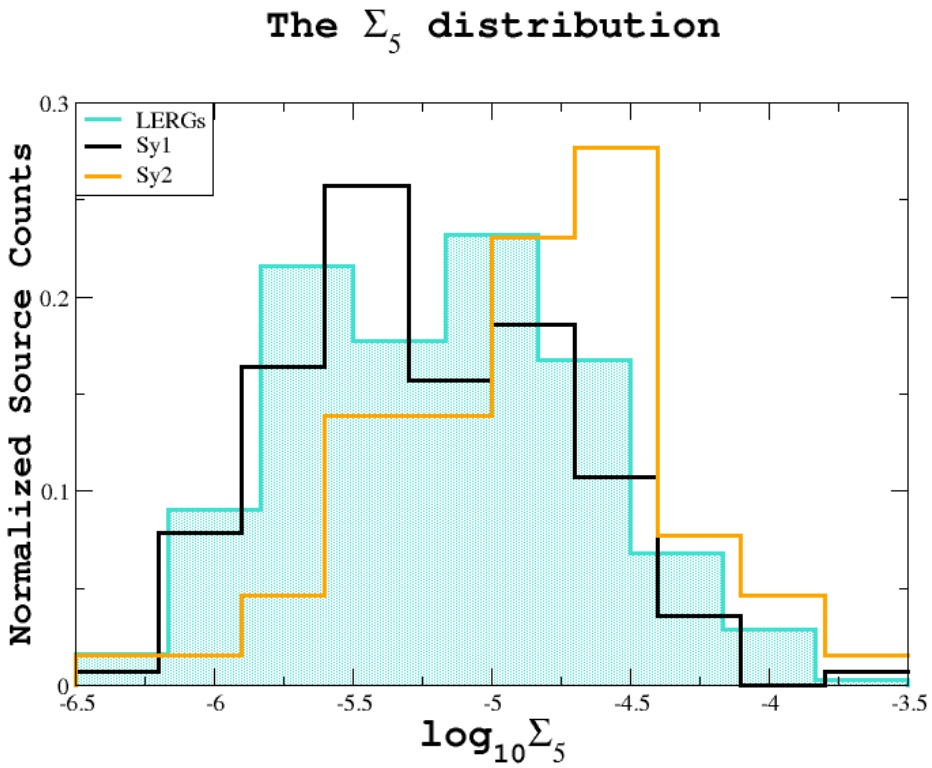

Figure 5.8: We show the normalized distribution of the Σ_5 parameter, i.e., the fifth nearest neighbor density. Type 2 Seyfert galaxies appear to have larger values of Σ_5 than type 1 Seyferts, while LERG distribution peaks between the two.

Chapter 6

Conclusions

This Ph.D. thesis is entirely focused on investigating properties of active galaxies, specifically blazars and Seyfert galaxies, through the creation and the development of source catalogs for these two AGN classes.

For the former class, the blazars, I described the ongoing quest to unveil the nature of potential lower energy counterpart of UGSs or confirm the blazar nature of BCUs in *Fermi*-LAT catalogs. I analyzed more than a hundred spectra, during my Ph.D. thesis and in my final summary, I showed that during the optical spectroscopic campaign I participated 371 out of 394 targets were all identified as blazars then associated with a γ-ray source in the latest release of the *Fermi*-LAT Point Source catalog. These sources were classified as 300 BL Lacs, 40 flat-spectrum radio quasars, and 31 blazars, which their host galaxy partially dominates the optical spectrum. Of the newly classified BL Lacs, we found 38 having a firm redshift estimate, where it is worth highlighting that finding redshift of BL Lac objects is extremely challenging due to the relatively weak spectral features in the optical spectra that in most of the cases appear featureless. All results of the optical spectroscopic campaign are summarized in Table 3.8, published in the works of our campaign that I participated (Peña-Herazo et al., 2019, 2017; de Menezes et al., 2019, 2020; Marchesini et al., 2019), those works of previous years (Álvarez Crespo et al., 2016c,b; Massaro et al., 2015b; Ricci et al., 2015; Landoni et al., 2015b; Paggi et al., 2014), and summarized recently on Peña-Herazo et al. (2020b).

I also searched for other groups' works presenting optical spectra of sources listed in the *Fermi*-LAT catalogs as UGSs or BCUs. According to my search, I found 123 blazars, 23 known blazars listed in the latest release of the Roma-BZCAT, and 19 targets collected from data available in the SDSS or the 6dF surveys while all the remaining ones newly discovered. I presented these results on Peña-Herazo et al (2020a), submitted to A&A.

As presented here, the second part of my thesis was entirely devoted to the 1^{st} release of the Turin-SyCAT, a catalog of Seyfert galaxies, homogeneously selected by their multifrequency properties and statically clean. This catalog lists 571 Seyferts, divided in 412 type 1s and 159 type 2s, in a redshift range of $0.001 < z < 0.4$, see Figure 4.3 for their redshift distribution whereas all sources listed therein have a published spectrum in the literature that we examined. I submitted the Turin-SyCAT

the 1^{st} release to publication on Astronomy and Astrophysics journal (Peña-Herazo et al. 2020b).

Studying the statistical properties of this catalog, I found a clear distinction between the two types of Seyfert galaxies using their $u-r$ color. We expected when considering their continuum spectral differences, where type 1s are considerably bluer than type 2s. I also found that mid-IR colors of type 1 Seyfert galaxies are more concentrated in the W1-W2 vs. W2-W3 color-color diagram concerning those of Seyfert 2 galaxies. Then comparing the Turin-SyCAT sample with blazar using mid-IR colors, I noticed a similarity of blazars and type 1 Seyferts and a similar behavior between type 2 Seyferts and quasars. These similarities barely contaminate blazar catalogs selected by infrared colors, since blazars are all radio-loud sources; thus, they can be neatly distinguished by their fraction of optical or infrared flux density to the radio-frequencies one. These results are part of the Turin-SyCAT publication, Peña-Herazo et al. (2020b).

Using Turin-SyCAT, I discovered a significant correlation between mid-IR fluxes at both 12 and 22μm (i.e., F_{12} and F_{22}, respectively) and hard X-ray fluxes between 15 and 150 keV. Both Seyfert classes appear to follow the same trend and share similar values of the ratio between F_{12} and F_{22} over F_{HX} in agreement with expectations of the AGN unification scenario. For SyCAT sources with a counterpart in the IRAS Point Source Catalog, we did not find any trend by comparing their far-IR fluxes and hard X-ray ones, implying that the cold dust emission at IRAS wavelengths is not dominated by the reprocessed emission of the central AGN by the dust torus. These multifrequency statistical analysis are part of the article on the 1^{st} release of the Turin-SyCAT, Peña-Herazo et al (2020b).

Followed by the creation of the Turin-SyCAT, we studied the large-scale environment of Seyfert galaxies. We did it using a statistical method based on the so-called cosmological neighbors. I found similarities in the environment up to 2 Mpc of type 1 and 2 Seyferts, supporting the unification scenario of AGNs for this radio-quiet class of sources. I also compared the Seyfert population's environment with one of the radio galaxies and found that the environment if the latter class is significantly richer than of the Seyferts. I conclude that in agreement with the predictions of the unification scenario type 1 and type 2 Seyfert galaxies live in the same large-scale environments thus confirming that their differences could be mainly ascribed to a different orientation of the central nucleus with respect to the line of sight. Then richer environments of radio galaxies compared to that of Seyfert galaxies is indeed in agreement with the expectations of their host galaxies, i.e., elliptical vs. spirals. These results are part of a publication I led and submitted to Astronomy and Astrophysics journal (Peña-Herazo et al 2020c).

Our observational campaign is still ongoing; we recently acquired an additional 62 spectra. Considering new observing runs already awarded to our group and considering the efficiency of how we acquired data to date, we expect to release results for an additional $\sim$ 500 targets by around 2022.

As future perspectives, I will continue using the Turin-SyCAT to search for heavily obscured Seyfert galaxies among unidentified hard X-ray sources given the correlation

discovered between their mid-IR and hard X-ray flux density. Then I will explore the possibility to investigate the large scale environments of Seyfert galaxies as a function of other parameters as emission line luminosity to search for possible differences. I am also starting the 2^{nd} release of the Turin-SyCAT, planned for the end of 2021, doubling the number of Seyfert galaxies listed therein. Finally, regarding blazars, I am investigating their optical spectral properties for those listed and observed thanks to the LAMOST survey.

Appendix A

List of Publications

2017

1. *Optical spectroscopic observations of gamma-ray blazar candidates. VII. Follow-up campaign in the southern hemisphere.*

   Peña-Herazo, H. A., Marchesini, E. J., Álvarez Crespo, N., Ricci, F., Massaro, F., Chavushyan, V., Landoni, M., Strader, J., Chomiuk, L., Cheung, C. C., Masetti, N., Jiménez-Bailón, E., D'Abrusco, R., Paggi, A., Milisavljevic, D., La Franca, F., Smith, H. A., & Tosti, G. (2017), Ap&SS, 362, 228.

2018

2. *Fermi Transient J1544-0649: A Flaring Radio-weak BL Lac.*

   Bruni, G., Panessa, F., Ghisellini, G., Chavushyan, V., **Peña-Herazo, H. A.**, Hernández-García, L., Bazzano, A., Ubertini, P., & Kraus, A. (2018), ApJ, 854, L23. 2018ApJ...854L..23B

2019

3. *Optical spectroscopic observations of gamma-ray blazar candidates VIII: the 2016-2017 follow up campaign carried out at SPM, NOT, KPNO and SOAR telescopes.*

   Marchesini, E. J.,**Peña-Herazo, H. A.**, Álvarez Crespo, N., Ricci, F., Negro, M., Milisavljevic, D., Massaro, F., Masetti, N., Landoni, M., Chavushyan, V., D'Abrusco, R., Jiménez-Bailón, E., La Franca, F., Paggi, A., Smith, H. A., & Tosti, G. (2019), Ap&SS, 364, 5.

4. *Optical spectroscopic observations of gamma-ray blazar candidates. IX. Optical archival spectra and further observations from SOAR and OAGH.*

   Peña-Herazo, H. A., Massaro, F., Chavushyan, V., Marchesini, E. J., Paggi, A., Landoni, M., Masetti, N., Ricci, F., D'Abrusco, R., Milisavljevic, D., Jiménez-Bailón, E., La Franca, F., Smith, H. A., & Tosti, G. (2019), Ap&SS, 364, 85.

5. *Optical characterization of WISE selected blazar candidates.*

   de Menezes, R., **Peña-Herazo, H. A.**, Marchesini, E. J., D'Abrusco, R., Masetti, N., Nemmen, R., Massaro, F., Ricci, F., Landoni, M., Paggi, A., & Smith, H. A. (2019), A&A, 630, A55.

2020

6. *Optical spectroscopic observations of gamma-ray blazar candidates. X. Results from the 2018-2019 SOAR and OAN-SPM observations of blazar candidates of uncertain type.*

   de Menezes, R., Amaya-Almazán, R. A., Marchesini, E. J., **Peña-Herazo, H. A.**, Massaro, F., Chavushyan, V., Paggi, A., Landoni, M., Masetti, N., Ricci, F., D'Abrusco, R., La Franca, F., Smith, H. A., Milisavljevic, D., Tosti, G., Jiménez-Bailón, E., & Cheung, C. C. (2020), Ap&SS, 365, 12. 2020Ap&SS.365...12D

7. *Fermi Large Area Telescope Fourth Source Catalog.*

   Abdollahi, S., Acero, F., Ackermann, M., Ajello, M., Atwood, W. B., Axelsson, M., Baldini, L., Ballet, J., Barbiellini, G., Bastieri, D., Becerra Gonzalez, J., Bellazzini, R., Berretta, A., Bissaldi, E., Blandford, R. D., Bloom, E. D., Bonino, R., Bottacini, E., Brandt, T. J., Bregeon, J., Bruel, P., Buehler, R., Burnett, T. H., Buson, S., Cameron, R. A., Caputo, R., Caraveo, P. A., Casandjian, J. M., Castro, D., Cavazzuti, E., Charles, E., Chaty, S., Chen, S., Cheung, C. C., Chiaro, G., Ciprini, S., Cohen-Tanugi, J., Cominsky, L. R., Coronado-Blázquez, J., Costantin, D., Cuoco, A., Cutini, S., D'Ammando, F., DeKlotz, M., Torre Luque, P. de . la ., de Palma, F., Desai, A., Digel, S. W., Lalla, N. D., Mauro, M. D., Venere, L. D., Domínguez, A., Dumora, D., Dirirsa, F. F., Fegan, S. J., Ferrara, E. C., Franckowiak, A., Fukazawa, Y., Funk, S., Fusco, P., Gargano, F., Gasparrini, D., Giglietto, N., Giommi, P., Giordano, F., Giroletti, M., Glanzman, T., Green, D., Grenier, I. A., Griffin, S., Grondin, M.-H., Grove, J. E., Guiriec, S., Harding, A. K., Hayashi, K., Hays, E., Hewitt, J. W., Horan, D., Jóhannesson, G., Johnson, T. J., Kamae, T., Kerr, M., Kocevski, D., Kovac'evic', M., Kuss, M., Landriu, D., Larsson, S., Latronico, L., Lemoine-Goumard, M., Li, J., Liodakis, I., Longo, F., Loparco, F., Lott, B., Lovellette, M. N., Lubrano, P., Madejski, G. M., Maldera, S., Malyshev, D., Manfreda, A., Marchesini, E. J., Marcotulli, L., Martí-Devesa, G., Martin, P., Massaro, F., Mazziotta, M. N., McEnery, J. E., Mereu, I., Meyer, M., Michelson, P. F., Mirabal, N., Mizuno, T., Monzani, M. E., Morselli, A., Moskalenko, I. V., Negro, M., Nuss, E., Ojha, R., Omodei, N., Orienti, M., Orlando, E., Ormes, J. F., Palatiello, M., Paliya, V. S., Paneque, D., Pei, Z., **Peña-Herazo, H.** , Perkins, J. S., Persic, M., Pesce-Rollins, M., Petrosian, V., Petrov, L., Piron, F., Poon, H., Porter, T. A., Principe, G., Rainò, S., Rando, R., Razzano, M., Razzaque, S., Reimer, A., Reimer, O., Remy, Q., Reposeur, T., Romani, R. W., Parkinson, P. M. S., Schinzel, F. K., Serini, D., Sgrò, C., Siskind, E. J., Smith, D. A., Spandre, G., Spinelli, P., Strong, A. W., Suson, D. J., Tajima, H., Takahashi, M. N., Tak, D., Thayer, J. B., Thompson,

D. J., Tibaldo, L., Torres, D. F., Torresi, E., Valverde, J., Klaveren, B. V., Zyl, P. van ., Wood, K., Yassine, M., & Zaharijas, G. (2020), ApJ, 247, 33. 2020ApJS..247...33A

8. *The Fourth Catalog of Active Galactic Nuclei Detected by the Fermi Large Area Telescope.*

   Ajello, M., Angioni, R., Axelsson, M., Ballet, J., Barbiellini, G., Bastieri, D., Becerra Gonzalez, J., Bellazzini, R., Bissaldi, E., Bloom, E. D., Bonino, R., Bottacini, E., Bruel, P., Buson, S., Cafardo, F., Cameron, R. A., Cavazzuti, E., Chen, S., Cheung, C. C., Ciprini, S., Costantin, D., Cutini, S., D'Ammando, F., de la Torre Luque, P., de Menezes, R., de Palma, F., Desai, A., Di Lalla, N., Di Venere, L., Domínguez, A., Dirirsa, F. F., Ferrara, E. C., Finke, J., Franckowiak, A., Fukazawa, Y., Funk, S., Fusco, P., Gargano, F., Garrappa, S., Gasparrini, D., Giglietto, N., Giordano, F., Giroletti, M., Green, D., Grenier, I. A., Guiriec, S., Harita, S., Hays, E., Horan, D., Itoh, R., Jóhannesson, G., Kovac'evic', M., Krauss, F., Kreter, M., Kuss, M., Larsson, S., Leto, C., Li, J., Liodakis, I., Longo, F., Loparco, F., Lott, B., Lovellette, M. N., Lubrano, P., Madejski, G. M., Maldera, S., Manfreda, A., Martí-Devesa, G., Massaro, F., Mazziotta, M. N., Mereu, I., Meyer, M., Migliori, G., Mirabal, N., Mizuno, T., Monzani, M. E., Morselli, A., Moskalenko, I. V., Negro, M., Nemmen, R., Nuss, E., Ojha, L. S., Ojha, R., Omodei, N., Orienti, M., Orlando, E., Ormes, J. F., Paliya, V. S., Pei, Z., **Peña-Herazo, H.***, Persic, M., Pesce-Rollins, M., Petrov, L., Piron, F., Poon, H., Principe, G., Rainò, S., Rando, R., Rani, B., Razzano, M., Razzaque, S., Reimer, A., Reimer, O., Schinzel, F. K., Serini, D., Sgrò, C., Siskind, E. J., Spandre, G., Spinelli, P., Suson, D. J., Tachibana, Y., Thompson, D. J., Torres, D. F., Torresi, E., Troja, E., Valverde, J., van Zyl, P., & Yassine, M. (2020), ApJ, 892, 105. 2020ApJ...892..105A

   *** As corresponding author.**

9. *Optical spectroscopic observations of low-energy counterparts of Fermi-LAT γ-ray sources*

   Peña-Herazo, H. A., Amaya-Almazán, R. A., Massaro, F., de Menezes, R., Marchesini, E. J., Chavushyan, V., Paggi, A., Landoni, M., Masetti, N., Ricci, F., D'Abrusco, R., Cheung, C.C., La Franca, F., Smith, H. A., Milisavljevic, D., Jiménez-Bailón, E., Patiño-Álvarez, V. M., Tosti, G. (2020), Submitted to A&A

10. *Turin-SyCAT: a multifrequency catalogue of Seyfert Galaxies*

    Peña-Herazo, H. A., Massaro, F., Chavushyan, V., Masetti, N., Paggi, A., Capetti, A. (2020), Submitted to A&A

11. *On the Large-Scale Environment of Seyfert Galaxies*

    Peña-Herazo, H. A., Massaro, F., Capetti, A., Chavushyan, V., Masetti, N., Paggi, A., (2020), Submitted to A&A

Astrophys Space Sci (2017) 362:228
DOI 10.1007/s10509-017-3208-7

ORIGINAL ARTICLE

Optical spectroscopic observations of gamma-ray blazar candidates. VII. Follow-up campaign in the southern hemisphere

H.A. Peña-Herazo[1,2,3] · E.J. Marchesini[1,2,4,5,6] · N. Álvarez Crespo[1,2] · F. Ricci[7] · F. Massaro[1,2] · V. Chavushyan[3] · M. Landoni[8] · J. Strader[9] · L. Chomiuk[9] · C.C. Cheung[10] · N. Masetti[6,11] · E. Jiménez-Bailón[12] · R. D'Abrusco[13] · A. Paggi[14] · D. Milisavljevic[14] · F. La Franca[7] · H.A. Smith[14] · G. Tosti[15]

Received: 28 July 2017 / Accepted: 11 November 2017 / Published online: 21 November 2017

Abstract Searching for low energy counterparts of γ-rays sources is one of the major challenges in modern γ-ray astronomy. In the third Fermi source catalog about 30% of detected sources are unidentified/unassociated Gamma-ray Sources (UGSs). We recently started an optical spectroscopic follow up campaign to confirm the blazar-like nature of candidates counterparts of UGSs. Here we report the spectra of *61* targets collected with the Southern Astrophysical Research Telescope (SOAR) between 2014 and the 2017. Our sample includes *33* potential counterparts of UGSs, selected on the basis of WISE colors, and *27* blazar candidates of uncertain type associated with gamma-ray sources of the last release of the Fermi catalog. We confirm the BZB nature of *20* sources lying within the positional uncertainty region of the UGSs. All the observed BCUs show blazar-like spectra, classified as 2 BZQs and *25* BZBs, for which we obtained 6 redshift estimates. Within the BCUs observations we report the redshift estimate for the BZB associated with, 3FGL J1106.4-3643 that is the second most distant BL Lac known to date, at $z \geq 1.084$.

Keywords Galaxies: active · Galaxies: BL Lacertae objects · Quasars: general

1 Introduction

Since the first release of the source catalog based on observations of the Energetic Gamma Ray Experiment Telescope (EGRET) (Fichtel et al. 1994), the nature of unidentified/unassociated gamma-ray sources (UGS) was under debate. With greater effective area and better angular resolution than previous γ-ray satellites, the Large Area Telescope (LAT), onboard of the Fermi Gamma-ray Space Telescope

H.A. Peña-Herazo
harold.penaherazo@edu.unito.it

1 Dipartimento di Fisica, Università degli Studi di Torino, via Pietro Giuria 1, 10125 Torino, Italy

2 Istituto Nazionale di Fisica Nucleare, Sezione di Torino, 10125 Torino, Italy

3 Instituto Nacional de Astrofísica, Óptica y Electrónica, Apartado Postal 51-216, 72840 Puebla, Mexico

4 Facultad de Ciencias Astronómicas y Geofísicas, Universidad Nacional de La Plata, Paseo del Bosque, B1900FWA La Plata, Argentina

5 Instituto de Astrofísica de La Plata, CONICET-UNLP, CCT La Plata, Paseo del Bosque S/N, B1900FWA La Plata, Argentina

6 INAF-Istituto di Astrofisica Spaziale e Fisica Cosmica di Bologna, via Gobetti 101, 40129 Bologna, Italy

7 Dipartimento di Matematica e Fisica, Università Roma Tre, via della Vasca Navale 84, 00146 Roma, Italy

8 INAF-Osservatorio Astronomico di Brera, Via Emilio Bianchi 46, 23807 Merate, Italy

9 Center for Data Intensive and Time Domain Astronomy, Department of Physics and Astronomy, Michigan State University, East Lansing, MI 48824, USA

10 Space Science Division, Naval Research Laboratory, Washington, DC 20375-5352, USA

11 Departamento de Ciencias Físicas, Universidad Andrés Bello, Fernández Concha 700, Las Condes, Santiago, Chile

12 Instituto de Astronomía, Universidad Nacional Autónoma de México, Apdo. Postal 877, Ensenada, 22800 Baja California, Mexico

13 Department of Physical Sciences, University of Napoli Federico II, via Cinthia 9, 80126 Napoli, Italy

14 Harvard-Smithsonian Center for Astrophysics, 60 Garden Street, Cambridge, MA 02138, USA

15 Dipartimento di Fisica, Università degli Studi di Perugia, 06123 Perugia, Italy

Astrophys Space Sci (2019) 364:85
https://doi.org/10.1007/s10509-019-3574-4

ORIGINAL ARTICLE

Optical spectroscopic observations of gamma-ray blazar candidates. IX. Optical archival spectra and further observations from SOAR and OAGH

H.A. Peña-Herazo[1,2,3] · F. Massaro[2,3,4,5] · V. Chavushyan[1] · E.J. Marchesini[2,3,6,7,8] · A. Paggi[2,3,4,5] · M. Landoni[9] · N. Masetti[8,10] · F. Ricci[11] · R. D'Abrusco[12] · D. Milisavljevic[12,13] · E. Jiménez-Bailón[14] · F. La Franca[15] · Howard A. Smith[12] · G. Tosti[16]

Received: 20 December 2018 / Accepted: 29 April 2019

Abstract Nearly one third of the sources in the *Fermi*-LAT catalogs lacks a lower energy counterpart, hence being referred as unidentified/unassociated gamma-ray sources (UGSs). In order to firmly classify them, dedicated multifrequency follow-up campaigns are necessary. These will permit to unveil their nature and identify the fraction that could belong to the class of active galaxies known as blazars that is the largest population of extragalactic γ-ray sources. In Fermi-LAT catalogs there are also gamma-ray sources associated with multifrequency blazar-like objects known as Blazars Candidates of Uncertain type (i.e., BCUs) for which follow up spectroscopic campaigns are mandatory to confirm their blazar nature. Thus, in 2013 we started an optical spectroscopic campaign to identify blazar-like objects potential counterparts of UGSs and BCUs. Here we report the spectra of 31 additional targets observed as part of our follow up campaign. Thirteen of them are BCUs for which we acquired spectroscopic observations at Observatorio Astrofísico Guillermo Haro (OAGH) and at Southern Astrophysical Research Observatory (SOAR) telescopes, while the rest has been identified thanks to the archival observations available from the Sloan Digital Sky Survey (SDSS). We confirm the blazar nature of all BCUs: three of them are in blazar of quasar type (BZQs) while the remaining ones can be spectroscopically classified as BL Lac objects (BZBs). Then we also discovered 18 BL Lac objects lying within the positional uncertainty regions of UGSs that could be their potential counterparts.

Keywords Galaxies: active · Galaxies: BL Lacertae objects · Quasars: general · Surveys · Radiation mechanisms: non-thermal

H.A. Peña-Herazo
harold.penaherazo@edu.unito.it

1 Instituto Nacional de Astrofísica, Óptica y Electrónica, Apartado Postal 51-216, 72000 Puebla, Mexico

2 Dipartimento di Fisica, Università degli Studi di Torino, via Pietro Giuria 1, 10125 Torino, Italy

3 Istituto Nazionale di Fisica Nucleare, Sezione di Torino, 10125 Torino, Italy

4 INAF-Osservatorio Astrofisico di Torino, via Osservatorio 20, 10025 Pino Torinese, Italy

5 Consorzio Interuniversitario per la Fisica Spaziale (CIFS), via Pietro Giuria 1, 10125 Torino, Italy

6 Facultad de Ciencias Astronómicas y Geofísicas, Universidad Nacional de La Plata, La Plata, Argentina

7 Instituto de Astrofísica de La Plata, CONICET-UNLP, CCT La Plata, La Plata, Argentina

8 INAF – Osservatorio di Astrofisica e Scienza dello Spazio, via Gobetti 93/3, 40129 Bologna, Italy

9 INAF – Osservatorio Astronomico di Brera, Via Emilio Bianchi 46, 23807 Merate, Italy

10 Departamento de Ciencias Físicas, Universidad Andrés Bello, Fernández Concha 700, Las Condes, Santiago, Chile

11 Instituto de Astrofísica and Centro de Astroingeniería, Facultad de Física, Pontificia Universidad Catolica de Chile, Casilla 306, Santiago 22, Chile

12 Center for Astrophysics | Harvard & Smithsonian, 60 Garden Street, Cambridge, MA 02138, USA

13 Department of Physics and Astronomy, Purdue University, 525 Northwestern Avenue, West Lafayette, IN 47907, USA

14 Instituto de Astronomía, Universidad Nacional Autónoma de México, Apdo. Postal 877, Ensenada, 22800 Baja California, Mexico

15 Dipartimento di Matematica e Fisica, Università Roma Tre, via della Vasca Navale 84, 00146 Roma, Italy

16 Dipartimento di Fisica, Università degli Studi di Perugia, 06123 Perugia, Italy

Published online: 10 May 2019

The Astrophysical Journal, 892:105 (23pp), 2020 April 1 https://doi.org/10.3847/1538-4357/ab791e

The Fourth Catalog of Active Galactic Nuclei Detected by the *Fermi* Large Area Telescope

M. Ajello[1], R. Angioni[2,3], M. Axelsson[4,5], J. Ballet[6], G. Barbiellini[7,8], D. Bastieri[9,10], J. Becerra Gonzalez[11], R. Bellazzini[12], E. Bissaldi[13,14], E. D. Bloom[15], R. Bonino[16,17], E. Bottacini[15,18], P. Bruel[19], S. Buson[20], F. Cafardo[21], R. A. Cameron[15], E. Cavazzuti[22], S. Chen[9,18], C. C. Cheung[23], S. Ciprini[3,2], D. Costantin[24], S. Cutini[25], F. D'Ammando[26], P. de la Torre Luque[13], R. de Menezes[17,21], F. de Palma[16], A. Desai[1], N. Di Lalla[15], L. Di Venere[13,14], A. Domínguez[27], F. Fana Dirirsa[28], E. C. Ferrara[29], J. Finke[23], A. Franckowiak[30], Y. Fukazawa[31], S. Funk[32], P. Fusco[13,14], F. Gargano[14], S. Garrappa[30], D. Gasparrini[2,3], N. Giglietto[13,14], F. Giordano[13,14], M. Giroletti[26], D. Green[33], I. A. Grenier[6], S. Guiriec[29,34], S. Harita[35], E. Hays[29], D. Horan[19], R. Itoh[36], G. Jóhannesson[37,38], M. Kovac'evic'[25], F. Krauss[39], M. Kreter[20,40], M. Kuss[12], S. Larsson[5,41,42], C. Leto[2], J. Li[30], I. Liodakis[15], F. Longo[7,8], F. Loparco[13,14], B. Lott[43], M. N. Lovellette[23], P. Lubrano[25], G. M. Madejski[15], S. Maldera[16], A. Manfreda[44], G. Martí-Devesa[45], F. Massaro[16,17,46], M. N. Mazziotta[14], I. Mereu[25,47], M. Meyer[32], G. Migliori[48,49], N. Mirabal[29,50], T. Mizuno[51], M. E. Monzani[15], A. Morselli[3], I. V. Moskalenko[15], M. Negro[50,52], R. Nemmen[21], E. Nuss[53], L. S. Ojha[29], R. Ojha[29], N. Omodei[15], M. Orienti[26], E. Orlando[15,54], J. F. Ormes[55], V. S. Paliya[30], Z. Pei[10], H. Peña-Herazo[16,17,46,56], M. Persic[7,57], M. Pesce-Rollins[12], L. Petrov[29], F. Piron[53], H. Poon[31], G. Principe[26], S. Rainò[13,14], R. Rando[9,18,58], B. Rani[29,59], M. Razzano[12,71], S. Razzaque[28], A. Reimer[15,45], O. Reimer[45], F. K. Schinzel[60,61], D. Serini[13], C. Sgrò[12], E. J. Siskind[62], G. Spandre[12], P. Spinelli[13,14], D. J. Suson[63], Y. Tachibana[35], D. J. Thompson[29], D. F. Torres[64,65], E. Torresi[66], E. Troja[29,67], J. Valverde[19], P. van Zyl[68,69,70], and M. Yassine[7,8]

[1] Department of Physics and Astronomy, Clemson University, Kinard Lab of Physics, Clemson, SC 29634-0978, USA
[2] Space Science Data Center—Agenzia Spaziale Italiana, Via del Politecnico, snc, I-00133, Roma, Italy; stefano.ciprini.asdc@gmail.com
[3] Istituto Nazionale di Fisica Nucleare, Sezione di Roma "Tor Vergata," I-00133 Roma, Italy; dario.gasparrini@ssdc.asi.it
[4] Department of Physics, Stockholm University, AlbaNova, SE-106 91 Stockholm, Sweden
[5] Department of Physics, KTH Royal Institute of Technology, AlbaNova, SE-106 91 Stockholm, Sweden
[6] AIM, CEA, CNRS, Université Paris-Saclay, Université Paris Diderot, Sorbonne Paris Cité, F-91191 Gif-sur-Yvette, France
[7] Istituto Nazionale di Fisica Nucleare, Sezione di Trieste, I-34127 Trieste, Italy
[8] Dipartimento di Fisica, Università di Trieste, I-34127 Trieste, Italy
[9] Istituto Nazionale di Fisica Nucleare, Sezione di Padova, I-35131 Padova, Italy
[10] Dipartimento di Fisica e Astronomia "G. Galilei," Università di Padova, I-35131 Padova, Italy
[11] Instituto de Astrofísica de Canarias, Observatorio del Teide, C/Via Lactea, s/n, E-38205, La Laguna, Tenerife, Spain
[12] Istituto Nazionale di Fisica Nucleare, Sezione di Pisa, I-56127 Pisa, Italy
[13] Dipartimento di Fisica "M. Merlin" dell'Università e del Politecnico di Bari, via Amendola 173, I-70126 Bari, Italy
[14] Istituto Nazionale di Fisica Nucleare, Sezione di Bari, I-70126 Bari, Italy
[15] W. W. Hansen Experimental Physics Laboratory, Kavli Institute for Particle Astrophysics and Cosmology, Department of Physics and SLAC National Accelerator Laboratory, Stanford University, Stanford, CA 94305, USA
[16] Istituto Nazionale di Fisica Nucleare, Sezione di Torino, I-10125 Torino, Italy
[17] Dipartimento di Fisica, Università degli Studi di Torino, I-10125 Torino, Italy
[18] Department of Physics and Astronomy, University of Padova, Vicolo Osservatorio 3, I-35122 Padova, Italy
[19] Laboratoire Leprince-Ringuet, École polytechnique, CNRS/IN2P3, F-91128 Palaiseau, France
[20] Institut für Theoretische Physik and Astrophysik, Universität Würzburg, D-97074 Würzburg, Germany
[21] Instituto de Astronomia, Geofísica e Ciências Atmosféricas, Universidade de São Paulo, Rua do Matão, 1226, São Paulo—SP 05508-090, Brazil
[22] Italian Space Agency, Via del Politecnico snc, I-00133 Roma, Italy
[23] Space Science Division, Naval Research Laboratory, Washington, DC 20375-5352, USA
[24] University of Padua, Department of Statistical Science, Via 8 Febbraio, 2, I-35122, Padova, Italy
[25] Istituto Nazionale di Fisica Nucleare, Sezione di Perugia, I-06123 Perugia, Italy
[26] INAF Istituto di Radioastronomia, I-40129 Bologna, Italy
[27] Grupo de Altas Energías, Universidad Complutense de Madrid, E-28040 Madrid, Spain
[28] Department of Physics, University of Johannesburg, P.O. Box 524, Auckland Park 2006, South Africa
[29] NASA Goddard Space Flight Center, Greenbelt, MD 20771, USA
[30] Deutsches Elektronen Synchrotron DESY, D-15738 Zeuthen, Germany
[31] Department of Physical Sciences, Hiroshima University, Higashi-Hiroshima, Hiroshima 739-8526, Japan
[32] Friedrich-Alexander Universität Erlangen-Nürnberg, Erlangen Centre for Astroparticle Physics, Erwin-Rommel-Str. 1, D-91058 Erlangen, Germany
[33] Max-Planck-Institut für Physik, D-80805 München, Germany
[34] The George Washington University, Department of Physics, 725 21st St, NW, Washington, DC 20052, USA
[35] Department of Physics, Tokyo Institute of Technology, Meguro City, Tokyo 152-8551, Japan
[36] Bisei Astronomical Observatory, 1723-70 Ookura, Bisei-cho, Ibara, Okayama 714-1411, Japan
[37] Science Institute, University of Iceland, IS-107 Reykjavik, Iceland
[38] Nordita, Royal Institute of Technology and Stockholm University, Roslagstullsbacken 23, SE-106 91 Stockholm, Sweden
[39] Department of Astronomy and Astrophysics, Pennsylvania State University, University Park, PA 16802, USA
[40] Centre for Space Research, North-West University, Potchefstroom Campus, Private Bag X6001, Potchefstroom 2520, South Africa
[41] The Oskar Klein Centre for Cosmoparticle Physics, AlbaNova, SE-106 91 Stockholm, Sweden
[42] School of Education, Health and Social Studies, Natural Science, Dalarna University, SE-791 88 Falun, Sweden
[43] Centre d'Études Nucléaires de Bordeaux Gradignan, Université de Bordeaux, IN2P3/CNRS, F-33175 Gradignan Cedex, France; lott@cenbg.in2p3.fr
[44] Università di Pisa and Istituto Nazionale di Fisica Nucleare, Sezione di Pisa I-56127 Pisa, Italy
[45] Institut für Astro- und Teilchenphysik, Leopold-Franzens-Universität Innsbruck, A-6020 Innsbruck, Austria
[46] Istituto Nazionale di Astrofisica-Osservatorio Astrofisico di Torino, via Osservatorio 20, I-10025 Pino Torinese, Italy
[47] Dipartimento di Fisica, Università degli Studi di Perugia, I-06123 Perugia, Italy

[48] Dipartimento di Astronomia, Università di Bologna, I-40127 Bologna, Italy
[49] Università di Bologna, I-40126 Bologna, Italy
[50] Department of Physics and Center for Space Sciences and Technology, University of Maryland Baltimore County, Baltimore, MD 21250, USA
[51] Hiroshima Astrophysical Science Center, Hiroshima University, Higashi-Hiroshima, Hiroshima 739-8526, Japan
[52] Center for Research and Exploration in Space Science and Technology (CRESST) and NASA Goddard Space Flight Center, Greenbelt, MD 20771, USA
[53] Laboratoire Univers et Particules de Montpellier, Université Montpellier, CNRS/IN2P3, F-34095 Montpellier, France
[54] Istituto Nazionale di Fisica Nucleare, Sezione di Trieste, and Università di Trieste, I-34127 Trieste, Italy
[55] Department of Physics and Astronomy, University of Denver, Denver, CO 80208, USA
[56] Instituto Nacional de Astrofísica, Óptica y Electrónica, Tonantzintla, Puebla 72840, Mexico; harold.penah@gmail.com
[57] Osservatorio Astronomico di Trieste, Istituto Nazionale di Astrofisica, I-34143 Trieste, Italy
[58] Center for Space Studies and Activities "G. Colombo," University of Padova, Via Venezia 15, I-35131 Padova, Italy
[59] Korea Astronomy and Space Science Institute, 776 Daedeokdae-ro, Yuseong-gu, Daejeon 305-348, Republic of Korea
[60] National Radio Astronomy Observatory, 1003 Lopezville Road, Socorro, NM 87801, USA
[61] University of New Mexico, MSC07 4220, Albuquerque, NM 87131, USA
[62] NYCB Real-Time Computing Inc., Lattingtown, NY 11560-1025, USA
[63] Purdue University Northwest, Hammond, IN 46323, USA
[64] Institute of Space Sciences (CSICIEEC), Campus UAB, Carrer de Magrans s/n, E-08193 Barcelona, Spain
[65] Institució Catalana de Recerca i Estudis Avançats (ICREA), E-08010 Barcelona, Spain
[66] INAF-Istituto di Astrofisica Spaziale e Fisica Cosmica Bologna, via P. Gobetti 101, I-40129 Bologna, Italy
[67] Department of Astronomy, University of Maryland, College Park, MD 20742, USA
[68] Hartebeesthoek Radio Astronomy Observatory, P.O. Box 443, Krugersdorp 1740, South Africa
[69] School of Physics, University of the Witwatersrand, Private Bag 3, WITS-2050, Johannesburg, South Africa
[70] Square Kilometre Array South Africa, Pinelands, 7405, South Africa
Received 2020 January 9; revised 2020 February 15; accepted 2020 February 17; published 2020 April 2

Abstract

The fourth catalog of active galactic nuclei (AGNs) detected by the *Fermi Gamma-ray Space Telescope* Large Area Telescope (4LAC) between 2008 August 4 and 2016 August 2 contains 2863 objects located at high Galactic latitudes ($|b| > 10^{\circ}$). It includes 85% more sources than the previous 3LAC catalog based on 4 yr of data. AGNs represent at least 79% of the high-latitude sources in the fourth *Fermi*-Large Area Telescope Source Catalog (4FGL), which covers the energy range from 50 MeV to 1 TeV. In addition, 344 gamma-ray AGNs are found at low Galactic latitudes. Most of the 4LAC AGNs are blazars (98%), while the remainder are other types of AGNs. The blazar population consists of 24% Flat Spectrum Radio Quasars (FSRQs), 38% BL Lac-type objects, and 38% blazar candidates of unknown types (BCUs). On average, FSRQs display softer spectra and stronger variability in the gamma-ray band than BL Lacs do, confirming previous findings. All AGNs detected by ground-based atmospheric Cerenkov telescopes are also found in the 4LAC.

Unified Astronomy Thesaurus concepts: Active galactic nuclei (16); Blazars (164); Gamma-ray sources (633); Relativistic jets (1390); Quasars (1319); BL Lacertae objects (158)

Supporting material: machine-readable tables

1. Introduction

Thanks to its broad energy range, excellent sensitivity, and all-sky monitoring capabilities, the *Fermi Gamma-ray Space Telescope* Large Area Telescope (LAT) has revolutionized our view of the gamma-ray sky. The fourth *Fermi*-LAT source catalog (4FGL, The Fermi-LAT collaboration 2020), based on the first 8 yr of data from the mission, contains 5064 sources in the energy range 50 MeV to 1 TeV.

The fourth catalog of active galactic nuclei (AGNs) detected by the LAT (4LAC), presented here, is derived from the 4FGL catalog. At high Galactic latitudes, AGNs represent by far the dominant class of gamma-ray sources in the 4FGL. The vast majority of these AGNs are of the blazar type, which are characterized by having relativistic jets closely aligned with our line of sight. The two main classes of blazars are Flat Spectrum Radio Quasars (FSRQs) and BL Lac-type objects (BL Lacs), distinguished according to the strength of their optical emission lines. FSRQs have strong, broad emission lines, while BL Lacs have weak, narrow, or no such lines. In addition to the improvements of the 4FGL relative to previous gamma-ray catalogs, the 4LAC has benefited from updated methods of associating gamma-ray AGNs with those known at other wavelengths. The 4LAC supersedes the third catalog of AGNs detected by the LAT (3LAC; Ackermann et al. 2015), which was based on 4 yr of data.

Gamma-ray AGN catalogs constitute unique resources for a broad range of astrophysics research. Recent applications include: population studies probing the BL Lac-FSRQ dichotomy (e.g., Ghisellini et al. 2017; Nalewajko & Gupta 2017); works on individual sources investigating the connections between gamma-ray loudness and brightness/polarization at other observational bands (e.g., Angelakis et al. 2016; Lico et al. 2017; Massaro et al. 2017; Fan & Wu 2018; Zargaryan et al. 2018); timing correlations between activity in the gamma-ray band and other wavelengths (e.g., Fuhrmann et al. 2016; Itoh et al. 2016); and tests of the possible link between gamma-ray AGNs and sources of ultra high-energy cosmic rays (e.g., Kagaya et al. 2017) or high-energy neutrinos (e.g., Padovani et al. 2016; Aartsen et al. 2017; Garrappa et al. 2019). These catalogs also enable probes of the extragalactic background light (EBL; e.g., Abdollahi et al. 2018) and the intergalactic magnetic field (e.g., Ackermann et al. 2018; Broderick et al. 2018), along with a measurement of the AGN contribution to the extragalactic diffuse gamma-ray background (e.g., Fornasa et al. 2016; Di Mauro et al. 2018).

The paper is organized as follows. Section 2 briefly describes the observations by the LAT and the analysis employed to

[71] Funded by contract FIRB-2012-RBFR12PM1F from the Italian Ministry of Education, University and Research (MIUR).

Astronomy & Astrophysics manuscript no. optctp_v5.2
July 13, 2020

Optical spectroscopic observations of low-energy counterparts of *Fermi*-LAT γ-ray sources

H. A. Peña-Herazo[1,2,3,4], R. A. Amaya-Almazán[2], F. Massaro[1,3,4,5], R. de Menezes[1,6], E. J. Marchesini[1,4,7,8,9], V. Chavushyan[2], A. Paggi[4,5], M. Landoni[10], N. Masetti[9,11], F. Ricci[12], R. D'Abrusco[13], C.C. Cheung[14], F. La Franca[15], H. A. Smith[13], D. Milisavljevic[16], E. Jiménez-Bailón[17], V. M. Patiño-Álvarez[2,18], and G. Tosti[19]

[1] Dipartimento di Fisica, Università degli Studi di Torino, via Pietro Giuria 1, I-10125 Torino, Italy.
[2] Instituto Nacional de Astrofísica, Óptica y Electrónica, Apartado Postal 51-216, 72000 Puebla, México.
[3] Istituto Nazionale di Fisica Nucleare, Sezione di Torino, I-10125 Torino, Italy.
[4] INAF-Osservatorio Astrofisico di Torino, via Osservatorio 20, 10025 Pino Torinese, Italy.
[5] Consorzio Interuniversitario per la Fisica Spaziale (CIFS), via Pietro Giuria 1, I-10125, Torino, Italy.
[6] Universidade de São Paulo, Departamento de Astronomia, São Paulo, SP 05508-090, Brazil.
[7] Facultad de Ciencias Astronómicas y Geofísicas, Universidad Nacional de La Plata, La Plata, Argentina.
[8] Instituto de Astrofísica de La Plata, CONICET-UNLP, CCT La Plata, La Plata, Argentina.
[9] INAF-Osservatorio di Astrofisica e Scienza dello Spazio, via Gobetti 93/3, I-40129, Bologna, Italy.
[10] INAF-Osservatorio Astronomico di Brera, Via Emilio Bianchi 46, I-23807 Merate, Italy.
[11] Departamento de Ciencias Físicas, Universidad Andrés Bello, Fernández Concha 700, Las Condes, Santiago, Chile.
[12] Instituto de Astrofísica and Centro de Astroingeniería, Facultad de Física, Pontificia Universidad Catolica de Chile, Casilla 306, Santiago 22, Chile.
[13] Harvard Smithsonian Center for Astrophysics, 60 Garden Street, Cambridge, MA 02138, USA.
[14] Naval Research Laboratory, Space Science Division, Code 7650, Washington, DC 20375, USA.
[15] Dipartimento di Matematica e Fisica, Università degli Studi Roma Tre, Via della Vasca Navale 84, I-00146, Roma, Italy.
[16] Department of Physics and Astronomy, Purdue University, 525 Northwestern Avenue, West Lafayette, IN 47907, USA.
[17] Instituto de Astronomía, Universidad Nacional Autónoma de México, Apdo. Postal 877, Ensenada, 22800 Baja California, México.
[18] Max-Planck-Institut für Radioastronomie, Auf dem Hügel 69, 53121 Bonn, Germany.
[19] Dipartimento di Fisica, Università degli Studi di Perugia, 06123 Perugia, Italy.

Received ... ; accepted ...

ABSTRACT

Context. A significant fraction of all γ-ray sources detected by the Large Area Telescope aboard the *Fermi* satellite is still lacking a low-energy counterpart. In addition, there is still a large population of γ-ray sources without a firm classification. In the last 10 years we have undertaken an optical spectroscopic campaign to address the problem of unassociated/unidentified γ-ray sources, mainly devoted to observe blazars and blazar candidates because they are the largest population of γ-ray sources associated to date.
Aims. Here we describe the impact of our optical spectroscopic campaign on the sources associated in *Fermi*-LAT catalogs, coupled with those found in the literature. In the literature search, we kept track of efforts of different teams that presented optical spectra of counterparts or potential counterparts of sources listed in *Fermi*-LAT catalogs. Our summary includes an additional 30 optical spectra of counterparts or potential counterparts of *Fermi*-LAT sources with unknown nature recently collected and analyzed here.
Methods. New spectra were acquired at Blanco 4-m and OAN-SPM 2.1-m telescopes and/or available in the Sloan Digital Sky Survey (data release 15).
Results. All new sources with optical spectra analyzed here are classified as blazars. Then, thanks to our campaign we discovered and classified 394 targets with an additional 123 collected from a literature search. We carried out our optical spectroscopic campaign between the release of the second and the third *Fermi*-LAT source catalog, classifying about 25% of sources with uncertain nature and discovering a blazar-like potential counterpart for ∼10% of UGSs listed therein. In the 1st data release of the 4FGL about 350 *Fermi*-LAT sources are classified to date thanks to our campaign.
Conclusions. The most elusive class of blazars is constituted by BL Lacs since the largest fraction of *Fermi*-LAT sources targeted in our observations showed a featureless optical spectrum. The same occurs among all spectra collected from the literature. Finally, we confirm the high reliability of methods based on mid-IR colors to select blazar-like candidate counterparts of unassociated/unidentified γ-ray sources.

Key words. Galaxies: Active – BL Lacertae objects: general – quasars: emission lines – galaxies: luminosity function

1. Introduction

With the launch in 2008 of the *Fermi* Large Area telescope (*Fermi*-LAT), a new era in the γ-ray astronomy began (Atwood et al. 2009). One of the most challenging key scientific objectives of the *Fermi*-LAT mission, highlighted well before the beginning of scientific operations, is to "identify currently unidentified/unassociated γ-ray sources (UGSs) in the sky" [1].

Amongst all associated γ-ray sources listed in the *Fermi*-LAT catalogs (1FGL, 2FGL, 3FGL and 4FGL, Abdo et al.

[1] https://fermi.gsfc.nasa.gov/science/resources/aosrd/

Astronomy & Astrophysics manuscript no. output
June 25, 2020

Turin-SyCAT: a multifrequency catalog of Seyfert Galaxies

Peña-Herazo, H. A.[1,2,3], Massaro, F.[1,3,4,5], Chavushyan, V.[2],
Masetti, N.[6,7], Paggi, A.[1,3,4,5], and Capetti, A.[4]

[1] Dipartimento di Fisica, Università degli Studi di Torino, via Pietro Giuria 1, I-10125 Torino, Italy.
[2] Instituto Nacional de Astrofísica, Óptica y Electrónica, Apartado Postal 51-216, 72000 Puebla, México.
[3] Istituto Nazionale di Fisica Nucleare, Sezione di Torino, I-10125 Torino, Italy.
[4] INAF-Osservatorio Astrofisico di Torino, via Osservatorio 20, 10025 Pino Torinese, Italy.
[5] Consorzio Interuniversitario per la Fisica Spaziale (CIFS), via Pietro Giuria 1, I-10125, Torino, Italy.
[6] INAF – Osservatorio di Astrofisica e Scienza dello Spazio, via Gobetti 93/3, I-40129, Bologna, Italy.
[7] Departamento de Ciencias Físicas, Universidad Andrés Bello, Fernández Concha 700, Las Condes, Santiago, Chile.

Received ... ; Accepted ...

ABSTRACT

We present the 1^{st} release of the Turin-SyCAT, a homogeneous catalog of Seyfert galaxies, created considering their multifrequency properties. We selected Seyfert galaxies on the basis of an extensive literature search and considering multifrequency selection criteria. We visually inspected all spectra available for all selected sources and applied several thresholds to their radio, infrared and optical properties. Our catalog includes 571 Seyfert galaxies distinguished in 412 type 1 and 159 type 2. From our analysis, we found that mid-IR colors of type 1 Seyfert galaxies are more concentrated in the W1-W2 vs. W2-W3 color-color diagram than those of Seyfert 2 galaxies. Then, type 1 Seyfert galaxies appear to have mid-IR colors similar to blazars, but can be distinguished from them on the basis of their radio-loudness. Additionally, Seyfert 2 galaxies have mid-IR colors similar to quasars but well distinct from those of BL Lac objects. As expected from their spectral properties, type 1 and 2 Seyfert galaxies have a neat distinction when using the $u-r$ color. Finally, we discovered a significant correlation between the mid-IR fluxes at both 12 and 22μm (i.e., F_{12} and F_{22}, respectively) and hard X-ray fluxes between 15 and 150 keV. Both Seyfert classes appear to follow the same trend and share similar values of the ratio between F_{12} and F_{22} over F_{HX} in agreement with expectations of the AGN unification scenario. As future perspectives our Turin-SyCAT will be then used to search for heavily obscured Seyfert galaxies among unidentified hard X-ray sources, given the correlation discovered, as well as to investigate the large scale environments of Seyfert galaxies.

Key words. Galaxies: Seyfert – Catalogs – Galaxies: Active

1. A brief historical introduction

The story of Seyfert galaxies begun at the beginning of the past century, when in 1908, Edward A. Fath discovered peculiar emission lines in the nuclear spectrum of the "spiral nebula" NGC 1068 (Fath 1909) at the Lick Observatory, later confirmed by Vesto M. Slipher in 1917 (Slipher 1917). At that epoch, the largest fraction of known extragalactic sources showed an optical spectrum dominated by absorption features due to stars while NGC 1068 presented several, relatively bright, emission lines.

About two decades later, Hubble (1926); Humason (1932); Mayall (1934) discovered similar, optical, emission lines in other "nebulae" then classifying them as extragalactic sources. However, we waited until 1943 when Carl Keenan Seyfert, reporting studying five more galaxies similar to NGC 1068, namely: NGC 1275, 3516, 4051, 4151, 7469 established the first class of active galactic nuclei (AGNs), showing emission dominated by their nuclear regions. By the end of the 1950s, the so-called "Seyfert galaxies" were mainly characterized by "extremely" compact nuclei (i.e., <100 pc) with masses of the order of 10^8-10^9 $M_\odot$ coupled with emission lines in their optical spectra that were not only unusually strong but also unusually wide. Assuming that the width of these spectral lines is due to the Doppler effect, caused by the motion of the ionized gas, gas velocities reach up to several thousand km s^{-1}, far higher than those measured in normal galaxies.

In the early '60s, after the discovery of quasars as cosmological sources (Schmidt 1963), it became clear that Seyfert galaxies shared a number of properties with this new class, certainly their cosmological distances (i.e., redshift z) but being less luminous. The luminosity gap between Seyfert galaxies and quasars was then filled with intermediate luminosity objects (Weedman 1976) found by different surveys. This was achieved thanks to the Markarian survey, including hundreds of galaxies characterized by a relatively strong ultraviolet emission (Markarian 1967), were ∼10% of galaxies listed therein are Seyferts (Huchra & Sargent 1973) or using galaxies selected by Zwicky (Sargent 1970) before and by Palomar-Green survey (Green 1976) later. As more Seyferts and quasars were discovered, their separation in luminosity narrowed down to being almost overlapped (see also Burbidge et al. 1963; Osterbrock & Parker 1965; Pacholczyk & Weymann 1968; Burbidge, & Hoyle 1968; Schmidt & Green 1983).

Send offprint requests to: Peña-Herazo, H. A., e-mail: harold.penah@gmail.com

Astronomy & Astrophysics manuscript no. output
August 5, 2020

On the Large-Scale Environment of Seyfert Galaxies

Peña-Herazo, H. A.[1,2], Massaro, F.[1,3,4,5], Capetti, A.[4], Chavushyan, V.[2], Masetti, N.[6,7], and Paggi, A.[1,3,4,5]

[1] Dipartimento di Fisica, Università degli Studi di Torino, via Pietro Giuria 1, I-10125 Torino, Italy.
[2] Instituto Nacional de Astrofísica, Óptica y Electrónica, Apartado Postal 51-216, 72000 Puebla, México.
[3] Istituto Nazionale di Fisica Nucleare, Sezione di Torino, I-10125 Torino, Italy.
[4] INAF-Osservatorio Astrofisico di Torino, via Osservatorio 20, 10025 Pino Torinese, Italy.
[5] Consorzio Interuniversitario per la Fisica Spaziale (CIFS), via Pietro Giuria 1, I-10125, Torino, Italy.
[6] INAF – Osservatorio di Astrofisica e Scienza dello Spazio, via Gobetti 93/3, I-40129, Bologna, Italy.
[7] Departamento de Ciencias Físicas, Universidad Andrés Bello, Fernández Concha 700, Las Condes, Santiago, Chile.

Received ... ; Accepted ...

ABSTRACT

We recently released the 1^{st} version of Turin-SyCAT, an extremely homogeneous and statistically "clean" (i.e. with accurate selection) catalog of Seyfert galaxies, one of the first discovered class of active galactic nuclei. Based on the potential use of the Turin-SyCAT to investigate the large-scale environments of Seyfert galaxies, we test the unification scenario of active galaxies. According to its predictions, we expect similar behavior of galaxies in the large-scale environments of type 1 and type 2 Seyferts, as their difference is only due to orientation respect to the line of sight. We adopted a procedure based on the spatial distribution of the so-called cosmological neighbors, lying within 2 Mpc from the Seyfert galaxy, i.e., sources with all SDSS magnitude flags indicating a galaxy-type object and having a spectroscopic redshift z with $\Delta z = |z_{\rm src} - z| \leq 0.005$, corresponding to the maximum velocity dispersion in groups and clusters of galaxies. We carried out our analysis in several redshift bins, a requirement strictly necessary to avoid cosmological biases and artifacts. From our analysis, we found no difference in the large-scale environments of type 1 and type 2 Seyfert galaxies up to redshift $z_{\rm src} = 0.15$. On the other hand, we found that radio galaxies inhabit richer large-scale environments than Seyfert galaxies. According to our investigation, we conclude that the large-scale environments of Seyfert galaxies are in agreement with the unification scenario of active galaxies and differences with respect to that of radio galaxies is indeed expected on the basis of their host galaxies, mostly spirals for the former class and elliptical for the latter one.

Key words. Galaxies: Seyfert – Catalogs – Galaxies: Active

1. Introduction

Seyfert galaxies are among the first classes of active galactic nuclei (AGNs) discovered at the beginning of the past century (Fath 1909; Slipher 1917; Hubble 1926; Humason 1932; Mayall 1934; Seyfert 1943). These are mainly radio-quiet AGNs, with power/luminosity at 1.4 GHz typically less than $\sim 10^{40}$ erg s^{-1} (Ho et al. 1995; Ho & Ulvestad 2001; Chiaraluce et al. 2019). Their infrared (IR) emission is due to several components: continuum emission, dominated by the re-processed radiation arising from the dusty torus heated by the central AGN, where IR luminosities accounts a significant percentage of the bolometric luminosity (see e.g., Tristram et al. 2007; Siebenmorgen et al. 2015; González-Martín et al. 2019) coupled with radiation arising from star forming regions (see e.g., LaMassa et al. 2012; Ruschel-Dutra et al. 2017; Esparza-Arredondo et al. 2018) and emissions lines from fine structure ionic species (Ruschel-Dutra et al. 2014) and silicate or other molecular components often associated with outflows (see e.g., Morganti et al. 2015; Feruglio et al. 2020).

In 1974 when Khachikian and Weedman proposed to classify Seyfert galaxies based on features in their optical spectra distinguishing between type 1 and type 2 on the relative width of their Balmer or forbidden emission lines, where type 2 Seyferts are those with similar relative width of Hβ to the [OIII] lines (see also Khachikian & Weedman 1971; Weedman 1977; Ho 2008).

Seyfert galaxies are also X-ray sources with luminosities $L_{2-10keV} \sim 10^{38-43}$ erg/s (see e.g., Panessa et al. 2006, for recent work on *XMM-Newton* and *Chandra* satellites, and references therein) with soft X-ray spectra showing a power law continuum with a high energy cut-off (see, e.g. Mushotzky et al. 1980; Haardt & Maraschi 1991; Singh et al. 2011) and a "soft excess" which origin is due to "unresolved" X-ray emission lines (Fabian et al. 1986; Walter & Fink 1993; Gliozzi & Williams 2020) while, around 6 keV, they generally show the Fe Kα fluorescent emission line (Nandra & Pounds 1994; Matt et al. 1996; Patrick et al. 2012).

According to the unification scenario of AGNs (Antonucci & Miller 1985; Antonucci 1993), differences between type 1 and 2 Seyfert galaxies are due to the orientation of the dusty torus obscuring the central "engine" respect to the line-of-sight.

However, several discoveries as (i) changing look Seyfert galaxies (e.g., Collin-Souffrin et al. 1973; Aretxaga et al. 1999), (ii) type 2 Seyferts without X-ray absorption features

Send offprint requests to: Peña-Herazo, H. A., e-mail: harold.penah@gmail.com

Appendix B

Optical Counterpart Tables

Here I report the first 12 lines of the two main tables summarizing results (i) obtained thanks to our optical spectroscopic campaign (see Table B.1) including all 394 targets and (ii) achieved in the literature (see Table B.2) listing a total of 123 sources.

Both tables contains: the *Fermi*-LAT name (4FGL for Table B.1 and 3FGL for Table B.2), *Fermi*-LAT classification provided int he catalog corresponding to the *Fermi*-LAT name, the assigned low-energy counterpart eventually associated in the corresponding *Fermi*-LAT catalog, the name of the pointed WISE counterpart, right ascension and declination (Equinox J2000) of the WISE counterpart, spectroscopic classification, redshift, references in our campaign (only for Table B.1), telescopes used for acquiring their spectra, and references for targets that are also reported in the literature.

Table B.1: Summary of the optical spectroscopic campaign.

Fermi-LAT name	*Fermi*-LAT class	Associated source	WISE counterpart	R.A. (J2000) hh:mm:ss	Dec. (J2000) dd:mm:ss	Class	z	Ref.	Telescope	Literature
4FGL J0003.9-1149	bll	PMN J0004-1148	J000404.91-114858.3	00:04:04.91	-11:48:58.33	bzb	–	d	6dF	
4FGL J0009.7-3217	rdg	IC 1531	J000935.55-321636.8	00:09:35.56	-32:16:36.85	bzg	0.0254	d	6dF	
4FGL J0015.6+5551	bll	GB6 J0015+5551	J001540.13+555144.7	00:15:40.14	+55:51:44.77	bzb	–	b	KPNO	
4FGL J0015.9+2440	bcu	GB6 J0016+2440	J001603.62+244014.7	00:16:03.62	+24:40:14.77	bzb	–	l	OAN	
FL8Y J0024.1+2401	ugs		J002406.10+240438.6	00:24:06.10	+24:04:38.67	bzb	0.062?	o	SDSS	
4FGL J0023.7-6820	bcu	PKS 0021-686	J002406.72-682054.5	00:24:06.72	-68:20:54.50	qso	0.354	f	SOAR	
4FGL J0028.4+2001	fsrq	TXS 0025+197	J002829.81+200026.7	00:28:29.82	+20:00:26.77	bzq	1.5517	d	SDSS DR12	
4FGL J0037.9+2612	bll	MG3 J003720+2613	J003719.15+261312.6	00:37:19.15	+26:13:12.60	bzg	0.1477	k	SDSS	
4FGL J0038.7-0204	rdg	3C 17	J003820.53-020740.5	00:38:20.53	-02:07:40.50	bzq	0.2204	k	SDSS	
4FGL J0040.4-2340	bll	PMN J0040-2340	J004024.90-234000.7	00:40:24.90	-23:40:00.70	bzg	0.213	f	SOAR	
4FGL J0043.5-0442	bll	1RXS J004333.7-044257	J004334.12-044300.6	00:43:34.12	-04:43:00.67	bzb	–	d	6dF	
4FGL J0043.7-1116	bcu	1RXS J004349.3-111612	J004348.66-111607.2	00:43:48.66	-11:16:07.23	bzb	0.264	c	SOAR,NOT	h

Column description: (1) Fermi name; (2) Fermi classification; (3) Fermi low-energy counterpart association name; (4) WISE counterpart name; (5) J2000 Right Ascension; (6) J2000 Declination; (7) Class; (8) Redshift; (9) References with: a, (Cowperthwaite et al., 2013); b, (Álvarez Crespo et al., 2016b); c, (Álvarez Crespo et al., 2016c); d, (Álvarez Crespo et al., 2016a); e, (Landoni et al., 2015b); f, (Marchesini et al., 2019); g, (Massaro et al., 2014); h, (Massaro et al., 2015c); i, (Massaro et al., 2015b); j, (Massaro et al., 2016); k, (de Menezes et al., 2019); l, (de Menezes et al., 2020); m, (Paggi et al., 2014); n, (Peña-Herazo et al., 2017); o, (Peña-Herazo et al., 2019); p, This work; q, (Ricci et al., 2015). (10) Telescope. (11) Reference for targets that are also reported in literature, with: a (Desai et al., 2019); b, (Falco et al., 1998); c, (Jones et al., 2009); d, (Hewitt & Burbidge, 1980); e, (Klindt et al., 2017); f, (La Mura et al., 2017); g, (Marchesi et al., 2018); h, (Marchesini et al., 2016); i, (Marlow et al., 2000); j, (Martí et al., 2004); k, (Masetti et al., 2013); l, (Paiano et al., 2017b); m, (Paiano et al., 2017a); n, (Shaw et al., 2013); o, (Titov et al., 2013); p, (Tsarevsky et al., 2005); q, (Vermeulen & Taylor, 1995); r, (Paiano et al., 2019).

Table B.2: Summary of literature search.

3FGL name	3FGL class	4FGL name	4FGL class	Associated name	WISE name	R.A. (J2000) hh:mm:ss	Dec. (J2000) dd:mm:ss	Class	z	Telescope	Literature
J0004.2+0843	ugs	J0004.0+0840	bcu	SDSS J000359.23+084138.1	J000359.23+084138.1	00:03:59.23	+08:41:38.15	bzb	>1.503	GTC	p
J0006.2+0135	ugs	J0006.4+0135	bcu	NVSS J000626+013611	J000626.90+013610.6	00:06:26.90	+01:36:10.70	bzb	0.787	GTC	p
J0008.0+4713	bll	J0008.0+4711	bll	MG4 J000800+4712	J000759.97+471207.7	00:07:59.98	+47:12:07.75	bzb	>1.659	GTC	n
J0031.3+0724	bcu	J0031.3+0726	bll	NVSS J003119+072456	J003119.71+072453.4	00:31:19.71	+07:24:53.50	bzb	>0.836	KPNO	j
J0040.3+4049	bcu	J0040.3+4050	bll	B3 0037+405	J004013.81+405004.5	00:40:13.82	+40:50:04.54	bzb	–	KPNO	j
J0043.7-1117	bcu	J0043.7-1116	bll	1RXS J004349.3-111612	J004348.66-111607.2	00:43:48.66	-11:16:07.23	bzb	–	NOT+Copernico	k;h
J0045.2-3704	bcu	J0045.1-3706	bcu	PKS 0042-373	J004512.06-370548.5	00:45:12.06	-37:05:48.54	bzq	1.033	SALT	g
J0049.0+4224	ugs	J0049.1+4223	bcu	GALEXASC J004859.14+422351.4	J004859.15+422351.1	00:48:59.16	+42:23:51.12	bzb	0.302	SDSS	o
J0049.7+0237	bll	J0049.7+0237	bll	PKS 0047+023	J004943.23+023703.7	00:49:43.23	+02:37:03.80	bzb	>0.55	GTC	n
J0102.1+0943	ugs	J0102.4+0942	bcu	2MASS J01021713+0944098	J010216.63+094411.1	01:02:17.10	+09:44:09.50	bzb	0.42	SDSS	o
J0127.2+0325	bcu	J0127.2+0324	bll	NVSS J012713+032259	J012713.94+032300.6	01:27:13.95	+03:23:00.64	bzb	–	KPNO	j
J0134.5+2638	bcu	J0134.5+2637	fsrq	RX J0134.4+2638	J013428.19+263843.0	01:34:28.20	+26:38:43.01	bzb	–	OAN+HET+KPNO	s;j

Column description: (1) 3FGL name; (2) 3FGL classification; (3) 4FGL name; (4) 4FGL classification; (5) Fermi low-energy counterpart association name (6) WISE counterpart name; (7) J2000 Right Ascension; (8) J2000 Declination; (9) Spectroscopic class; (10) Redshift; (11) Telescope (12) References with: a, (Britzen et al., 2007); b, (Caccianiga et al., 2002); c, (Álvarez Crespo et al., 2016b); d, (Álvarez Crespo et al., 2016c); e, (Desai et al., 2019); f, (Hewitt & Burbidge, 1980); g, (Klindt et al., 2017); h, (La Mura et al., 2017); i, (Landoni et al., 2018); j, (Marchesi et al., 2018); k, (Marchesini et al., 2016); l, (Massaro et al., 2015c); m, (Paggi et al., 2014); n, (Paiano et al., 2017b); o, (Paiano et al., 2017a); p, (Paiano et al., 2019); q, (Peterson et al., 1976); r, (Ricci et al., 2015); s, (Shaw et al., 2013); t, (Wisotzki et al., 2000).

Appendix C

Turin-SyCAT Tables

Here we report the first five rows for each table of the Turin-SyCAT as described in the following.

In Table C.1 there are all 571 Turin-SyCAT sources with (i) their unique catalog identification number (ID); (ii) their SyCAT name; (iii,iv,v) radio names from SUMSS, FIRST and NVSS catalogs if a counterpart is present; (vi) name of the unique WISE counterpart as well as (vii) that in the optical from the Pan-STARRS if in the footprint above Declination of ∼33 °; (viii,ix,x,xi) X-ray names from the ROSAT, 3PBC, BAT105 and IBIS4CAT, respectively. This table is extremely important to carry out crossmatches easily with other catalogs/survey/samples.

Table C.2 reports the main properties of the catalog as (i) unique catalog ID; (ii) SyCAT name; (iii) name of the mid-IR WISE counterpart; (iv,v) WISE coordinates; (vi,vii) redshift and luminosity distance computed according to the chosen cosmology, respectively; (viii) the type 1 or type 2 classification provided by our analysis; (ix) the reference for the redshift; (x,xi) the class indicated in the literature and the reference for it.

In Table C.3, we provide all information regarding the mid-IR properties as all WISE and 2MASS magnitudes, including their uncertainties, and the $L_{3.4\mu m}$ luminosity used to avoid quasar selection compared to the 10^{11} $L_{\odot}$ threshold.

Main optical information (i.e., magnitudes and spectral classification, if any) concerning the crossmatches obtained with the SDSS, and the Pan-STARRS databases are indeed reported in Table C.4, together with their (1) unique ID; (2) SyCAT name; (3) name in Pan-STARRS survey. Columns(4), (5), (6), (7), and (8) are the PSF magnitudes from Pan-STARRS in *g, r, i, z, and y* bands and their uncertainties in parenthesis. The following columns contain SDSS information: (9) flag of presence in SDSS; (10) magnitude from SDSS in u band and its 1σ uncertainty in parenthesis; (11) spectroscopic redshift; (12) automatic classification; and (13) automatic sub-classification. This information is provided only for Seyfert galaxies lying in the Pan-STARRS footprint.

Table C.1: All Turin-SyCAT sources with names of their counterparts in the catalogs/surveys explored (First five rows, full table available in the on-line material)

ID	SyCAT name	SUMSS name	FIRST name	NVSS name	WISE name	Pan-STARRS PSO name	ROSAT name	3PBC name	BAT105 SWIFT name	IBIS4CAT IGR name
1	SY1 J0002+0322				J000226.41+032107.0	J000226.415+032106.991	J000226.6+032105	J0002.5+0322	J0002.5+0323	
2	SY2 J0004+7020				J000401.97+701918.2	J000401.990+701918.250		J0004.0+7018	J0005.0+7021	J00040+7020
3	SY1 J0005-5006				J000543.06-500654.7		J000543.1-500703			
4	SY1 J0006+2013			J000619+201210	J000619.53+201210.6	J000619.529+201210.662		J0006.3+2012	J0006.2+2012	
5	SY1 J0008+1450				J000805.61+145023.6	J000805.625+145023.383	J000805.6+145027			

Column description: (1) Unique catalog identified (ID); (2) SyCAT name; (3) name in SUMSS; (4) name in FIRST; (5) name in NVSS; (6) name in WISE; (7) name in Pan-STARRS; (8) name in ROSAT; (9) name in 3PBC; (10) name in BAT105; (11) name in IBIS4CAT.

Table C.2: 1^{st} release of the Turin-SyCAT (First five rows)

ID	SyCAT name	WISE name	R.A. (J2000) hh:mm:ss.ss	Dec. (J2000) dd:mm:ss.s	z	D_L Mpc	class	z ref.	class lit.	class ref.
1	SY1 J0002+0322	J000226.41+032107.0	00:02:26.41	+03:21:06.9	0.0255	112.02	1	rz1	1	rc1
2	SY2 J0004+7020	J000401.97+701918.2	00:04:01.97	+70:19:18.3	0.0960	443.61	2	rz2	2	rc2
3	SY1 J0005-5006	J000543.06-500654.7	00:05:43.06	-50:06:55.0	0.0334	147.72	1	rz3	1	rc3
4	SY1 J0006+2013	J000619.53+201210.6	00:06:19.53	+20:12:10.5	0.0258	113.22	1	rz1	1	rc4
5	SY1 J0008+1450	J000805.61+145023.6	00:08:05.62	+14:50:23.3	0.0451	200.96	1	rz5	1	rc5

Column description: (1) ID; (2) SyCAT name; (3) name in WISE; (4) WISE Right Ascension in J2000 Equinox; (5) WISE Declination in J2000 Equinox; (6) redshift; (7) luminosity distance; (8) Seyfert type classification (1 or 2); (9) Redshift reference with: rz1, Huchra et al. (1999); rz2, Masetti et al. (2008); rz3, Dressler & Shectman (1988); rz5, Pietsch et al. (1998). (10) Classification in the literature. (11) Reference for the literature classification, with: rc1,Rafanelli & Schulz (1991); rc2, Masetti et al. (2008); rc3, Dressler et al. (1985); rc4, Osterbrock & Martel (1993); rc5, Pietsch et al. (1998).

Finally, in Table C.5, we report all parameters related to the X-ray counterparts of the Turin-SyCAT sources collected from the ROSAT, the 3PBC, the BAT105, and the IBSI4CAT catalogs. This information is shown in the table only for those sources having at least one X-ray counterpart in one of the surveys previously indicated and again the (i) unique ID; (ii) SyCAT name; (iii) name of the mid-IR WISE counterpart are in the first three columns, respectively.

Table C.3: Mid-IR and near-IR properties of Turin-SyCAT sources (First five rows)

ID	SyCAT name	WISE name	W1 (mag)	W2 (mag)	W3 (mag)	W4 (mag)	J (mag)	H (mag)	K_s (mag)	$L_{3.4\mu\,m}$ (10^9 $L_\odot$)
1	SY1 J0002+0322	J000226.41+032107.0	10.78±0.02	10.16±0.02	6.96±0.02	4.78±0.03	13.87±0.10	13.02±0.11	12.34±0.06	5.1
2	SY2 J0004+7020	J000401.97+701918.2	11.86±0.02	10.81±0.021	7.75±0.02	5.06±0.03	15.3±0.08	14.23±0.08	13.40±0.06	1.9
3	SY1 J0005−5006	J000543.06−500654.7	10.72±0.02	9.76±0.021	6.94±0.02	4.85±0.03	13.84±0.05	13.02±0.07	12.12±0.04	9.5
4	SY1 J0006+2013	J000619.53+201210.6	9.06±0.02	8.08±0.02	5.72±0.01	3.58±0.02	12.62±0.03	11.73±0.04	10.59±0.02	25.6
5	SY1 J0008+1450	J000805.61+145023.6	12.50±0.02	12.19±0.023	9.39±0.04	7.10±0.09	14.67±0.06	14.01±0.07	13.51±0.07	3.4

WISE and 2MASS magnitudes, including their uncertainties, and the $L_{3.4\mu\,m}$ luminosity used to avoid quasar selection compared to the 10^{11} $L_\odot$ threshold.
Column description: (1) ID; (2) SyCAT name; (3) name in WISE; (4) WISE W1 3.4 μm magnitude and its 1σ uncertainty in parenthesis; (5) WISE W2 [4.6] μm magnitude and its 1σ uncertainty in parenthesis; (6) WISE W3 [12] μm magnitude and its 1σ uncertainty in parenthesis; (7) WISE W4 [22] μm magnitude and its 1σ uncertainty in parenthesis; (8) 2MASS J magnitude and its 1σ uncertainty in parenthesis; (9) 2MASS H magnitude and its 1σ uncertainty in parenthesis; (10) 2MASS K magnitude and its 1σ uncertainty in parenthesis; (11) Luminosity at $3.4\mu\,m$. In this example table magnitudes are rounded for space reasons.

Table C.4: Optical properties of Turin-SyCAT sources (First five rows)

ID	SyCAT name	PanSTARRS name	g (mag)	r (mag)	i (mag)	z (mag)	y (mag)	SDSS flag	u (mag)	z_{sp}	class	sclass
1	SY1 J0002+0322	J000226.415+032106.991	16.13±0.01	15.75±0.03	15.70±0.04	15.37±0.04	15.21±0.05	n				
2	SY2 J0004+7020	J000401.990+701918.250	20.28±0.04	19.34±0.03	18.36±0.04	17.91±0.06	17.62±0.06	n				
4	SY1 J0006+2013	J000619.529+201210.662	14.58±0.01	14.12±0.02	14.21±0.01	14.21±0.01	14.11±0.03	n				
5	SY1 J0008+1450	J000805.625+145023.383	17.15±0.03	16.63±0.02	16.43±0.01	16.24±0.05	16.21±0.04	y	19.04±0.02	0.0456	QSO	BL
6	SY2 J0010−0442	J001009.970−044237.823	17.03±0.04	16.54±0.02	16.37±0.03	16.01±0.03	15.79±0.03	n				

WISE and 2MASS magnitudes, including their uncertainties, and the $L_{3.4\mu\,m}$ luminosity used to avoid quasar selection compared to the 10^{11} $L_{\odot}$ threshold.
Column description: (1) ID; (2) SyCAT name; (3) Pan-STARRS name; (4) PSF magnitude from Pan-STARRS in g band and its 1σ uncertainty in parenthesis; (5) PSF magnitude from Pan-STARRS in r band and its 1σ uncertainty in parenthesis; (6) PSF magnitude from Pan-STARRS in i band and its 1σ uncertainty in parenthesis; (7) PSF magnitude from Pan-STARRS in z band and its 1σ uncertainty in parenthesis; (8) PSF magnitude from Pan-STARRS in y band and its 1σ uncertainty in parenthesis; (9) SDSS flag (y= in the SDSS footprint); (10) magnitude from SDSS in u band and its 1σ uncertainty in parenthesis; (11) spectroscopic redshift from SDSS; (12) SDSS automatic classification; (13) SDSS automatic sub-classification, BL: Broad line.

Table C.5: X-ray properties of Turin-SyCAT sources (First five rows)

ID	SyCAT name	ROSAT name	counts	ϑ_{rw} (arcsec)	3PBC name	3PBC counterpart name	3PBC class	F_{HX} erg s^{-1} cm^{-2}	ϑ_{3w} (arcsec)	BAT105 name	BAT105 class	ϑ_{bw} (arcsec)	IBIS name	IBIS class	ϑ_{iw} (arcsec)
1	SY1 J0002+0322	J000226.6+032105	0.226±0.027	3.22	J0002.5+0322	NGC 7811	Sy1	1.39±0.18e−11	0.69	J0002.5+0323	Sy1.5	0.94			
2	SY2 J0004+7020				J0004.0+7018	2MASX J00040192+7019185	AG?	1.10±0.13e−11	0.26	J0005.0+7021	Sy1.9	0.18	J00040+7020	Sy2	0.4
3	SY1 J0005−5006	J000543.1−500703	0.379±0.070	8.26											
4	SY1 J0006+2013				J0006.3+2012	Mrk 335	Sy1	1.76±0.14e−11	0.12	J0006.2+2012	Sy1.2	0.4			
5	SY1 J0008+1450	J000805.6+145027	0.179±0.019	3.39											

WISE and 2MASS magnitudes, including their uncertainties, and the $L_{3.4\mu m}$ luminosity used to avoid quasar selection compared to the 10^{11} $L_{\odot}$ threshold.
Column description: (1) Catalog ID; (2) SyCAT name; (3) WISE name; (4) ROSAT name; (5) X-ray counts from the ROSAT catalog and its 1σ uncertainty in parenthesis; (6) Angular Separation between ROSAT and WISE positions in arcseconds; (7) 3PBC name; (8) counterpart listed in the 3PBC; (9) 3PBC classification; (10) F_{HX} and its 1σ uncertainty in parenthesis (in units of erg s^{-1} cm^{-2}); (11) Angular Separation between 3PBC and WISE positions in arcseconds; (12) BAT105 name; (13) BAT105 classification; (14) Angular Separation between BAT105 and WISE positions in arcseconds; (15) INTEGRAL name from IBIS4CAT; (16) INTEGRAL classification from IBIS4CAT; (17) Angular Separation between IBIS4CAT and WISE positions in arcseconds.

List of Figures

List of Tables

Bibliography

Abazajian, K., Adelman-McCarthy, J. K., Agüeros, M. A., et al. 2005, AJ, 129, 1755

Abdo, A. A., Ackermann, M., Ajello, M., et al. 2010a, ApJS, 188, 405

—. 2010b, ApJ, 722, 520

—. 2010c, ApJ, 715, 429

Abdo, A. A., Ackermann, M., Agudo, I., et al. 2010d, ApJ, 716, 30

Abdollahi, S., Acero, F., Ackermann, M., et al. 2020, ApJS, 247, 33

Abolfathi, B., Aguado, D. S., Aguilar, G., et al. 2018, ApJS, 235, 42

Acero, F., Donato, D., Ojha, R., et al. 2013, ApJ, 779, 133

Acero, F., Ackermann, M., Ajello, M., et al. 2015, ApJS, 218, 23

Ackermann, M., Ajello, M., Allafort, A., et al. 2012, ApJ, 753, 83

Ackermann, M., Ajello, M., Allafort, A., et al. 2012, Science, 338, 1190

Ackermann, M., Ajello, M., Atwood, W. B., et al. 2015, ApJ, 810, 14

Adams, T. F. 1977, ApJS, 33, 19

Aguado, D. S., Ahumada, R., Almeida, A., et al. 2019, ApJS, 240, 23

Ahn, C. P., Alexandroff, R., Allende Prieto, C., et al. 2012, ApJS, 203, 21

Ajello, M., Romani, R. W., Gasparrini, D., et al. 2014, ApJ, 780, 73

Ajello, M., Gasparrini, D., Sánchez-Conde, M., et al. 2015, ApJ, 800, L27

Ajello, M., Angioni, R., Axelsson, M., et al. 2020, ApJ, 892, 105

Almaini, O., Boyle, B. J., Griffiths, R. E., et al. 1995, MNRAS, 277, L31

Alonso-Herrero, A., Ramos Almeida, C., Mason, R., et al. 2011, ApJ, 736, 82

Alonso-Herrero, A., García-Burillo, S., Pereira-Santaella, M., et al. 2019, A&A, 628, A65

Álvarez Crespo, N., Massaro, F., D'Abrusco, R., et al. 2016a, Ap&SS, 361, 316

Álvarez Crespo, N., Masetti, N., Ricci, F., et al. 2016b, AJ, 151, 32

Álvarez Crespo, N., Massaro, F., Milisavljevic, D., et al. 2016c, AJ, 151, 95

Antonucci, R. 1993, ARA&A, 31, 473

Antonucci, R. R. J., & Miller, J. S. 1985, ApJ, 297, 621

Aretxaga, I., Joguet, B., Kunth, D., Melnick, J., & Terlevich, R. J. 1999, ApJ, 519, L123

Arnaud, K. A., Branduardi-Raymont, G., Culhane, J. L., et al. 1985, MNRAS, 217, 105

Arsioli, B., Fraga, B., Giommi, P., Padovani, P., & Marrese, P. 2015, Astronomy & Astrophysics, 579, A34

Ashby, M. L. N., Stern, D., Brodwin, M., et al. 2009, ApJ, 701, 428

Atwood, W. B., Abdo, A. A., Ackermann, M., et al. 2009, ApJ, 697, 1071

Awaki, H., Ueno, S., Taniguchi, Y., & Weaver, K. A. 2000, ApJ, 542, 175

Baldi, R. D., Capetti, A., & Giovannini, G. 2015, A&A, 576, A38

Baldi, R. D., Capetti, A., & Massaro, F. 2018, A&A, 609, A1

Baldry, I. K., Balogh, M. L., Bower, R. G., et al. 2006, MNRAS, 373, 469

Baldwin, J. A., Phillips, M. M., & Terlevich, R. 1981, PASP, 93, 5

Baskin, A., & Laor, A. 2018, MNRAS, 474, 1970

Beasley, A. J., Gordon, D., Peck, A. B., et al. 2002, ApJS, 141, 13

Becker, R. H., White, R. L., & Helfand, D. J. 1995, ApJ, 450, 559

Beckert, T., Driebe, T., Hönig, S. F., & Weigelt, G. 2008, A&A, 486, L17

Beckmann, V., & Shrader, C. R. 2012, Active Galactic Nuclei

Beckmann, V., Soldi, S., Ricci, C., et al. 2009, A&A, 505, 417

Bennett, C. L., Larson, D., Weiland, J. L., & Hinshaw, G. 2014, ApJ, 794, 135

Berlin, A., & Hooper, D. 2014, Phys. Rev. D, 89, 016014

Berlind, A. A., Frieman, J., Weinberg, D. H., et al. 2006, ApJS, 167, 1

Best, P. N., & Heckman, T. M. 2012, MNRAS, 421, 1569

Bird, A. J., Malizia, A., Bazzano, A., et al. 2007, ApJS, 170, 175

Biviano, A. 2000, in Constructing the Universe with Clusters of Galaxies, 1

Blandford, R. D., & Königl, A. 1979, ApJ, 232, 34

Blandford, R. D., & McKee, C. F. 1982, ApJ, 255, 419

Blandford, R. D., & Znajek, R. L. 1977a, MNRAS, 179, 433

—. 1977b, MNRAS, 179, 433

Boissay, R., Paltani, S., Ponti, G., et al. 2014, A&A, 567, A44

Brightman, M., & Nandra, K. 2011, MNRAS, 413, 1206

Britzen, S., Brinkmann, W., Campbell, R. M., et al. 2007, A&A, 476, 759

Bruni, G., Panessa, F., Ghisellini, G., et al. 2018, ApJ, 854, L23

Burbidge, E. M. 1968, ApJ, 154, L109

Burbidge, G. R., Burbidge, E. M., & Sandage, A. R. 1963, Reviews of Modern Physics, 35, 947

Burtscher, L., Jaffe, W., Raban, D., et al. 2009, ApJ, 705, L53

Burtscher, L., Meisenheimer, K., Tristram, K. R. W., et al. 2013, A&A, 558, A149

Caccianiga, A., Marchã, M. J., Antón, S., Mack, K. H., & Neeser, M. J. 2002, MNRAS, 329, 877

Calzetti, D. 2011, in EAS Publications Series, Vol. 46, EAS Publications Series, ed. C. Joblin & A. G. G. M. Tielens, 133–141

Capetti, A., Massaro, F. Paggi, A., Baldi, R. D., et al. 2020, Accepted on A&A

Capetti, A., Massaro, F., & Baldi, R. D. 2017a, A&A, 598, A49

—. 2017b, A&A, 601, A81

Cardelli, J. A., Clayton, G. C., & Mathis, J. S. 1989, The Astrophysical Journal, 10, 245

Carilli, C. L., & Barthel, P. D. 1996, A&A Rev., 7, 1

Chiaraluce, E., Bruni, G., Panessa, F., et al. 2019, MNRAS, 485, 3185

Cid Fernandes, R., Heckman, T., Schmitt, H., González Delgado, R. M., & Storchi-Bergmann, T. 2001, ApJ, 558, 81

Clemens, J. C., Crain, J. A., & Anderson, R. 2004, in Society of Photo-Optical Instrumentation Engineers (SPIE) Conference Series, Vol. 5492, Ground-based Instrumentation for Astronomy, ed. A. F. M. Moorwood & M. Iye, 331–340

Cohen, A. S., Lane, W. M., Cotton, W. D., et al. 2007, AJ, 134, 1245

Cohen, M. H., Kellermann, K. I., Shaffer, D. B., et al. 1977, Nature, 268, 405

Colless, M., Dalton, G., Maddox, S., et al. 2001, MNRAS, 328, 1039

Collin-Souffrin, S., Alloin, D., & Andrillat, Y. 1973, A&A, 22, 343

Condon, J. J., Cotton, W. D., Greisen, E. W., et al. 1998, AJ, 115, 1693

Contini, M., & Viegas, S. M. 2000, ApJ, 535, 721

Corral, A., Della Ceca, R., Caccianiga, A., et al. 2011, A&A, 530, A42

Cowperthwaite, P. S., Massaro, F., D'Abrusco, R., et al. 2013, AJ, 146, 110

Croom, S. M., Smith, R. J., Boyle, B. J., et al. 2004, MNRAS, 349, 1397

Crummy, J., Fabian, A. C., Gallo, L., & Ross, R. R. 2006, MNRAS, 365, 1067

Cusumano, G., La Parola, V., Segreto, A., et al. 2010, A&A, 524, A64

D'Abrusco, R., Longo, G., & Walton, N. A. 2009, MNRAS, 396, 223

D'Abrusco, R., Massaro, F., Ajello, M., et al. 2012, ApJ, 748, 68

D'Abrusco, R., Massaro, F., Paggi, A., et al. 2013, ApJS, 206, 12

—. 2014, ApJS, 215, 14

D'Abrusco, R., Álvarez Crespo, N., Massaro, F., et al. 2019, ApJS, 242, 4

Dadina, M. 2008, A&A, 485, 417

Dahari, O. 1984, AJ, 89, 966

Davies, R. I., Müller Sánchez, F., Genzel, R., et al. 2007, ApJ, 671, 1388

de Grijp, M. H. K., Keel, W. C., Miley, G. K., Goudfrooij, P., & Lub, J. 1992, A&AS, 96, 389

de Menezes, R., Peña-Herazo, H. A., Marchesini, E. J., et al. 2019, A&A, 630, A55

de Menezes, R., Amaya-Almazán, R. A., Marchesini, E. J., et al. 2020, Ap&SS, 365, 12

De Robertis, M. M., Hayhoe, K., & Yee, H. K. C. 1998, ApJS, 115, 163

den Brok, J. S., Cantalupo, S., Mackenzie, R., et al. 2020, MNRAS, 495, 1874

Desai, A., Marchesi, S., Rajagopal, M., & Ajello, M. 2019, ApJS, 241, 5

Diamond-Stanic, A. M., & Rieke, G. H. 2012, ApJ, 746, 168

Djannati-Atai , A., Piron, F., Barrau, A., et al. 1999, A&A, 350, 17

Doert, M., & Errando, M. 2014, ApJ, 782, 41

Domínguez, A., Primack, J. R., Rosario, D. J., et al. 2011, MNRAS, 410, 2556

Douglas, J. N., Bash, F. N., Bozyan, F. A., Torrence, G. W., & Wolfe, C. 1996, AJ, 111, 1945

Dressler, A., & Shectman, S. A. 1988, AJ, 95, 284

Dressler, A., Thompson, I. B., & Shectman, S. A. 1985, ApJ, 288, 481

Dultzin-Hacyan, D., Krongold, Y., Fuentes-Guridi, I., & Marziani, P. 1999, ApJ, 513, L111

Durré, M., & Mould, J. 2018, ApJ, 867, 149

Edge, D. O., Shakeshaft, J. R., McAdam, W. B., Baldwin, J. E., & Archer, S. 1959, MmRAS, 68, 37

Efstathiou, A., & Rowan-Robinson, M. 1995, MNRAS, 273, 649

Eke, V. R., Baugh, C. M., Cole, S., et al. 2004, MNRAS, 348, 866

Elvis, M., Risaliti, G., Nicastro, F., et al. 2004, ApJ, 615, L25

Esparza-Arredondo, D., González-Martín, O., Dultzin, D., et al. 2018, ApJ, 859, 124

Evans, I. N., Primini, F. A., Glotfelty, K. J., et al. 2010, ApJS, 189, 37

Evans, P. A., Osborne, J. P., Beardmore, A. P., et al. 2014, ApJS, 210, 8

Fabian, A. C., Guilbert, P. W., Arnaud, K. A., et al. 1986, MNRAS, 218, 457

Fabian, A. C., Iwasawa, K., Reynolds, C. S., & Young, A. J. 2000, PASP, 112, 1145

Falco, E. E., Kochanek, C. S., & Muñoz, J. A. 1998, ApJ, 494, 47

Fanaroff, B. L., & Riley, J. M. 1974, MNRAS, 167, 31P

Fath, E. A. 1909, PASP, 21, 138

Ferland, G. J., & Netzer, H. 1983, ApJ, 264, 105

Feruglio, C., Fabbiano, G., Bischetti, M., et al. 2020, ApJ, 890, 29

Fey, A. L., Gordon, D., Jacobs, C. S., et al. 2015, AJ, 150, 58

Fischer, T. C., Crenshaw, D. M., Kraemer, S. B., & Schmitt, H. R. 2013, ApJS, 209, 1

Fomalont, E. B., Petrov, L., MacMillan, D. S., Gordon, D., & Ma, C. 2003, AJ, 126, 2562

Fossati, G., Maraschi, L., Celotti, A., Comastri, A., & Ghisellini, G. 1998, MNRAS, 299, 433

Fritz, J., Franceschini, A., & Hatziminaoglou, E. 2006, MNRAS, 366, 767

Fukugita, M., Ichikawa, T., Gunn, J. E., et al. 1996, AJ, 111, 1748

Gallimore, J. F., Yzaguirre, A., Jakoboski, J., et al. 2010, ApJS, 187, 172

García-Bernete, I., Ramos Almeida, C., Acosta-Pulido, J. A., et al. 2016, MNRAS, 463, 3531

García-Burillo, S., Combes, F., Usero, A., et al. 2014, A&A, 567, A125

George, I. M., & Fabian, A. C. 1991, MNRAS, 249, 352

Giommi, P., Ansari, S. G., & Micol, A. 1995, A&AS, 109, 267

Giroletti, M., Massaro, F., D'Abrusco, R., et al. 2016, Astronomy & Astrophysics, 588, A141

Gliozzi, M., & Williams, J. K. 2020, MNRAS, 491, 532

González-Martín, O., Masegosa, J., García-Bernete, I., et al. 2019, ApJ, 884, 11

Gordon, Y. A., Owers, M. S., Pimbblet, K. A., et al. 2017, MNRAS, 465, 2671

Goulding, A. D., & Alexander, D. M. 2009, MNRAS, 398, 1165

Goulding, A. D., Alexander, D. M., Bauer, F. E., et al. 2012, ApJ, 755, 5

Gower, J. F. R., Scott, P. F., & Wills, D. 1967, MmRAS, 71, 49

Gravity Collaboration, Pfuhl, O., Davies, R., et al. 2020a, A&A, 634, A1

Gravity Collaboration, Dexter, J., Shangguan, J., et al. 2020b, A&A, 635, A92

Green, A. R., McHardy, I. M., & Lehto, H. J. 1993, MNRAS, 265, 664

Green, R. F. 1976, PASP, 88, 665

Green, R. F., Schmidt, M., & Liebert, J. 1986, ApJS, 61, 305

Guainazzi, M., Matt, G., & Perola, G. C. 2005, A&A, 444, 119

Haardt, F., & Maraschi, L. 1991, ApJ, 380, L51

Haas, M. R., Schaye, J., & Jeeson-Daniel, A. 2012, MNRAS, 419, 2133

Halpern, J. P., & Filippenko, A. V. 1984, ApJ, 285, 475

Hao, L., Weedman, D. W., Spoon, H. W. W., et al. 2007, ApJ, 655, L77

Hartman, R. C., Bertsch, D. L., Bloom, S. D., et al. 1999, ApJS, 123, 79

Healey, S. E., Romani, R. W., Taylor, G. B., et al. 2007, ApJS, 171, 61

Heckman, T. M. 1978, PASP, 90, 241

—. 1980, A&A, 500, 187

Heckman, T. M., & Best, P. N. 2014, ARA&A, 52, 589

Hewitt, A., & Burbidge, G. 1980, ApJS, 43, 57

Hine, R. G., & Longair, M. S. 1979, MNRAS, 188, 111

Ho, L. C. 2008, ARA&A, 46, 475

Ho, L. C., Filippenko, A. V., & Sargent, W. L. 1995, ApJS, 98, 477

Ho, L. C., Filippenko, A. V., & Sargent, W. L. W. 2003, ApJ, 583, 159

Ho, L. C., Filippenko, A. V., Sargent, W. L. W., & Peng, C. Y. 1997, ApJS, 112, 391

Ho, L. C., & Peng, C. Y. 2001, ApJ, 555, 650

Ho, L. C., & Ulvestad, J. S. 2001, ApJS, 133, 77

Hönig, S. F., Kishimoto, M., Antonucci, R., et al. 2012, ApJ, 755, 149

Hopkins, P. F., Cox, T. J., Kereš, D., & Hernquist, L. 2008, ApJS, 175, 390

Hovatta, T., Lister, M. L., Aller, M. F., et al. 2012, AJ, 144, 105

Hoyle, F., & Fowler, W. A. 1963, Nature, 197, 533

Hubble, E. P. 1926, ApJ, 64, 321

Huchra, J., & Burg, R. 1992, ApJ, 393, 90

Huchra, J., & Sargent, W. L. W. 1973, ApJ, 186, 433

Huchra, J. P., Vogeley, M. S., & Geller, M. J. 1999, ApJS, 121, 287

Humason, M. L. 1932, PASP, 44, 267

Jaffe, W., Meisenheimer, K., Röttgering, H. J. A., et al. 2004, Nature, 429, 47

Jensen, J. J., Hönig, S. F., Rakshit, S., et al. 2017, MNRAS, 470, 3071

Jiang, N., Wang, H., Mo, H., et al. 2016, ApJ, 832, 111

Jones, D. H., Saunders, W., Colless, M., et al. 2004, MNRAS, 355, 747

Jones, D. H., Read, M. A., Saunders, W., et al. 2009, MNRAS, 399, 683

Kammoun, E. S., Miller, J. M., Zoghbi, A., et al. 2019, ApJ, 877, 102

Kaspi, S., Brandt, W. N., George, I. M., et al. 2002, ApJ, 574, 643

Kataoka, J., Mattox, J. R., Quinn, J., et al. 1999, Astroparticle Physics, 11, 149

Katarzyński, K., Sol, H., & Kus, A. 2001, A&A, 367, 809

Kauffmann, G., Heckman, T. M., Tremonti, C., et al. 2003, MNRAS, 346, 1055

Keel, W. C. 1980, AJ, 85, 198

Kellermann, K. I., Sramek, R., Schmidt, M., Shaffer, D. B., & Green, R. 1989, AJ, 98, 1195

Kellermann, K. I., Sramek, R. A., Schmidt, M., Green, R. F., & Shaffer, D. B. 1994, AJ, 108, 1163

Kerr, M. 2019, ApJ, 885, 92

Kewley, L. J., Dopita, M. A., Sutherland, R. S., Heisler, C. A., & Trevena, J. 2001, ApJ, 556, 121

Kewley, L. J., Groves, B., Kauffmann, G., & Heckman, T. 2006, MNRAS, 372, 961

Khachikian, E. E., & Weedman, D. W. 1971, Astrofizika, 7, 389

Khachikian, E. Y., & Weedman, D. W. 1974, ApJ, 192, 581

Kishimoto, M., Hönig, S. F., Antonucci, R., et al. 2011, A&A, 527, A121

Klindt, L., van Soelen, B., Meintjes, P. J., & Väisänen, P. 2017, MNRAS, 467, 2537

Kormendy, J., & Richstone, D. 1995, ARA&A, 33, 581

Koshida, S., Yoshii, Y., Kobayashi, Y., et al. 2009, ApJ, 700, L109

Koshida, S., Minezaki, T., Yoshii, Y., et al. 2014, ApJ, 788, 159

Koski, A. T. 1978, ApJ, 223, 56

Koss, M., Trakhtenbrot, B., Ricci, C., et al. 2017, ApJ, 850, 74

Kotilainen, J. K., & Ward, M. J. 1994, MNRAS, 266, 953

Koulouridis, E., Chavushyan, V., Plionis, M., Krongold, Y., & Dultzin-Hacyan, D. 2006a, ApJ, 651, 93

Koulouridis, E., Plionis, M., Chavushyan, V., et al. 2013, A&A, 552, A135

—. 2006b, ApJ, 639, 37

Koulouridis, E., Georgantopoulos, I., Loukaidou, G., et al. 2016, A&A, 586, A3

Krolik, J. H. 1998, Active Galactic Nuclei: From the Central Black Hole to the Galactic Environment

Krongold, Y., Dultzin-Hacyan, D., & Marziani, P. 2002, ApJ, 572, 169

La Mura, G., Busetto, G., Ciroi, S., et al. 2017, European Physical Journal D, 71, 95

Lagos, C. D. P., Padilla, N. D., Strauss, M. A., Cora, S. A., & Hao, L. 2011, MNRAS, 414, 2148

Laing, R. A., Jenkins, C. R., Wall, J. V., & Unger, S. W. 1994, in Astronomical Society of the Pacific Conference Series, Vol. 54, The Physics of Active Galaxies, ed. G. V. Bicknell, M. A. Dopita, & P. J. Quinn, 201

LaMassa, S. M., Heckman, T. M., Ptak, A., et al. 2012, ApJ, 758, 1

Lamer, G., McHardy, I. M., Uttley, P., & Jahoda, K. 2003, MNRAS, 338, 323

Landi, R., Bassani, L., Stephen, J. B., et al. 2015, A&A, 581, A57

Landoni, M., Falomo, R., Treves, A., & Sbarufatti, B. 2014, A&A, 570, A126

Landoni, M., Falomo, R., Treves, A., Scarpa, R., & Reverte Payá, D. 2015a, AJ, 150, 181

Landoni, M., Paiano, S., Falomo, R., Scarpa, R., & Treves, A. 2018, ApJ, 861, 130

Landoni, M., Massaro, F., Paggi, A., et al. 2015b, AJ, 149, 163

Laurikainen, E., & Salo, H. 1995, A&A, 293, 683

Lebouteiller, V., Barry, D. J., Goes, C., et al. 2015, ApJS, 218, 21

Lebouteiller, V., Barry, D. J., Spoon, H. W. W., et al. 2011, ApJS, 196, 8

Lintott, C. J., Schawinski, K., Slosar, A., et al. 2008, MNRAS, 389, 1179

Liodakis, I., & Blinov, D. 2019, MNRAS, 486, 3415

Lipovetskij, V. A., Neizvestnyj, S. I., & Neizvestnaya, O. M. 1987, Soobshcheniya Spetsial'noj Astrofizicheskoj Observatorii, 55

Lipovetsky, V. A., Neizvestny, S. I., & Neizvestnaya, O. M. 1988, Soobshcheniya Spetsial'noj Astrofizicheskoj Observatorii, 55, 5

Lira, P., Videla, L., Wu, Y., et al. 2013, ApJ, 764, 159

López-Gonzaga, N., Burtscher, L., Tristram, K. R. W., Meisenheimer, K., & Schartmann, M. 2016, A&A, 591, A47

López-Gonzaga, N., Jaffe, W., Burtscher, L., Tristram, K. R. W., & Meisenheimer, K. 2014, A&A, 565, A71

Lynden-Bell, D. 1969, Nature, 223, 690

MacKenty, J. W. 1989, ApJ, 343, 125

—. 1990, ApJS, 72, 231

Magdziarz, P., Blaes, O. M., Zdziarski, A. A., Johnson, W. N., & Smith, D. A. 1998, MNRAS, 301, 179

Magdziarz, P., & Zdziarski, A. A. 1995, MNRAS, 273, 837

Magorrian, J., Tremaine, S., Richstone, D., et al. 1998, AJ, 115, 2285

Maiolino, R., & Rieke, G. H. 1995, ApJ, 454, 95

Maiolino, R., Salvati, M., Bassani, L., et al. 1998, A&A, 338, 781

Malkan, M. A., Gorjian, V., & Tam, R. 1998, ApJS, 117, 25

Mandal, A. K., Rakshit, S., Kurian, K. S., et al. 2018, MNRAS, 475, 5330

Mandarakas, N., Blinov, D., Liodakis, I., et al. 2019, A&A, 623, A61

Mantovani, G., Nandra, K., & Ponti, G. 2016, MNRAS, 458, 4198

Marchesi, S., Kaur, A., & Ajello, M. 2018, AJ, 156, 212

Marchesini, E. J., Paggi, A., Massaro, F., et al. 2020, A&A, 638, A128

Marchesini, E. J., Masetti, N., Chavushyan, V., et al. 2016, A&A, 596, A10

Marchesini, E. J., Peña-Herazo, H. A., Álvarez Crespo, N., et al. 2019, Ap&SS, 364, 5

Markarian, B. E. 1967, Astrofizika, 3, 55

Markarian, B. E., Lipovetsky, V. A., Stepanian, J. A., Erastova, L. K., & Shapovalova, A. I. 1989, Soobshcheniya Spetsial'noj Astrofizicheskoj Observatorii, 62, 5

Markowitz, A., Reeves, J. N., Miniutti, G., et al. 2008, PASJ, 60, S277

Marlow, D. R., Rusin, D., Jackson, N., et al. 2000, AJ, 119, 2629

Martí, J., Paredes, J. M., Bloom, J. S., et al. 2004, A&A, 413, 309

Martini, P., Elias, J., Points, S., et al. 2014, in Society of Photo-Optical Instrumentation Engineers (SPIE) Conference Series, Vol. 9147, Ground-based and Airborne Instrumentation for Astronomy V, 91470Z

Masetti, N., Palazzi, E., Bassani, L., Malizia, A., & Stephen, J. B. 2004, A&A, 426, L41

Masetti, N., Mason, E., Bassani, L., et al. 2006, A&A, 448, 547

Masetti, N., Mason, E., Morelli, L., et al. 2008, A&A, 482, 113

Masetti, N., Parisi, P., Palazzi, E., et al. 2009, A&A, 495, 121

—. 2010, A&A, 519, A96

Masetti, N., Parisi, P., Jiménez-Bailón, E., et al. 2012, A&A, 538, A123

Masetti, N., Parisi, P., Palazzi, E., et al. 2013, A&A, 556, A120

Mason, R. E., Levenson, N. A., Shi, Y., et al. 2009, ApJ, 693, L136

Massaro, E., Giommi, P., Leto, C., et al. 2009, A&A, 495, 691

Massaro, E., Maselli, A., Leto, C., et al. 2015a, Ap&SS, 357, 75

Massaro, E., Nesci, R., & Piranomonte, S. 2012a, MNRAS, 422, 2322

Massaro, F., Álvarez-Crespo, N., Capetti, A., et al. 2019, ApJS, 240, 20

Massaro, F., & D'Abrusco, R. 2016, ApJ, 827, 67

Massaro, F., D'Abrusco, R., Ajello, M., Grindlay, J. E., & Smith, H. A. 2011, ApJ, 740, L48

Massaro, F., D'Abrusco, R., Giroletti, M., et al. 2013, The Astrophysical Journal Supplement Series, 207, 4

Massaro, F., D'Abrusco, R., Paggi, A., et al. 2013, ApJS, 206, 13

Massaro, F., D'Abrusco, R., Tosti, G., et al. 2012b, ApJ, 750, 138

Massaro, F., Landoni, M., D'Abrusco, R., et al. 2015b, A&A, 575, A124

Massaro, F., Marchesini, E. J., D'Abrusco, R., et al. 2017, ApJ, 834, 113

Massaro, F., Masetti, N., D'Abrusco, R., Paggi, A., & Funk, S. 2014, AJ, 148, 66

Massaro, F., Paggi, A., Errando, M., et al. 2013, The Astrophysical Journal Supplement Series, 207, 16

Massaro, F., D'Abrusco, R., Landoni, M., et al. 2015c, ApJS, 217, 2

Massaro, F., Álvarez Crespo, N., D'Abrusco, R., et al. 2016, Ap&SS, 361, 337

Massaro, F., Capetti, A., Paggi, A., et al. 2020, ApJS, 247, 71

Matt, G. 2000, A&A, 355, L31

Matt, G., Brandt, W. N., & Fabian, A. C. 1996, MNRAS, 280, 823

Matt, G., Fabian, A. C., & Ross, R. R. 1993, MNRAS, 262, 179

Matt, G., Marinucci, A., Guainazzi, M., et al. 2014, MNRAS, 439, 3016

Mauch, T., Murphy, T., Buttery, H. J., et al. 2003, MNRAS, 342, 1117

Mayall, N. U. 1934, PASP, 46, 134

Mehdipour, M., Branduardi-Raymont, G., Kaastra, J. S., et al. 2011, A&A, 534, A39

Menezes, R. B., da Silva, P., & Steiner, J. E. 2018, MNRAS, 473, 2198

Merloni, A., Dwelly, T., Salvato, M., et al. 2015, MNRAS, 452, 69

Mirabal, N., & Halpern, J. P. 2009, ApJ, 701, L129

Miraghaei, H., & Best, P. N. 2017, MNRAS, 466, 4346

Mooney, S., Quinn, J., Callingham, J. R., et al. 2019, A&A, 622, A14

Moore, B., Frenk, C. S., & White, S. D. M. 1993, MNRAS, 261, 827

Mor, R., & Netzer, H. 2012, MNRAS, 420, 526

Mor, R., Netzer, H., & Elitzur, M. 2009, ApJ, 705, 298

Moran, E. C., Kay, L. E., Davis, M., Filippenko, A. V., & Barth, A. J. 2001, ApJ, 556, L75

Morganti, R., Oosterloo, T., Oonk, J. B. R., Frieswijk, W., & Tadhunter, C. 2015, A&A, 580, A1

Mulchaey, J. S., Colbert, E., Wilson, A. S., Mushotzky, R. F., & Weaver, K. A. 1993, ApJ, 414, 144

Mulchaey, J. S., Koratkar, A., Ward, M. J., et al. 1994, ApJ, 436, 586

Müller-Sánchez, F., Prieto, M. A., Hicks, E. K. S., et al. 2011, ApJ, 739, 69

Mushotzky, R. F., Marshall, F. E., Boldt, E. A., Holt, S. S., & Serlemitsos, P. J. 1980, ApJ, 235, 377

Nandra, K., O'Neill, P. M., George, I. M., & Reeves, J. N. 2007, MNRAS, 382, 194

Nandra, K., & Pounds, K. A. 1994, MNRAS, 268, 405

Nenkova, M., Sirocky, M. M., Ivezić, Ž., & Elitzur, M. 2008a, ApJ, 685, 147

Nenkova, M., Sirocky, M. M., Nikutta, R., Ivezić, Ž., & Elitzur, M. 2008b, ApJ, 685, 160

Netzer, H. 2013, The Physics and Evolution of Active Galactic Nuclei

—. 2015, ARA&A, 53, 365

Nolan, P. L., Abdo, A. A., Ackermann, M., et al. 2012, ApJS, 199, 31

Nori, M., Giroletti, M., Massaro, F., et al. 2014, The Astrophysical Journal Supplement Series, 212, 3

Oh, K., Koss, M., Markwardt, C. B., et al. 2018, ApJS, 235, 4

Ordovás-Pascual, I., Mateos, S., Carrera, F. J., et al. 2017, MNRAS, 469, 693

Orr, M. J. L., & Browne, I. W. A. 1982, MNRAS, 200, 1067

Osterbrock, D. E. 1981, ApJ, 249, 462

Osterbrock, D. E., & Ferland, G. J. 2006, Astrophysics of gaseous nebulae and active galactic nuclei

Osterbrock, D. E., & Martel, A. 1993, ApJ, 414, 552

Osterbrock, D. E., & Mathews, W. G. 1986, ARA&A, 24, 171

Osterbrock, D. E., & Parker, R. A. R. 1965, ApJ, 141, 892

Osterbrock, D. E., & Pogge, R. W. 1985, ApJ, 297, 166

Pacholczyk, A. G., & Weymann, R. 1968, AJ, 73, 836

Paggi, A., Massaro, F., D'Abrusco, R., et al. 2013, ApJS, 209, 9

Paggi, A., Milisavljevic, D., Masetti, N., et al. 2014, AJ, 147, 112

Paiano, S., Falomo, R., Franceschini, A., Treves, A., & Scarpa, R. 2017a, ApJ, 851, 135

Paiano, S., Falomo, R., Treves, A., Franceschini, A., & Scarpa, R. 2019, ApJ, 871, 162

Paiano, S., Landoni, M., Falomo, R., Treves, A., & Scarpa, R. 2017b, ApJ, 844, 120

Panessa, F., & Bassani, L. 2002, A&A, 394, 435

Panessa, F., Bassani, L., Cappi, M., et al. 2006, A&A, 455, 173

Pappa, A., Georgantopoulos, I., Stewart, G. C., & Zezas, A. L. 2001, MNRAS, 326, 995

Parisi, P., Masetti, N., Jiménez-Bailón, E., et al. 2012, A&A, 545, A101

Patrick, A. R., Reeves, J. N., Porquet, D., et al. 2012, MNRAS, 426, 2522

Peña-Herazo, H. A., Massaro, F., Chavushyan, V., et al. 2020a, Submitted to A&A

Peña-Herazo, H. A., Marchesini, E. J., Álvarez Crespo, N., et al. 2017, Ap&SS, 362, 228

Peña-Herazo, H. A., Massaro, F., Chavushyan, V., et al. 2019, Ap&SS, 364, 85

—. 2020b, Submitted to A&A

Peeters, E., Spoon, H. W. W., & Tielens, A. G. G. M. 2004, ApJ, 613, 986

Peterson, B. A., Jauncey, D. J., Wright, A. E., & Condon, J. J. 1976, ApJ, 207, L5

Peterson, B. M. 1993, PASP, 105, 247

—. 1997, An Introduction to Active Galactic Nuclei

Petrosian, A. R. 1982, Astrofizika, 18, 548

Petrov, L., Mahony, E. K., Edwards, P. G., et al. 2013, MNRAS, 432, 1294

Pian, E., Vacanti, G., Tagliaferri, G., et al. 1998, ApJ, 492, L17

Pier, E. A., & Krolik, J. H. 1992, ApJ, 401, 99

—. 1993, ApJ, 418, 673

Pietsch, W., Bischoff, K., Boller, T., et al. 1998, A&A, 333, 48

Pilkington, J. D. H., & Scott, J. F. 1965, MmRAS, 69, 183

Pogge, R. W. 1988, ApJ, 332, 702

Ponti, G., Miniutti, G., Fabian, A. C., Cappi, M., & Palumbo, G. G. C. 2006, Astronomische Nachrichten, 327, 1055

Pounds, K., & Vaughan, S. 2006, MNRAS, 368, 707

Pounds, K. A., Warwick, R. S., Culhane, J. L., & de Korte, P. A. J. 1986, MNRAS, 218, 685

Prieto, M. A., Mezcua, M., Fernández-Ontiveros, J. A., & Schartmann, M. 2014, MNRAS, 442, 2145

Raban, D., Jaffe, W., Röttgering, H., Meisenheimer, K., & Tristram, K. R. W. 2009, MNRAS, 394, 1325

Rafanelli, P., & Schulz, H. 1991, Astronomische Nachrichten, 312, 167

Rafanelli, P., Violato, M., & Baruffolo, A. 1995, AJ, 109, 1546

Rees, M. J. 1984, ARA&A, 22, 471

Reyes, R., Zakamska, N. L., Strauss, M. A., et al. 2008, AJ, 136, 2373

Ricci, C. 2011, PhD thesis, University of Geneva

Ricci, C., Ueda, Y., Koss, M. J., et al. 2015, ApJ, 815, L13

Richards, G. T., Nichol, R. C., Gray, A. G., et al. 2004, ApJS, 155, 257

Risaliti, G., Maiolino, R., & Salvati, M. 1999, ApJ, 522, 157

Roche, P. F., Packham, C., Aitken, D. K., & Mason, R. E. 2007, MNRAS, 375, 99

Rojas, A. F., Masetti, N., Minniti, D., et al. 2017, A&A, 602, A124

Ross, R. R., & Fabian, A. C. 1993, MNRAS, 261, 74

Ruschel-Dutra, D., Pastoriza, M., Riffel, R., Sales, D. A., & Winge, C. 2014, MNRAS, 438, 3434

Ruschel-Dutra, D., Rodríguez Espinosa, J. M., González Martín, O., Pastoriza, M., & Riffel, R. 2017, MNRAS, 466, 3353

Sabater, J., Best, P. N., & Argudo-Fernández, M. 2013, MNRAS, 430, 638

Salpeter, E. E. 1964, ApJ, 140, 796

Salvato, M., & Rafanelli, P. 1997, Astronomische Nachrichten, 318, 237

Salvetti, D., Chiaro, G., La Mura, G., & Thompson, D. J. 2017, MNRAS, 470, 1291

Sandage, A., & Tammann, G. A. 1987, A Revised Shapley-Ames Catalog of Bright Galaxies

Sani, E., Lutz, D., Risaliti, G., et al. 2010, MNRAS, 403, 1246

Sargent, W. L. W. 1970, ApJ, 160, 405

Saxton, R. D., Read, A. M., Esquej, P., et al. 2008, A&A, 480, 611

Sbarufatti, B., Falomo, R., Treves, A., & Kotilainen, J. 2006, A&A, 457, 35

Schawinski, K., Thomas, D., Sarzi, M., et al. 2007, MNRAS, 382, 1415

Scheuer, P. A. G., & Readhead, A. C. S. 1979, Nature, 277, 182

Schinzel, F. K., Petrov, L., Taylor, G. B., & Edwards, P. G. 2017, ApJ, 838, 139

Schinzel, F. K., Petrov, L., Taylor, G. B., et al. 2015, ApJS, 217, 4

Schlafly, E. F., & Finkbeiner, D. P. 2011, ApJ, 737, 103

Schlegel, D. J., Finkbeiner, D. P., & Davis, M. 1998, ApJ, 500, 525

Schmidt, M. 1963, Nature, 197, 1040

Schmidt, M., & Green, R. F. 1983, ApJ, 269, 352

Schmitt, H. R. 2001, AJ, 122, 2243

Schmitt, H. R., & Kinney, A. L. 1996, ApJ, 463, 498

Scott, A. E., Stewart, G. C., Mateos, S., et al. 2011, MNRAS, 417, 992

Segreto, A., Cusumano, G., Ferrigno, C., et al. 2010, A&A, 510, A47

Seibert, M., Wyder, T., Neill, J., et al. 2012, in American Astronomical Society Meeting Abstracts, Vol. 219, American Astronomical Society Meeting Abstracts #219, 340.01

Seyfert, C. K. 1943, ApJ, 97, 28

Shablovinskaya, E. S., Afanasiev, V. L., & Popović, L. č. 2020, ApJ, 892, 118

Shaw, M. S., Romani, R. W., Cotter, G., et al. 2013, ApJ, 764, 135

Shi, Y., Rieke, G. H., Smith, P., et al. 2010, ApJ, 714, 115

Siebenmorgen, R., Heymann, F., & Efstathiou, A. 2015, A&A, 583, A120

Simkin, S. M., Su, H. J., & Schwarz, M. P. 1980, ApJ, 237, 404

Singh, K. P., Garmire, G. P., & Nousek, J. 1985, ApJ, 297, 633

Singh, V., Shastri, P., & Risaliti, G. 2011, A&A, 532, A84

Skrutskie, M. F., Cutri, R. M., Stiening, R., et al. 2006, AJ, 131, 1163

Slipher, V. M. 1917, Lowell Observatory Bulletin, 3, 59

Souchay, J., Andrei, A. H., Barache, C., et al. 2009, A&A, 494, 799

Stalevski, M., Fritz, J., Baes, M., Nakos, T., & Popović, L. Č. 2012, MNRAS, 420, 2756

Stasińska, G. 1984, A&A, 135, 341

Stasińska, G., Cid Fernandes, R., Mateus, A., Sodré, L., & Asari, N. V. 2006, MNRAS, 371, 972

Stern, D., Assef, R. J., Benford, D. J., et al. 2012, ApJ, 753, 30

Stickel, M., Padovani, P., Urry, C. M., Fried, J. W., & Kuehr, H. 1991, ApJ, 374, 431

Stocke, J. T., Morris, S. L., Gioia, I. M., et al. 1991, ApJS, 76, 813

Stocke, J. T., Morris, S. L., Weymann, R. J., & Foltz, C. B. 1992, ApJ, 396, 487

Storchi-Bergmann, T., Fernandes, R. C., & Schmitt, H. R. 1998, ApJ, 501, 94

Strand, N. E., Brunner, R. J., & Myers, A. D. 2008, ApJ, 688, 180

Stroh, M. C., & Falcone, A. D. 2013, ApJS, 207, 28

Sturm, E., Schweitzer, M., Lutz, D., et al. 2005, ApJ, 629, L21

Suganuma, M., Yoshii, Y., Kobayashi, Y., et al. 2006, ApJ, 639, 46

Tadhunter, C. 2008, J New Astronomy Reviews, 52, 227

Titov, O., Stanford, L. M., Johnston, H. M., et al. 2013, AJ, 146, 10

Tody, D., & Doug. 1986, in IN: Instrumentation in astronomy VI; Proceedings of the Meeting, Tucson, AZ, Mar. 4-8, 1986. Part 2 (A87-36376 15-35). Bellingham, WA, Society of Photo-Optical Instrumentation Engineers, 1986, p. 733., ed. D. L. Crawford, Vol. 627, 733–748

Torrealba, J., Chavushyan, V., Cruz-González, I., et al. 2012, RMxAA, 48, 9

Tran, H. D. 2001, ApJ, 554, L19

—. 2003, ApJ, 583, 632

Treister, E., Castander, F. J., Maccarone, T. J., et al. 2005, ApJ, 621, 104

Tristram, K. R. W., Meisenheimer, K., Jaffe, W., et al. 2007, A&A, 474, 837

Tsarevsky, G., de Freitas Pacheco, J. A., Kardashev, N., et al. 2005, A&A, 438, 949

Tueller, J., Mushotzky, R. F., Barthelmy, S., et al. 2008, ApJ, 681, 113

Turner, T. J., & Pounds, K. A. 1989, MNRAS, 240, 833

Ulrich, M.-H., Maraschi, L., & Urry, C. M. 1997, ARA&A, 35, 445

Urry, C. M., & Padovani, P. 1995, PASP, 107, 803

van Dokkum, P. G. 2001, PASP, 113, 1420

Vaughan, S., Edelson, R., Warwick, R. S., & Uttley, P. 2003, MNRAS, 345, 1271

Vaughan, S., & Fabian, A. C. 2004, MNRAS, 348, 1415

Veilleux, S., & Osterbrock, D. E. 1987, ApJS, 63, 295

Vermeulen, R. C., & Taylor, G. B. 1995, AJ, 109, 1983

Veron-Cetty, M. P., & Veron, P. 1989, European Southern Observatory Scientific Report, 7, 1

Véron-Cetty, M. P., & Véron, P. 2006, A&A, 455, 773

—. 2010, A&A, 518, A10

Villarroel, B., & Korn, A. J. 2014, Nature Physics, 10, 417

Villarroel, B., Nyholm, A., Karlsson, T., et al. 2017, ApJ, 837, 110

Visnovsky, K. L., Impey, C. D., Foltz, C. B., et al. 1992, ApJ, 391, 560

Voges, W., Aschenbach, B., Boller, T., et al. 1999, A&A, 349, 389

—. 2000, IAU Circ., 7432, 3

Wada, K. 2012, ApJ, 758, 66

Wada, K., Papadopoulos, P. P., & Spaans, M. 2009, ApJ, 702, 63

Walter, R., & Fink, H. H. 1993, A&A, 274, 105

Warwick, R. S., Saxton, R. D., & Read, A. M. 2012, A&A, 548, A99

Weaver, K. A., Heckman, T. M., Strickland, D. K., & Dahlem, M. 2002, ApJ, 576, L19

Webb, J. R., Smith, A. G., Leacock, R. J., et al. 1988, AJ, 95, 374

Weedman, D. W. 1976, QJRAS, 17, 227

—. 1977, ARA&A, 15, 69

Weigelt, G., Hofmann, K. H., Kishimoto, M., et al. 2012, A&A, 541, L9

White, R. L., Becker, R. H., Helfand, D. J., & Gregg, M. D. 1997, ApJ, 475, 479

Wisotzki, L., Christlieb, N., Bade, N., et al. 2000, A&A, 358, 77

Worpel, H., Brown, M. J. I., Jones, D. H., Floyd, D. J. E., & Beutler, F. 2013, ApJ, 772, 64

Wright, A. E., Griffith, M. R., Burke, B. F., & Ekers, R. D. 1994, ApJS, 91, 111

Wright, E. L., Eisenhardt, P. R. M., Mainzer, A. K., et al. 2010, AJ, 140, 1868

Xanthopoulos, E. 1996, MNRAS, 280, 6

Xie, Y., Li, A., & Hao, L. 2017, ApJS, 228, 6

Yee, H. K. 1983, ApJ, 272, 473

Zechlin, H.-S., & Horns, D. 2012, Journal of Cosmology and Astroparticle Physics, 2012, 050

Zel'dovich, Y. B. 1964, Soviet Physics Doklady, 9, 195

Zhou, X. L., Zhao, Y. H., & Soria, R. 2011, MNRAS, 413, L61